REHABILITATION OF THE DAMAGED BRICK INFILLED RC FRAMES BY CFRP OVERLAYS AND EPOXY INJECTION

by

Ozan KARATAŞ

B.S., in C.E., Boğaziçi University, 2006

Submitted to the Institute for Graduate Studies in
Science and Engineering in partial fulfillment of
the requirements for the degree of
Master of Science

Graduate Program in Civil Engineering
Boğaziçi University

2009

ACKNOWLEDGEMENTS

First, I would like to express my sincere gratitude to my thesis supervisor, Prof. Dr. Cengiz Karakoç for his guidance, support and encouragement throughout the preparation of this thesis. Without her sympathy, patience and guidance, the accomplishment would be impossible.

I would also like to thank Dr. Şevket Özden and Dr. Savaş Atmaca for their kind and supportive attitude to me and showing high interests and valuable advices to my thesis.

I can not find the proper words to thank my dear friends and colleagues; M. Oğuz Gedikli, Aysegül Korkmaz and Alper Firat Delice for their generous helps and supports during my thesis.

ABSTRACT

REHABILITATION OF THE DAMAGED BRICK INFILLED RC FRAMES BY CFRP OVERLAYS AND EPOXY INJECTION

The effect of damage and comparison with the undamaged specimen considering the engineering properties (stiffness, strength, energy dissipation, ductility…etc.) of infilled RC frames with or without CFRP were evaluated experimentally and analytically. Two single-bay, two-story damaged specimens at 1/3 scale were tested in a vertical position under quasi-static reversed cyclic seismic loading. Vertical and lateral loads were applied concurrently. These specimens were strengthened with CFRP unidirectional overlays in various configurations and the cracks were repaired with epoxy injection. The specimens had some deficiencies commonly seen in pre-1998 Turkish construction. The specimens had detailing deficiencies; such as insufficient confinement, 90^0 hooks, no transverse reinforcement in the joints, design deficiencies; such as weak column-strong beam, and construction deficiencies; such as poor material quality, and inadequate lap splice length. They also had different damage levels and aspect ratio which was tested under same circumstances by Atmaca in 2008. To eliminate the existing deficiencies and capacity loss due to the damage and cracks, unidirectional CFRP overlays were applied in the form of vertical strips and/or cross diagonals on both sides of the infill panel and anchored to the surrounding RC frames. The brick loss were repaired and the cracks were filled with epoxy. The application of CFRP overlays and epoxy injection improved the load carrying capacity and the energy dissipation capacity of damaged specimen, close to the undamaged strengthened condition. Generally, as the peak loads increased, their corresponding drifts also increased and the general behavior of damaged specimens were approximately same with the one Atmaca's experimental undamaged specimens. Some stiffness improvements were also recorded depending on damage level and the aspect ratio of the frames. The experimental capacity of the specimens was compared with both analytical calculation and experimental values of the Atmaca's undamaged strengthened specimens with same conditions.

ÖZET

HASARLI TUĞLA DOLGU DUVARLI BETONARME ÇERÇEVELERİN KARBON FİBER ESASLI KOMPOZİT YAYGILARLA VE EPOKSİ ENJEKSİYONU İLE REHABİLİTASYONU

Hasarlı olarak tamir edilen ve güçlendirilen dolgulu betonarme çerçeveler üzerinde hasar etkisi ve bu etkinin hasarsız güçlendirilmiş numunelerlere karşılaştırlmasını mühendislik özellikleri bakımından (rijitlik, dayanım, enerji yutma, düktilite…vs.) deneysel ve nümerik olarak değerlendirilmiştir. 1/3 ölçekli, tek açıklıklı, iki katlı ve düşey olarak test alanına yerleştirilen 2 farklı seviyede hasarlı numune statik tersinir yanal yükler altında deneye tabi tutulmuştur. Düşey ve yatay yükler birbirinden bağımsız olarak numuneye etkittirilmiştir. İki numunede hasarlı olarak karbon lifleriyle güçlendirilip, çatlak bölgelerine epoksi enjeksiyonu yapılmıştır. Numuneler 1998'den önce Türkiye'de yapılan yapılarda yaygın bir şekilde görülen kusurlara sahiptir. Bu kusurlar yetersiz sargı, 90^0 kanca ve birleşim bölgelerinde etriye bulunmaması gibi detay kusurları, zayıf kolon-güçlü kiriş gibi dizayn kusurları ve düşük malzeme kalitesi, yetersiz bindirme boyu gibi yapım kusurlarıdır. Bu kusurlara ek olarak numuneler farklı yükseklik uzunluk oranına ve hasar seviyelerine sahiptir. Numuneler 2008 yılında Atmaca tarafından yapılan deneydeki aynı karakteristik özelliklere sahip olup bu yapılan deneyde hasar görmüştür. Bu mevcut kusurları azaltmak, çatlaklardan oluşan hasarın getirdiği kapasite azalmasını kompanse etmek ve sismik performanslarını arttırmak için tek yönlü karbon fiberli kompozit yaygılar düşey şeritler ve/veya eğik diyagonaller biçiminde dolgu duvarın her iki tarafına da yapıştırılmış ve betonarme çerçeveye ankrajlanmıştır. Tüm tuğla kayıpları giderilmiş, çatlamış yüzeyler özel bir epoksi malzemeyle doldurulup tamir edilmiştir. Karbon fiberli kompozit yaygılar ve epoksi enjeksiyonu numunelerin yük taşıma ve enerji yutma kapasitelerini, Atmaca tarafından 2008 yılında hasarsız olarak güçlendirilmiş numune seviyesine çok yakın değerlere kadar arttırmıştır. Maksimum yüklere tekabül eden yatay deplasmanlar da artmıştır. Hasarlı numunelerin deneysel kapasiteleri hasarsız güçlendirlmiş numuneler üzerinde yapılan teorik ve deneysel değerlerle karşılaştırılmış ve yakın değerlere ulaşılmıştır.

TABLE OF CONTENTS

LIST OF FIGURES

LIST OF TABLES

LIST OF SYMBOLS/ABBREVIATIONS

b_{column}	Column section width
b_{FRP}	Width of FRP
d_{column}	Column effective depth
E_{bm}	The modulus of elasticity of the masonry infill
E_{bmp}	The modulus of elasticity of the plastered infill wall
E_c	The modulus of elasticity of concrete in the frame
E_p	The modulus of elasticity of the plaster
E_s	Modulus of elasticity of re-bars
f_{bm}	Compressive strength of masonry (excluding plaster)
f_{bmp}	Compressive strength of masonry (including plaster)
f_{bmpF}	Compressive strength of the strengthened infill wall
f_{ck}	Characteristic compressive strength of concrete
f_{ctk}	Characteristic tensile strength of concrete
f_m’	The prism compressive strength of the masonry
f_p, f_m, f_{mortar}	Nominal compressive strength of 50x50x50mm mortar cubes
f_s	Maximum stress in the re-bars of the tension column
f_{sp}	Splitting tensile strength of concrete
f_u	Characteristic ultimate strength of rebars
f_{yk}	Characteristic yield strength of re-bars
h_1	Story height
h_{bmp}, h_m	Height of the infill wall
h_{column}	Column section height
H_{ult}	Corner crushing strength of the infill
I_g	Moment of inertia of column
k	Modification factor
l, L_f	Length of the frame between centers of the columns
l_b	Insufficient lap splice length
l_{bmp}, l_m	Length of the infill wall
N_d	Axial load on the column

P	Overturning failure load
R_c	Diagonal compression failure force
R_s	Diagonal compression strut force
R_{strut}	Capacity of the equivalent compression strut
s	Spacing of the transverse reinforcement
t	The thickness of the infill
t_{bm}	Thickness of the infill wall excluding plaster
t_{frp}	Thickness of CFRP overlay
t_p	Thickness of the plaster
V_{column}	Shear capacity of the column (either tension or compression)
$V_{cr\text{-}compression}$	Shear resistance of concrete under compression
$V_{cr\text{-}tension}$	Shear resistance of concrete under tension
V_f	The maximum shear force resisted by the wall
$V_{f\text{-}column}$	Total shear force carried by column
V_i	The sliding shear capacity of the infilled frame
V_w	Shear strength contribution of transverse steel
z_{clm}	Vertical contact length between masonry panel and the column
ε_y	Yield strain of re-bars
μ	Coefficient of friction
θ, θ_{strut}	Inclination of the diagonal compressive strut
θ_{FRP}	Inclination of the cross FRP diagonals
τ_{bm}	Shear strength of masonry (excluding plaster)
τ_p, τ_m	Shear strength of plaster or mortar
ASTM	American Society for Testing and Materials
CFRP	Carbon Fiber Reinforced Plastic
LVDT	Linear Variable Differential Transducers
RC	Reinforced Concrete
TDY	Turkish Earthquake Code

1. INTRODUCTION

1.1. General Concepts

Previous observations showed that disastrous earthquakes which cause catastrophic damages, (Erzincan, Afyon-Dinar, Adana-Ceyhan, Marmara and Bolu-Düzce) originated from the lack of lateral strength, ductility and stiffness. The other issue that is not taken into account is the masonry infill walls. Masonry infill walls can interact with the surrounding frame and influence the stiffness and strength capacity unless they are isolated from the structural system. However commonly used type of masonry is the hollow clay tile has a non ductile behavior which causes a rapid degradation in stiffness and strength under seismic loads.

Masonry infill influence on the basic frame can differ according to the condition of designs and the structural system that masonry infill is at contact. As in the previous earthquakes occurred in Turkey, if masonry walls have not been designed to resist lateral loads, at a certain level of displacement, infill walls behave in a brittle manner. At this instant the huge lateral forces are redistributed to the main structural system which causes severe damages to the main frame, due to the fact that they are not designed to resist the increased lateral loads.

Otherwise, infill walls have a positive effect considering the stiffer walls attract more seismic loads until the damage level. This feature of the infill walls save the main frame from large deformations while dissipating the seismic energy. Beside this, frames with infill walls have lower inter-story drift values under the seismic action if the seismic action creates a smaller displacement than the failure displacement of masonry infill.

Apart from the design issue, deficiencies at the construction phase may result in severe damages under the seismic actions. The interaction forces occur between the infill walls and the frame elements in case of the lack of mortar and other construction materials which may create severe damages as a consequence.

Experimental studies showed that during an earthquake, masonry walls do not have the inertia force absorption capacity due to the fact that unreinforced masonry is brittle and weak in tension. Unreinforced masonry is a cheap construction material; therefore it is widely used at developing countries such as, Turkey. As a consequence of poor seismic behavior of the constructions, made up of unreinforced masonry, necessity of rehabilitation emerged.

Rehabilitation techniques which are generally divided into two groups as pre-earthquake (strengthening) and post-earthquake (repair) have lots of different ways considering the advancing technology. Economy, time, and application convenience are the main concerns while deciding the rehabilitation technique. With the help of advancing technology Fiber Reinforced Plastic, (FRP) occurred as a new repairing or strengthening method. It has lots of advantages considering the application convenience, less disturbance to the people living, less weight added to the complete system and suitable mechanical properties. However, compared with the other techniques, FRP materials' long term behaviors could not be evaluated and should be explored in the future.

FRP material can be easily applied to the both column-beam joints, infill walls, shear walls and other structural load bearing elements. The ease of application creates time saving for the researches. The most important issue is that, this application has to be held on the same condition as in the most of buildings in Turkey. As it is mentioned before masonry walls have lack of tensile strength and behave brittle manner under the seismic action. FRP application, highlighted as high tensile strength capacity maybe the good solution as both pre and post earthquake retrofitting technique. Not only the high mechanical properties but also the rapid application and the minimum disturbance to the dwellers are the dominant features compared with the conventional techniques such as adding new shear walls instead of masonry walls and steel jacketing methods.

At this point, as a structural engineer one should develop the most feasible and applicable solution considering experimental studies including the lots of structures for rehabilitation and retrofitting. The most important part of these studies has to include the deficiencies and vulnerability of the existing building in order to find justifiable solutions.

The effect of an earthquake can be determined by the level of damage to the buildings. However, level of damage is not only affected by the earthquake seismic loads but also the soil condition and the deficiencies of the existing buildings. In order to apply the correct rehabilitation or retrofitting technique, one has to determine the deficiencies and vulnerabilities of a building. After the Marmara earthquake, Turkish Earthquake Code had also been rehabilitated and finally in 2007 latest earthquake codes are published in Turkey. Deficiencies of a building result in poor seismic performance in terms of stiffness, strength and ductility.

Most important deficiency among the existing building is strong beam –weak column construction. In Turkish Earthquake Code (TDY) 2007 it is strictly emphasized that strong columns should be stronger than beams in order to develop suitable side-sway mechanism. Joints consisting of strong beam weak column result in plastic hinge formation at columns. This type of behavior is a non-ductile mechanism which can cause catastrophic damages. Other type of deficiency is the inadequate confinement and splice length. After the big earthquakes observations showed that, lack of transverse reinforcement and lap splice lengths are the main deficiency among the damaged buildings. 90 degree bending ends for transverse reinforcement, lack of adequate anchorage length and improper reinforcement details decrease the confinement effect, therefore buckling in longitudinal reinforcement and column shear failure occurs. This is the most sudden and brittle failure mode.

Soft\weak story is the other vulnerability for the buildings in case of seismic action. It is originated from the lack of stiffness and lateral strength compared with the neighboring stories. Irregularities on the infill structures may also create column hinging which can result in a sudden damage. Beside this, short column effect creates the same type of damages due to decrease in the effective length of column. This decrease can be originated from the large openings from one column to another in the infill walls.

All of these deficiencies made our buildings vulnerable to the earthquake. Because we have huge numbers of these type of building, conventional rehabilitation methods such as adding new structural walls, are not quick enough and not feasible. Therefore, FRP application technique arises from these needs of the engineering demands.

1.2. Scope and Objective

In this study main targets are to investigate the damage effect on the behavior of hollow clay tile infilled RC frames, repaired by means of CFRP and epoxy injection. As it is mentioned above chapter, our aim is to determine the most feasible, time saving repairing rehabilitation methods even in the damaged frames with deficiencies observed in Turkey. The behavior of FRP for strengthening, was investigated before, however, under cracked and damaged condition, FRP effectiveness and efficiency with epoxy injection to the cracks are the main issues that would be investigated, by comparing the other experimental works.

The study is limited to planar single bay and two storey infilled frames. Frames are composed of beams, columns and hollow clay tiles with repair and rehabilitation material FRP. These models were tested until the failure, under reversed cyclic loading. Now, main goal is to repair the damaged frames and masonry, and rehabilitate them in order to reach the uncracked or undamaged condition. After testing the repaired frames comparison with the other experimental works will be done and it is aimed to find the effect of the damage can be compensated or not. The analytical capacity calculation methods of undamaged models are going to be investigated whether it is suitable for damage and repaired case or not.

The second chapter of this study includes the existing literature review on the topic and composed of the summary of some papers and researches about the infill frames and rehabilitation techniques. Third chapter gives the information about materials and the test setup. The material and specimen features are summarized at this chapter. Chapter four and five consists of test results, comparison with the undamaged frames and other experimental works and their evaluations. Finally chapter seven provides the recommendation and conclusion considering this study and the future studies.

2. LITERATURE REVIEW

2.1. Previous Studies

Throughout the years lots of researches and paper had been released considering the brick infill frames. However, FRP repairing or strengthening has emerged as a new rehabilitation technique. It is anticipated that the use of FRP on masonry will involve walls resisting in-plane and out of plane loads. But, most of the studies and experimental works have been on the out of plane capacity of walls with externally applied FRP.

FRP is a new and challenging issue in civil engineering due to the fact that it has lots of advantages compared with the conventional methods. Apart from this there are some issues that have to be further investigated such as the moisture effect on the FRP bonding, fire resistance and long term behavior. Studies about the strengthening and repairing of the infill reinforced concrete frames by means of the reinforced concrete walls and FRP composite materials are summarized in this chapter.

Ersoy,U. tested and studied on the reinforced concrete infills in 1971. The frames were one bay and one story RC infilled walls. They were tested under monotonically increasing lateral loads. Frame aspect ratio was approximately 2.0. Main parameters investigated were the relative rigidities of frame members, infill thickness, frame-wall interface type, and the ratio of horizontal load to vertical load. As a conclusion, researchers have found that RC infilled walls assured significant rigidity by increasing the lateral load capacity 700% and decreasing the failure deformation 65%. Also, the RC walls increased the initial stiffness as much as 5 times.[1]

Mainstone, R.J. investigated and tested the steel frames with brickwork in 1971. In order to make a clear judgment, Mainstone, R.J. also tested the walls without frames apart from three brickwork infilled frames. As expected, sudden and brittle failure occurred. Failure mode was originated from diagonal cracks and crushing. At the end of the report, he proposed three curves to clarify the equivalent strut considering the stiffness, cracking and strength.[2]

Altın, S. completed a research considering the behavior of RC frames with conventional strengthening methods, reinforced concrete infills in 1990. This investigation was the upgrade of the one that is mentioned above (Ersoy 1971). This experiment consisted of 14 one-third scale, one bay, but two storey specimens. Infills were used as a strengthening method rather than a repair because the frames were undamaged. Main variables were the pattern of RC infill reinforcement detail, its connection to the frames, effect of axial load and the strength. Under lateral cyclic load the specimen were tested and it was concluded that under the proper frame to infill connection detail, the strength and stiffness values increased dramatically. In addition to this, axial forces on the columns and the strength of the columns also increased the lateral load capacity.[3]

Sieble, F. and Weeks, J. performed lots of tests on the full scale five storey masonry building reinforced with FRP.(1994) They investigated both strengthening and repairing conditions that focus on the in-plane strength. All of the results indicated that dramatic increases revealed considering the ductility and load carrying capacity.[4]

Marjani, F. studied the behavior of RC frames with brick infills in 1997. The effect of the brick infill tested and author found out that the stiffness and strength values significantly increased. The effect of the plaster on the bricks was the other subject that had been evaluated. It was seen that plastering the both sides of the specimen improved the behavior of the frames and ductility by delaying the diagonal cracking pattern of the brick.[5]

Ehsani, M. R. and Al-Saidy, A. investigated the contribution of the FRP overlays on the shear strength of the clay brick infills in 1997. 37 specimens had been tested under displacement controlled static loading. The shear strength provided by mortar had been diminished, by placing the plywood between the bricks. The effect of this gap under FRP rehabilitation was examined by the researchers. The main studied parameters were the strength of FRP, fiber orientation and the anchorage length. It is concluded that, FRP strength and anchorage length influenced the failure modes. Increase in the strength of the fabric, caused the limited usage of the capacity of the FRP. In order to obtain full strength

of the FRP, the anchorage length of the fabrics should be adequate. Finally 45^{o} orientation of the FRP produced the higher ultimate load compared with the 90^{o} [6]

Triantafillou, T. C. examined the strength of the masonry walls strengthened with externally applied FRP overlays in 1998. In order to determine dimensioning of the FRP reinforcement he had studied the models under monotonically out of plane bending, in plane bending and shear under the axial load. Four bending test had been executed to 12 specimen which consisted of six out of plane and six in plane. The researcher concluded that high stress zones should be reinforced intensively with FRP laminates in order to find out a strength increase. Secondly, under lower axial load condition, in plane shear capacity of the strengthened masonry walls increases. Finally, short length of the specimens and inadequate bond development length result in peeling off of FRP laminates and fully in plane flexure strength was not achieved. However, it was stated that, FRP application noticeably improved the both in plane and out plane bending and shear capacity [7]

Kolsch, H. studied the different method for out of plane retrofitting of masonry infill walls in 1998. This strengthening technique had been executed by using carbon fabrics inside the cement based matrix. On the other hand there was a control specimen which is not strengthened by carbon fabrics. Both full scale masonry walls were tested in out of plane bending and under cyclic loading condition. It is concluded by the author that, compared with the control specimen, the capacity of the strengthened masonry wall was 3 times greater. In addition to this conclusion, it has stated that carbon fiber embedded cement matrix hindered the any collapse of the infill panels.[8]

Trovilion, J. C. and Marshall, O. S. investigated the applicability of FRP for the strengthening technique on unreinforced masonry walls in corporation with the U.S. Army Construction Engineering Research Laboratory in 2000. For this study four different FRP system systems were applied to the 40 wall panels. Main variables that had been investigated were the width and thickness of FRP, different fiber orientations and multiple FRP layers. Firstly it has observed that the diagonal tension test were incapable for the evaluation of the behavior of the FRP on the masonry walls due to the fact that, stress distribution on the specimens was not uniform. However, the triplet test enabled that the evaluation of the relationship between width of FRP and its direct effect on the

strengthening of mortar joint in bricks. On the other hand, using the multiple layers FRP technique had a result that, shear strength of the mortar joint exceeded the compressive strength of the brick. [9]

Albert, M.L. and Cheng, R.J. had tested unreinforced masonry walls that are subjected to out of plane flexure loads in 2001. Main objective of this test was to show the effectiveness of FRP materials in increasing the load capacity of the walls. Ten walls used in this test and conducted 13 experiments. The effect of both damaged and undamaged walls were tested. Parameters that have been checked were type of reinforcement layout and amount of FRP, axial load and cyclic behavior. It was concluded by the authors that general behavior of the specimens were similar, strength and ductility of the specimens was increased dramatically when strengthened with FRP. Also the layout and the amount of fiber reinforcement affect the stiffness and other parameters including the ductility.[10]

Hamilton, H.W. and Dolan, C.V. investigated out of plane behavior of the masonry walls which are consisted of normal and lightweight concrete and strengthened with glass FRP in 2001. For this investigation they have tested six unreinforced concrete masonry walls (4 short walls and 2 tall walls). Main variables were the height of the specimen and type of concrete masonry wall. Test results show that bonding of glass FRP strips enable the walls to increase deformation capacity and stiffness due to increased integrity. Three different type of failure modes observed: Glass FRP fracture, delamination and the combination of both fracture and delamination.[11]

Tumialan, G. J. examined an alternative technique to Fiber Reinforced Polymer (FRP) externally-bonded laminates, which is the use near surface mounted (NSM) FRP bars in 2002. This technique consists of placing a bar in a groove cut into the surface of the member being strengthened. This paper describes three applications of FRP bars for the strengthening of URM and reports on the obtained experimental results. In the first application, FRP bars are applied vertically to resist out-of-plane forces acting on the masonry walls (i.e. flexural strengthening). In the second application, bars are inserted horizontally in the masonry joints to strengthen the wall when subjected to in-plane forces (i.e. shear strengthening). Finally, the third application deals with the retrofitting of masonry walls showing deficient anchorage to the base beam. In this application, FRP bars

are placed in the toe region of the wall acting as anchors to increase flexural capacity. In each of these three applications, the strengthening was remarkably effective. Conclusions can be listed as follows. Masonry walls strengthened with NSM FRP bars exhibited similar performance to walls strengthened with FRP laminates. For flexural strengthening, increments ranging between 4 and 14 times of the original masonry capacity may be achieved. These large increments should be taken as a reference only in walls that can be idealized as simply supported (i.e. when arching mechanism is not observed) Remarkable increases in shear capacity ranging between 30 and 80% may be achieved by FRP structural repointing. However, these increment levels should not be generalized for walls built with clay bricks, where different masonry characteristics (i.e. compressive strength) and wall geometries (i.e. number of wythes and number of layers) are observed. The use of FRP NSM bars for anchorage improvement may provide increases over 100% in in-plane flexural capacity. [12]

Li, T. carried out a research including the comparison of the three different walls retrofitted with FRP in 2001. One of the specimens was control specimen, and the others were reinforced with vertical FRP and horizontal FRP rods respectively. These specimens were tested under in-plane loading and results of the test showed that the response of two retrofitted walls was same until the deboning of the vertical strips. Finally the capacity of the horizontally retrofitted wall was 2 times compared with the vertical one. However the vertical strips increased the load capacity of the control specimen by 300%.[13]

Al-Chaar, G. examined a three-story, three-bay reinforced concrete frame with masonry infill panels was constructed and subjected to a series of damaging lateral forces for the purpose of assessing the effectiveness of CFRP overlays in increasing strength, stiffness, and deformation capacity in 2002. The test structure was a half scale model designed to incorporate the essential structural characteristics of a general class of military buildings constructed in the 1950s. The damaged test structure was then strengthened with CFRP wraps intended to restore its structural integrity to near-pretest condition. Prior to strengthening, damaged infill panels were replaced with new masonry and cracks in the concrete frame were injected with epoxy. Seismic performance of the –rehabilitated structure was then re-evaluated using a series of reversed and repeated lateral displacements and forces. This paper compares the load-deformation performance of the

rehabilitated test structure with that of the original frame-infill system. Test results are discussed with respect to measurements of strength, stiffness, and deformation capacity as well as observed damage patterns and apparent performance limit states. It was concluded that the effectiveness of adhered FRP wraps exhibited in the slight increase in the strength of the rehabilitated structure compared to the strength of the undamaged structure. Most important, the peak load of the rehabilitated occurred at a higher drift ratio and more cycles than the original structure.[14]

Borri, A. conducted a research on the damaged structures after the Umbria Marche earthquake in 2002. This research includes the behavior of masonry and the effectiveness of the seismic strengthening of both damaged and undamaged walls. Main tested systems were the traditional grout injection and upgrading with FRP. As a conclusion of the research, the traditional injection technique was more effective when used as a repair method for the damaged panels. On the other hand the application of the FRP was found out to be more effective in case of panels made of adequately connected masonry multiple-leaf walls or brick panels. [15]

Hanoglu K. B. tested four ductile four non-ductile framed single-bay-single story specimens with and without infill panels in 2002. A new method for tensile strength testing of the hollow clay tile units proposed and used coupling with finite element models to establish a tile tensile strength estimate. Glass fiber woven sheet and carbon fiber reinforced plastic laminates were used to confine and brace the hollow clay tile infill. Addition of glass-fiber overlays and carbon fiber laminates increased the strength of the infilled frames above the conventionally infilled frames. Corner crushing type of failure was observed in all strengthened specimens. Strengthening of infilled frames with FRP enhanced the probability of sudden and brittle failures. Analytically, a new finite element modeling approach was developed based on the use of plane-framework analysis methods, for plane stress analysis. The calculated pushover curves showed a good agreement with the test results for the detailed model, and the engineering model was regarded amenable for the future calibration. [16]

Valuzzi, M. R. examined an experimental study based on brick masonry panels strengthened by FRP in 2002. Main goal was to find out the efficiency of the FRP as an alternative shear reinforcement technique. 33 different panels were subjected to diagonal compression tests. Experimental results indicated that FRP laminates applied only one side of the panels did not upgrade the shear collapse mechanism dramatically. However, panels that were reinforced double side by FRP laminates provided more ductile behavior and significant ultimate capacity increase. [17]

Mertol, H. C. performed an experiment on two specimens which were one-third scale, one bay and two story plastered hollow clay tile infilled reinforced concrete frames in 2002. One of them was control specimen with no CFRP reinforcement. Other one was strengthened with CFRP overlays on both sides of the infill walls. There were no anchorage to the columns and beams. The result showed that strengthening of the masonry infill walls without anchoring the CFRP to beams and columns was not an efficient strengthening method. The increase in the strength and ultimate load capacity was very small compared with the control specimen with no CFRP overlays. Considering the economic issues, the overall performance improvement of strengthened specimen was not satisfactory. [18]

Akgüzel, U. examined the behavior of one third scale, two-story infilled frames upgraded by CFRP overlays in 2003. One of the specimens was bare frame, one of them masonry infilled and the others were strengthened with CFRP overlays. One of the most important deficiencies among all specimens was the insufficient lapped splice above the floor level. Uniaxial CFRP sheets were used to strengthen the specimen and these specimens were tested under reversed cyclic loading. The results can be summarized as : Lateral load carrying capacity and dissipated energy increased significantly. The change in stiffness was not noticeable however; stiffness degradation of the specimen with CFRP sheets was faster compared with the bare frame. Deformation capacity decreased but for the specimen with columns confined with CFRP overlays around lap splice regions, deformation capacity was increased. Finally, most important conclusion was stated that, insufficient lapped splice deficiency was diminished by the pattern in which column were confined by CFRP around the lap splice region. [19]

Stratford, T. examined the behavior of clay and concrete brick walls upgraded with glass FRP in 2004. 2 unreinforced walls and 4 reinforced walls were tested under monotonic loading which were consisted of lateral and vertical loading types. The one side of reinforced specimens was covered by biaxial GFRP overlays. After the test, author made conclusion that, for clay brick walls load carrying capacity increased 65% in case of GFRP strengthening However, load carrying capacity for concrete masonry walls increased between 40% and 63%. Stiffness and deformation capacity were not affected compared with the unreinforced specimen. In order to reach a ductile failure within the masonry, it is stated that premature failure has to be eliminated at the ultimate limit state. Therefore high strain adhesive required instead of high strength one. [20]

Erdem, I. has tested the performance of two different type of strengthening method in 2006. Three bays, two storey specimens were used under reversed cyclic loading. The frames had the general deficiencies seen Turkey. The middle bays of the frames were filled with either reinforced concrete or diagonally applied CFRP on the masonry wall. CFRP sheets applied diagonally on the brick infill wall and anchored to the surrounding frame. Beside this, lap splice regions on the columns were wrapped with uniaxial lateral displacement control load applied to the second story and vertical constant load to the columns. After the test the conclusions are as follows. Failure behavior of FRP applied specimen was resulted from the initial failure of FRP anchor at foundation. From this conclusion one can say that the anchor length and amount has significant effect on the effectiveness of FRP. When compared with the bare frame, reinforced concrete infill provided 5 times increase in ultimate load, although FRP strengthened frame enabled 4.6 times. Initial stiffness parameter was also showed a dramatic increase both in RC in filled and FRP upgraded. However, strength degradation of FRP applied frame was much more compared with the RC in filled one, due to the initial failure of FRP anchors. [21]

Yuksel investigated the features of single bay two story masonry infilled RC frames. Aspect ratio for the specimens was 1.7. There were 6 specimens. Two of them were bare frame, another 2 of them was masonry infilled only and the last ones were CFRP strengthened frames. For each group one specimen had lack of lapped splice length and had consisted of plain bars. All of the specimens were tested under quasi-static reversed cyclic loading and displacement controlled type of loading. Axial loads on columns were

23% of the capacity of columns and kept constant throughout the test. Strengthening pattern is the cross diagonal on both faces which were anchored to the surrounding frame. Also vertical CFRP sheets anchored to the foundation of the specimen. Finally in order to eliminate lap splice deficiency FRP applied to the bottom of columns. It can be concluded that: no critical damage seen at the second stories of specimens. Presence of infill walls shifts the behavior of the specimen from bare frame to shear wall type. The peak load of the infilled specimen with lap splices was 15% higher than that of the infilled specimen without lap splices. Retrofitting the infilled specimens with CFRP improved the strength and energy dissipation capacities of unstrengthened ones. [22]

ElGawady et al. examined the behavior of FRP strengthened hollow clay masonry walls in 2007. One side of three damaged and one undamaged walls was rehabilitated and specimens tested in plane under cyclic loading. The axial load of the half scale specimens was kept constant. Test variables were axial rigidity of FRP and effective moment to shear ratio. Bidirectional or double layer unidirectional FRP was applied to the specimens. They stated that FRP improved stiffness, strength and energy dissipation of the unreinforced specimens. The increase in lateral load was in the range of 42% for low axial rigidity and high moment to shear ratio and 493% for high axial rigidity and low moment to shear ratio respectively. The damage level and type of damage adversely influenced the maximum load of the retrofitted specimens. As the axial rigidity increased, the probability of occurrence of brittle failure mode increased. [23]

Almusallam, T. H. investigated the suitability and effectiveness of fiber-reinforced polymers FRP in strengthening and/or repairing unreinforced masonry infill walls in reinforced concrete frames which are subjected to in-plane seismic/cyclic loading in 2007. For this purpose, a detailed experimental program was conducted. Specimen geometry, test setup, instrumentation, and a loading procedure that simulates earthquake loading are presented in a detailed fashion. Results of experimental observations are discussed in the form of load-displacement hysteretic loops and envelopes; column profiles; strain diagrams, and wall shear distortion. The test results, in general, indicate that the use of glass FRP GFRP sheets as strengthening materials provides a degree of enhancement to the infill wall, upgrades its deformation capacity, and makes the wall work as one unit. These results thus show great potential for externally bonded GFRP sheets in upgrading and

strengthening the infill walls under in-plane seismic loads. As a conclusion, the behavior of three types of infill walls, namely, unstrengthened control, repaired, and strengthened was experimentally investigated. The results of tested specimens showed that the GFRP provides a degree of enhancement to the infill wall and increases its strength and ductility considerably. In addition, it also upgrades the deformation capacity and makes the wall work as one unit. For specimens of the present study, it was observed that use of GFRP strengthening increases the deformation capacity of infill walls up to 3 times its corresponding unstrengthened control specimen. These results thus show the great potential of externally bonded GFRP sheets in upgrading and strengthening rehabilitation infill walls under in-plane seismic loads. [24]

Della Corte, G. carried out a research about the effect of FRP strengthening on real RC building including the infill masonry frames in 2008. Two lateral-loading inelastic tests on a real masonry-infilled reinforced concrete RC building are presented. The first test has been carried out on the original building. Extensive damage to both masonry panels and RC elements columns and staircase structure has been produced, with out-of-plane collapse of almost all the walls parallel to the loading direction. The second test has been carried out on the repaired building. Namely, perimeter masonry panels were completely rebuilt and also strengthened by placing fiber-reinforced polymer FRP rods into the mortar bed joints of masonry. Extensive damage was produced also during this second test. Test results are discussed and compared to each other. Besides, the ability of current analytical methods in predicting the shear strength of both unreinforced and FRP-reinforced masonry panels is investigated. Eventually, simple analytical models are proposed for the lateral response of the whole building, including also contribution from the staircase structure. Some of the conclusions are as follows: However, out-of-plane collapse only occurred for a relatively large drift of about 0.05 rad. But, this last conclusion requires a word of caution, because the test was in plane static loading and, then, it did not consider out-of-plane dynamic effects possibly acting along with the in-plane dynamic load. The near surface mounted FRP rods, placed in the mortar bed joints, revealed to be effective in changing the failure mode of masonry panels from dominant diagonal tension cracking to prevailing shear sliding mode. [25]

Choi, T. H. conducted an investigation on the flexural behavior of partially bonded fiber-reinforced polymer FRP strengthened concrete beams focusing on the improvement of ductility in 2008. An analytical model was developed based on the curvature approach to predict the behavior of beams strengthened with partially bonded FRP systems. The result of the analysis showed that ductility of the partially bonded system was improved while sustaining high load carrying capacity in comparison to the fully bonded system. To verify the analytical model, an experimental program was carried out with reinforced concrete beams strengthened with the externally bonded FRP system. A comparison of the analytical prediction and experimental results showed good agreement. It was concluded that, the analytical model, developed based on the curvature approach, could predict the general behavior of the partially bonded beams with any unbonded length, and showed the potential to improve ductility with high load carrying capacity. However, the premature debonding failure and the FRP slip could not be considered. The analysis considering those effects and the experimental verification should be conducted in the future. [26]

Atmaca, S. investigated the effects of aspect ratio on the engineering properties of infilled RC frames with or without CFRP were evaluated experimentally and analytically in 2008. Ten single-bay, two-story specimens at 1/3 scale were tested in a vertical position under quasi-static reversed cyclic seismic loading. Two out of ten specimens were control specimens (with no CFRP) and the rest of them were strengthened with CFRP unidirectional overlays in various configurations. The specimens had some deficiencies commonly seen in pre- 1998 Turkish construction. The specimens had detailing and construction deficiencies mostly seen in Turkey. To eliminate the existing deficiencies of the specimens and improve their seismic performance, unidirectional CFRP overlays were applied in the form of vertical strips and/or cross diagonals on both sides of the infill panel and anchored to the surrounding RC frames. The application of CFRP overlays improved the load carrying capacity and the energy dissipation capacity significantly. Generally, as the peak loads increased, their corresponding drifts also increased. Some stiffness improvements were also recorded depending on the configuration of the CFRP overlays and the aspect ratio of the frames. The test results were compared with the numerical results obtained from the nonlinear static pushover analysis. The analytical model incorporated the equivalent diagonal compression strut concept for the infill panel. [27]

3. TEST PROGRAM

3.1 General

Past earthquakes and collapses showed that there is a strong need for repairing and rehabilitation of existing buildings in Turkey. In case of an earthquake, the deficiencies of the existing buildings emerges and therefore, investigations were carried on the specimens which includes common deficiencies such as, poor material strength, detailing deficiencies and strong column weak beam presence.

In 2008, Atmaca investigated and tested 10 specimens with these deficiencies with different aspect ratio and different FRP strengthening pattern were the main parameters. 2 of the specimens with aspect ratio 1.0 and 2.3 were the control specimen and were tested without FRP application. Same specimens without no damage were also tested with FRP application and the results were checked at the end of the test.

In our experimental program, these unstrengthened, damaged specimens were tested after different repairing and FRP application techniques. The pattern of the FRP application was the same with the one that was undamaged and strengthened with FRP in Atmaca's experiment. At the end of the test, our aim is to investigate the strength, stiffness and energy dissipation characteristic of FRP applied damaged specimen. These behaviors of damaged specimens with different aspect ratio, were compared with the ones at Atmaca‘s experiment. Three type of specimen would be checked and compared: Undamaged-strengthened (Atmaca 2008), damaged-strengthened and undamaged control specimen.

After the comparison of the behaviors, the efficiency of the repairing methods such as epoxy injection and FRP application would be checked. Effect of different damage levels and aspect ratios would also be investigated. Finally the analytical studies were carried out considering the damage effect on the load carrying capacities. It is believed that the observed failure modes, characteristics of the behavior, and the parameters investigated, like the frame aspect ratio, will be an important step for future studies.

3.2. Test Specimens

As stated above, two damaged specimen with different aspect ratio and damage level, were used for this experiment. One of the specimens, namely O1, had an aspect ratio 1.0 and low damage level without any brick loss. The other specimen O2, with aspect ratio 2.3, had medium damage and brick loss due to compression strut under the lateral cyclic load and axial load on columns. The main difference and variables between these specimens is the level of damage and aspect ratio.

On the other hand, both of the specimens had common properties such as, column beam dimensions, reinforcement details, CFRP pattern, brick and plaster type. All test specimens were designed and detailed considering deficiencies faced in practice. All test specimens were two-story, one bay, and one-third scale reinforced concrete infilled frames. Axial load on the columns was given considering column capacities

Dimensions of the columns and beams were 100/150 mm and 150/150 mm respectively. The thickness of the infill was about 70 mm excluding plaster. Strong beam-weak column design philosophy which was prohibited in the current code was employed to simulate previous applications. The height of the specimens from the foundation level was 1800 mm with various spans. The spans of the specimens between column outer faces for aspect ratios 1.0, 2.3 were 930 mm and 2000 mm respectively. Column and beam stirrups were Φ4@95mm, and Φ4@100mm respectively. Details of the specimens were listed at Table 3.1

During the production of the specimens, it was intended that both of the specimens had the same deficiencies common in practice. The deficiencies of the specimens were; low quality concrete, insufficient confinement, hooks with 90 degree ends, plain bars and inadequate lap splice length in columns and beam bottom reinforcement, no transverse steel in the joints and strong beams-weak columns. Longitudinal plain reinforcing bars in the columns were Φ8 with a lap splice length of 20Φ. Spacing and the diameter of the stirrups are illustrated in Table 3.1. Inadequate confinement was also a common practice in the existing buildings.

Table 3.1. Properties of test specimens

Spec.	Aspect Ratio	Damage Level	Repairing Pattern	Column Reinf.	Beam Reinf.	F_{ck} (MPa)	F_{mortar} (MPa)
O1	1.0	Low (No Brick Loss, Cracks at the Bottom of Columns)	High strength epoxy injection and CFRP application both vertical and diagonal scheme.	4Φ8(ρ=0.0134) Tie Φ4@95 mm	6Φ8(ρ=0.0074) Tie Φ4@100 mm	8.0	5.2
O2	2.3	Medium (Brick Loss at 1st story and Cracks on columns under the 1st Story)	High Strength Epoxy Injection and CFRP application both vertical and diagonal scheme.	4Φ8(ρ=0.0134) Tie Φ4@95 mm	6Φ8(ρ=0.0074) Tie Φ4@100 mm	11.0	6.5

3.3. Materials

3.3.1. Concrete

Concrete mix was prepared in the laboratory in order to produce a low nominal compressive strength concrete (Atmaca 2008). To fulfill this aim, a high water to cement ratio was used. Two types of mix design were used. The mix design values for the specimens O1 and O2 are listed in Table 3.2. In order to determine the compressive and tensile strength of concrete, cylinder samples with a diameter of 150 mm and height of 300 mm were used. Compressive strength of cylinder samples is listed in Table 3.1 for each specimen.

Table 3.2. Concrete mix proportion for specimen O1 and O2

Specimens O1 and O2	
Material	Weight for m^3 (kg/m^3)
Cement, (PKC/B 32.5-R)	270
Water	233
0-3 Sand	450
3-7 Sand (Crushed Sand)	450
7-15 Gravel (Coarse Aggregate)	916
Super plasticizer	0.8

3.3.2. Steel Reinforcement

Plain bars with different nominal diameters were used for the longitudinal reinforcement, stirrups and ties. Longitudinal bars with a diameter of 8 mm were used for beams and columns. The plain wires with a diameter of 4 mm were used as stirrups and ties. Characteristic values for these bars are given in Table 3.3.

Table 3.3. Properties of reinforcements

Diameter	Category	f_{yk} (MPa)	E_s (MPa)	f_u (MPa)	ε_y
ϕ8	Longitudinal Steel	347	195000	448	0.0018
ϕ4	Stirrup, Tie	241	198600	423	0.0012

As mentioned before, plain bars of 8 mm diameter were used as longitudinal reinforcement for beams and columns. In columns there were the lap splices with a length of approximately 16 cm at floor levels. Moreover, there was no any transverse reinforcement at the joints. Plain bars used for beams had hooks of 135^0. Plain wires of 4 mm diameter were used as ties and stirrups. Transverse reinforcement had 90^0 hook ends. The arrangement of longitudinal and transverse steel was the same for all the specimens. The details of reinforcement were drawn and illustrated in Figures 3.1 and 3.2.

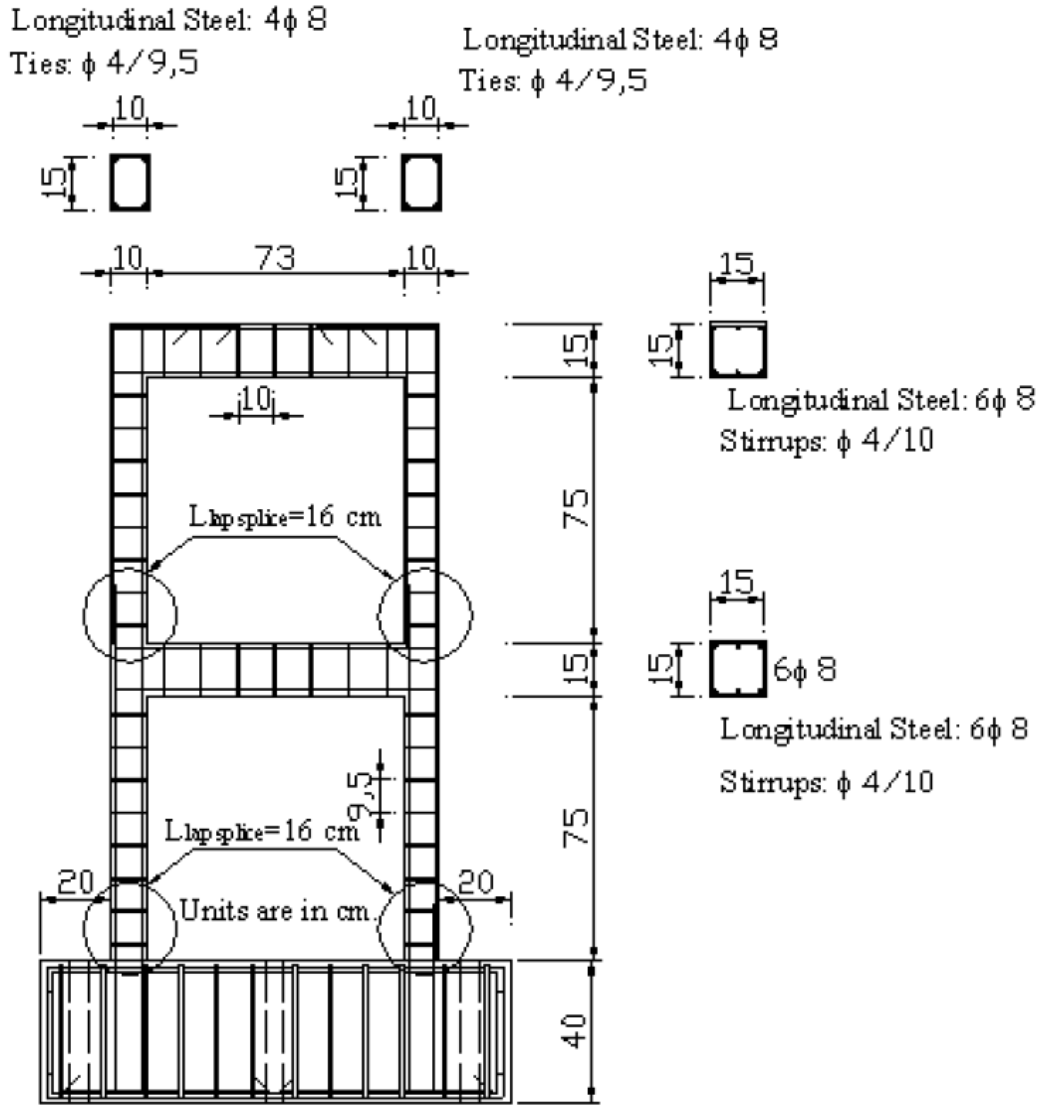

Figure 3.1. Reinforcement details of specimen O1

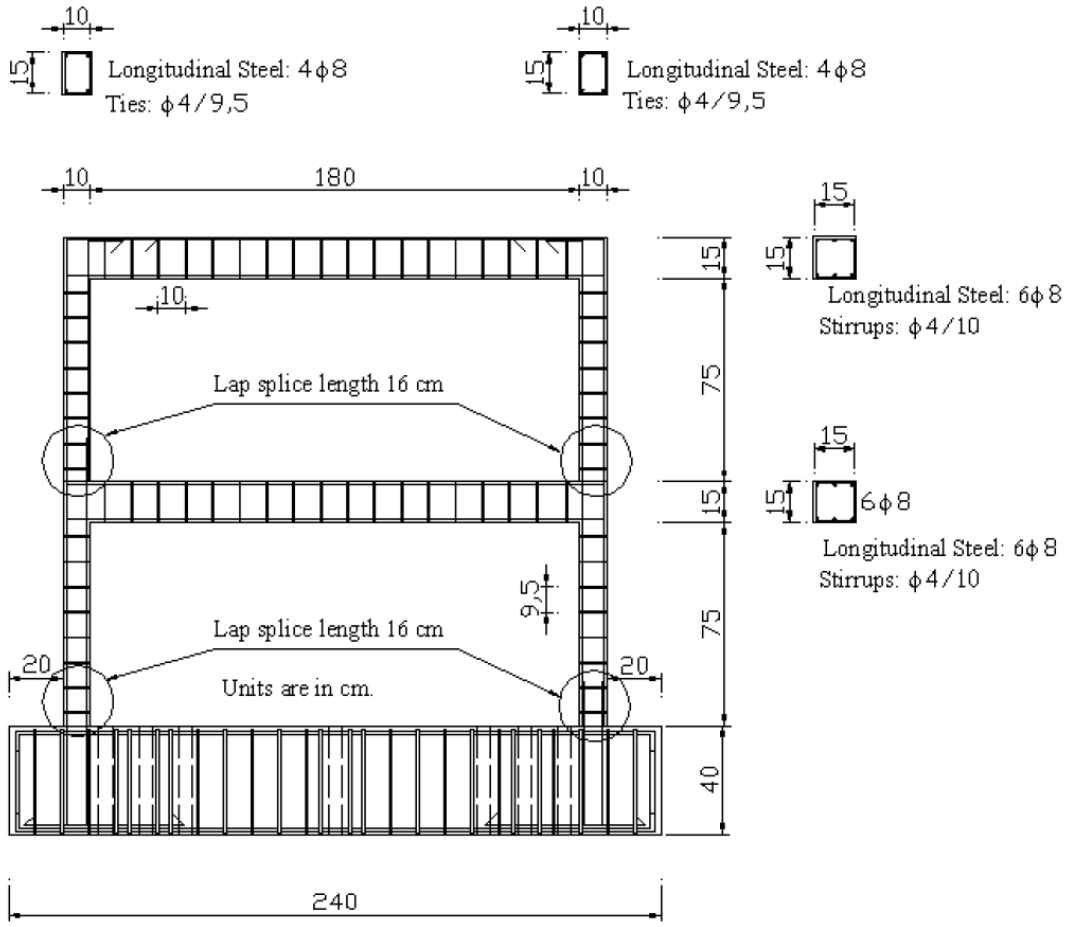

Figure 3.2. Reinforcement details of specimen O2

3.3.3. Infill Plaster and Brick Mortar

The same mix design was used for both mortar and the plaster. The plaster thickness was approximately 10 mm while the thickness of mortar between bricks was approximately 3 mm. The mix design is given in Table 3.6. In order to determine the compressive strength of mortar, 50 mm*50 mm *50 mm cube specimens were prepared and tested. Nominal compressive strength of mortar cubes are listed in Table 3.1 for each specimen. In order to repair the damaged frames' plaster, new mixture prepared with same mix proportion. It was essential to reach the same compressive strength value with the one Atmaca prepared before his test. After the repair the cube specimens were tested and it was observed that the compressive strength of new repairing mortar was 6.2 MPa, which was very close the original one.

Table 3.4. Mix ratio of mortar and plaster

Material	Ratio in the mix (by Weight,%)
0-3 Sand	60
Lime	11
Cement	11
Water	18

3.3.4. Infill Masonry

Hollow-clay tile was used as the infill material. Tiles used in specimens were specially produced for this experimental research and were scaled down to simulate the real tile. Dimensions of the hollow clay tiles are given in Figure. 3.1. In all specimens both faces of the wall were plastered. In order to determine the shear and compressive strength of the infilling material quadlet and triplet tests were performed respectively (Atmaca 2008).

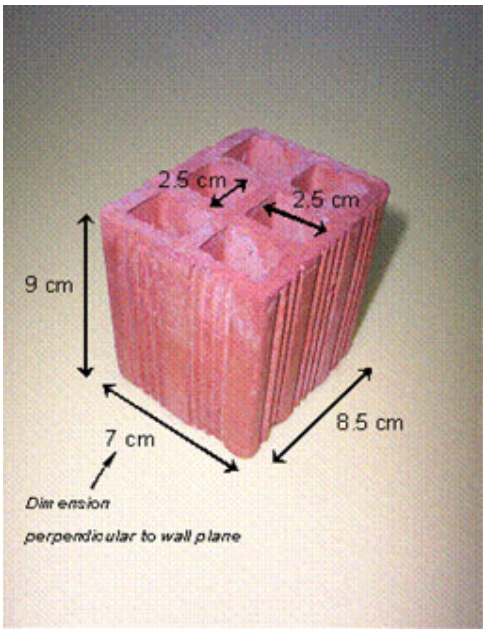

Figure 3.3. Dimensions of the hollow clay tile

3.3.5. Carbon Fiber Reinforced Polymer

Recent developments in the fields of fiber reinforced polymers and composites have resulted in the development of new materials with excellent potentials for retrofitting of concrete and masonry structures in areas where conventional materials have failed to provide satisfactory performance and service life.

It is obvious that in civil engineering the use of fiber reinforced polymer (FRP) composites has grown very rapidly in recent years. Appealing characteristics of fiber reinforcement are small thickness, high strength-to-weight ratio, high modulus of elasticity, and the ease of application. The use of FRP materials offers important advantages in addition to their mechanical characteristics and ease of installation. To name some, the disturbance of the occupants of the facility is minimized and there is minimal loss of usable space during strengthening. Low fire resistance, weakness for ultraviolet light and some chemicals are among the disadvantages. In civil engineering structures, FRP has large application areas such as bridges, buildings (beams, columns, and masonry), bridge decks etc. In this dissertation CFRP which has unidirectional fibers was used. Since it is anisotropic, orientation of fibers where they are used is very important to get the highest advantage.

Since FRP composites have not existed long, the civil engineering community is newly beginning to explore these materials as an economical and effective alternative to steel and reinforced concrete. As used in civil engineering applications, the most common FRP composites have been E-glass, carbon, and/or aramid fiber reinforcement in a polyester, vinyl ester, or epoxy matrix.

Strengthening of the back and front face of the specimens as well as the anchorage dowels were done with a continuous CFRP fabric overlay commercially available by the name of SikaWrap Hex®-230C and a epoxy based impregnating resin which is used as a seal coat during application is Sikadur®-330. Mechanical properties of the carbon fiber fabric and the epoxy resin, as supplied by the manufacturer, are given in Table 3.5 and Table 3.6 respectively.

Table 3.5. Technical data for epoxy based impregnating resin

Sikadur-330 Impregnating Resin	
APPEARANCE	Comp. A: white Comp. B: grey
DENSITY	1.31 kg/l (mixed)
MIXING RATIO	A:B = 4:1 by weight
POT LIFE	15˚C : 90 min (5 kg) 35˚C : 30 min (5 kg)
OPEN TIME	30 min (at + 35˚C)
VISCOSITY	Plasty, not flowable
APPLICATION TEMPERATURE	+15˚C to + 35˚C (ambient and substrate)
ADHESIVE TENSILE STRENGTH ON CONCRETE (EN 24624)	Concrete failure after 1 day (cured at > 15˚C on sandblasted substrate)
TENSILE STRENGTH (DIN 53455)	30 N/mm^2 (cured at 7 days at +23˚C)
FLEXURAL E-MODULUS (DIN 53452)	3,800 N/mm^2 (cured 7 days at +23˚C)
HEAT DEFLECTION TEMPERATURE (Astm D 648)	Cured : 7 days, 15˚C : 41˚C 7 days, 23˚C : 47˚C 7 days, 35˚C : 53˚C
SHELF LIFE	18 months from manufacturing date in original packing stored at temperatures from +5˚ to 25˚C
PACKAGING	Pre dosed units (A + B) at 5 kg

Table 3.6. Technical data for carbon fiber reinforced polymer

SIKAWRAP HEX-230 C WOVEN CARBON FIBER FIBRIC FOR STRUCTURAL STRENGTHENING	
DESCRIPTION	A unidirectional woven carbon fiber fabric for the dry application process
TYPE	Mid strength carbon fibers
CONSTRUCTION	Fiber orientation:0^0 (unidirectional) Warp: black carbon fibers (99% of total areal weight) Weft: white thermoplastic heat-set fibers
FABRIC WIDTH;LENGTH/ROLL	300/600 mm ≥50 m
STORAGE	24 months from date of production if stored properly
AREAL WEIGHT	225 gr/m2
DESIGN THICKNESS	0.13 mm (based on fiber content)
TENSILE STRENGTH	3500 MPa (nominal)
TENSILE E-MODULUS	230000 MPa (nominal)
ELONGATION AT BREAK	1.5% (nominal)

3.3.6. Epoxy Based Crack Repairing and Injection Mortar

Test specimens O1 and O2 had both different types of cracks and concrete damages especially on columns at 1st story. In order to eliminate the lack of strength and to reach the original load carrying capacity of columns, epoxy based repairing mortar and injection technique were used.

For this repairing and injection works, 2 types of material were used, commercially available by the name Sikadur® 31 and Sikadur® 52. Both of them are epoxy based 2 component resin that used together for the repairing of cracks between 0.5mm and 5mm. Out of this crack range, only Sikadur® 31 were used as a high strength repair mortar. It has an ease of application because, it is a thixotropic material which can be used at vertical and overhead application. It hardens without shrinkage and has very good adhesion to most construction material. Most important feature is to have high initial and ultimate stress with a short time. Main disadvantage is that, this material can only be applied to the pure concrete or cement surface, which forced us to remove all the paint and gypsum on the mortar. Technical data and mechanical properties are listed in Table 3.7.

Sikadur® 52 is another high strength epoxy resin which was used as injection liquid to the cracks. It has very good adhesion to concrete and has very low viscosity. It is shrinkage free while strengthening. This material has very high adhesive and mechanical strength; however brittle behavior cannot be observed. Main advantage of this component is that, it could be used with single component pumps, due to the fact that it has very low viscosity. This high strength injection epoxy resin can only be used for the cracks between 0.5mm and 5 mm. Before the injection application all dust and loose materials should be removed from the cracks. There are two type of Sikadur® 52 considering the climate conditions. Sikadur® 52 Type N, were used for this experiment due to the fact that the temperature never exceed the 30 degree during the application. Technical data and mechanical properties are listed in Table 3.8.

Table 3.7. Technical data for Sikadur 31 repair mortar

Sikadur 31 Epoxy Repair Mortar	
APEARENCE	Comp. A: white Comp. B: dark grey Comp A+B : concrete grey
DENSİTY	1.65 kg/l (mixed at 20 ^{o}C)
MİXİNG RATİO	A:B = 5:1 (by weight)
POT LİFE	120 mins at 10^{o}C 60 mins at 20 ^{o}C 25 mins at 30 ^{o}C
VISCOSITY	Plasty, not flowable
SHELF LIFE	24 month from manufacturing date in orginal packing stored between 5^{o}C and 30^{o}C
PACKAGING	Predosed unit (A+B) at 7.2 kg
APPLICATION TEMPRATURE	10^{o}C to 30^{o}C (Ambient and substrate)
TENSILE STRENGTH	Curing 10 days between 10^{o}C to 20 ^{o}C : 15-20 N/mm^2
COMPRESSIVE STRENGTH	Curing 10 days between 10^{o}C to 20 ^{o}C : 60-70 N/mm^2
FLEXURAL STREGTH	Curing 10 days between 10^{o}C to 20 ^{o}C : 30-40 N/mm^2
BOND STREGTH	Curing 10 days between 10^{o}C to 20 ^{o}C : 4 N/mm^2(concrete), 15 N/mm^2 (steel)
E-MODULUS	4.300 N/mm^2

Table 3.8. Technical data for Sikadur 52 injection resin

Sikadur 52 Epoxy Injection Resin	
APEARENCE	Comp. A: transparent Comp. B: Brownish Comp A+B :Yellowish-Brownish
DENSİTY	1.085 kg/l (mixed at 20 ^{o}C)
MİXİNG RATİO	A:B = 2:1 (by weight)
POT LİFE	80 mins at 10^{o}C 25 mins at 23 ^{o}C 10 mins at 30 ^{o}C
VISCOSITY	1.200 mPA.s at 10 ^{o}C 430 mPa.s at 20 ^{o}C 220 mPa.s at 30 ^{o}C
SHELF LIFE	24 month from manufacturing date in original packing stored between 5^{o}C and 30^{o}C
PACKAGING	Predosed unit (A+B) at 3 kg
APPLICATION TEMPRATURE	5^{o}C to 30^{o}C (Ambient and substrate)
TENSILE STRENGTH	Curing 7 days at 23 ^{o}C : 37 N/mm^{2}
COMPRESSIVE STRENGTH	Curing 7 days at 23 ^{o}C : 52 N/mm^{2}
FLEXURAL STREGTH	Curing 7 days at 23 ^{o}C : 61 N/mm^{2}
BOND STREGTH	Curing 7 days at 23 ^{o}C : 4 N/mm^{2}(concrete)
E-MODULUS	1.800 N/mm^{2}

3.4. Repairing and Rehabilitation of Test Specimens

Test specimens O1 and O2 are both damaged and same repairing methods had been applied. The only difference between the specimens was brick loss at first story of specimen O2. The damage levels are different such that crack formations on columns and plaster loss. In order to start repairing, brick loss had to be recovered. After that, plaster repairs applied and finally high strength epoxy resin were injected into the cracks on the columns which has width between 0.5mm and 5 mm. Following the repairing of the specimens, rehabilitation procedure with CFRP overlays had been applied to them. CFRP strengthening pattern was replica of the one Atmaca (2008) has applied to his specimen SA1.0 CV and SA2.3 CV. By this way our aim was to see the effect of the damage levels and epoxy injection on the specimen and to see whether the damaged specimen could reach the desired strength or not after the repairing and rehabilitation techniques. First and second floor view of test specimens are shown at Fig. 3.4 and Fig.3.5

Figure 3.4. First floor of test specimens

Figure 3.5. Second floor of test specimens

3.4.1. Brick and Plaster Repairs

As it was seen from the Fig.3.4, brick loss was appeared at only test specimen O2 with an aspect ration 2.3. For the specimen O1, only plaster repairs had been applied for the backside. Two different repairing options for the brick repair had been examined. One of them was to demolish all first floor brick and rebuilt it. The other one was only repairing and filling the missing parts. The second way of repair had been chosen due to the fact that, repairing philosophy had to be feasible and realistic. Also, there was a problem if we would choose the way to demolish such that, the plaster and mortar strength and condition might change compared with the results of Atmaca's specimen.

Before starting the repair, the mortar had been prepared according the values at Table 3.4. The concrete surfaces facing the bricks were roughened with the help of a chisel in order to increase the adherence between the brick mortar and concrete. This application can be seen at Figure 3.6. Following these works, bricks were installed and cement based plaster applied to the missing surfaces with 1 cm thickness. Only specimen O2 was needed brick and plaster repair as shown at Figure 3.7. Specimen O1 had lack of plaster at backside only as it is seen at Figure. 3.8

Figure 3.6. Roughing of concrete surface

Figure 3.7. Brick and plaster repairs for specimen O2

Figure 3.8. Plaster repairs for specimen O1

3.4.2. Crack Repairs and Epoxy Injection

Second phase of the repairing works was the filling of the cracks on the column and beams. After the tests of Atmaca(2008), it is seen that cracks occurred especially at column beam joints and at the column foundation joints. Width of these cracks was approximately between 2 and 5 mm. Beside that there were lots of micro cracks smaller than the 0.5 mm which high strength epoxy injection method could not be used. However, these surface cracks were repaired with the help of repair mortar Sikadur 31.

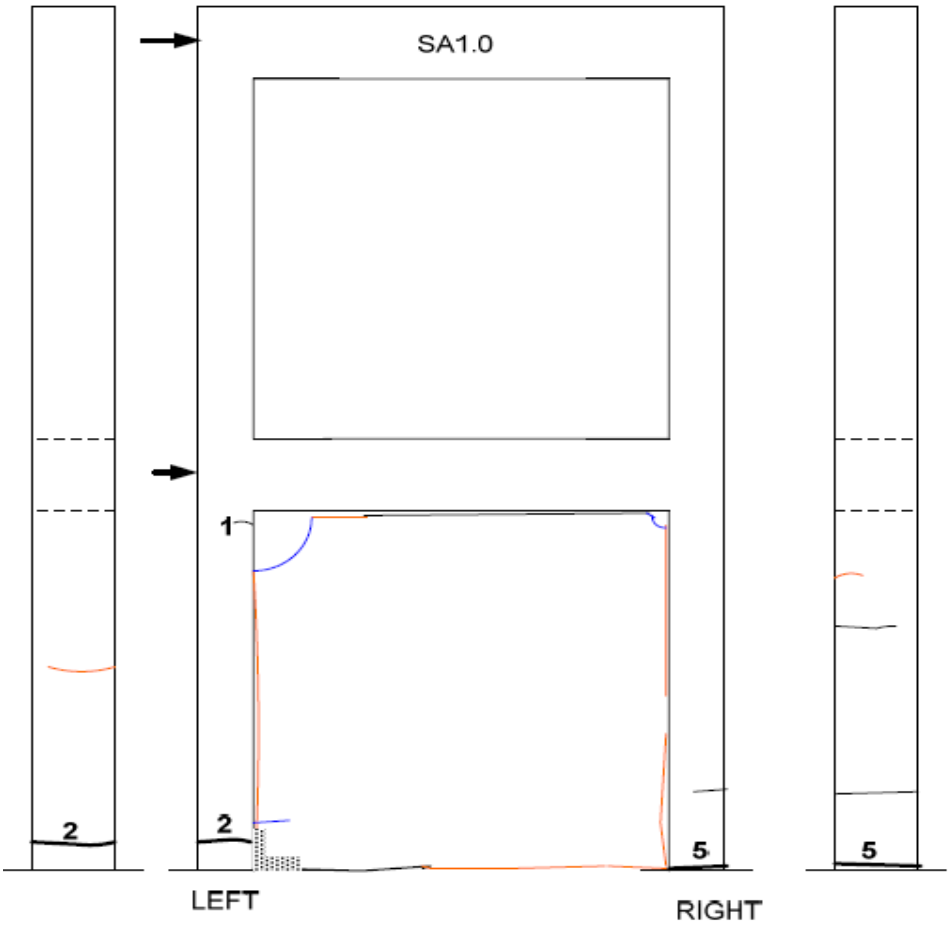

Figure 3.9. Cracks distribution at specimen O1

Firstly, the cracks on the specimen explored and decided that which type of cracks will be filled with epoxy. For the specimen O1, as it is seen from the Fig 3.9, cracks at the foundation level of columns were the main points to apply the epoxy injection. Other cracks on the columns and beams were smaller than 0.5 mm, so that no need for injection but surface repair had been applied to them. Specimen O2 had much more cracks on

columns as illustrated at Fig 3.10. At this specimen critical cracks wider than 0.5 mm had been occurred at the first story column beam joints and foundation level of column. These 4 critical points were injected by high strength epoxy resin.

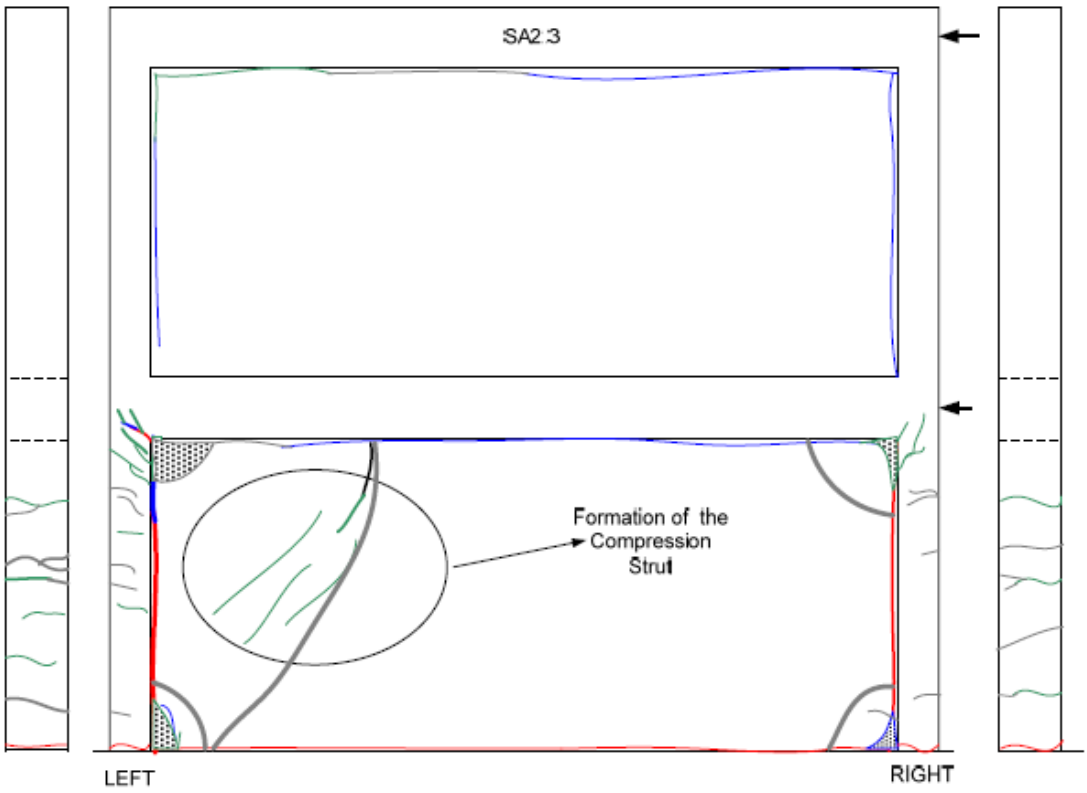

Figure 3.10. Cracks distribution at specimen O2

Before starting the epoxy injection the paint on the columns had to be removed in order to increase repair mortar adhesion to the concrete surface. All of the specimens were painted by Atmaca in order to observe the cracks during the test. Before the application all of the paints were removed with the help of mechanical sandpaper. After clearing the dust and any loose particles, the injection dowels were placed and fixed with high strength epoxy based repair mortar Sikadur 31. After placement of the injection dowels, outer face of the cracks all around the dowel were filled with Sikadur 31. Sikadur 31 would help us to seal the injected epoxy resin during the application. By this way, the injected epoxy inside the cracks would spread into the smaller cracks. The Sikadur 31 application were shown at Fig 3.11 and 3.12

Figure 3.11. Placement of injection dowel

Figure 3.12. Finished application of Sikadur 31 and injection dowel

After a curing time of 24 hours, the repair mortars around the injecting zone reached the desired strength value. The curing time depends on the weather condition. First of all, the high strength epoxy resin prepared carefully with the guidance of professional Sika worker. Then, we choose to use hand pump instead of mechanical one due to the fact that, our cracks were not so wide and long enough to use it. After filling the hand pump with Sikadur 52, injection through the injection dowels were started. Pumping had to be stopped until the low viscosity epoxy resin flow throughout a different capillary space in the concrete. As it is seen from Figure 3.13, 3.14, 3.15 and 3.16, both specimen O1 and O2 subjected to the injection especially on columns. After the injection the non-viscous epoxy filled the crack and flow out from another weak zone of the concrete. This meant that cracks were fully filled and the excessive amount of epoxy flowing out.

Figure 3.13. Pumping the epoxy resin for specimen O2

Figure 3.14. The flow-out of epoxy resin after injection for Specimen O2

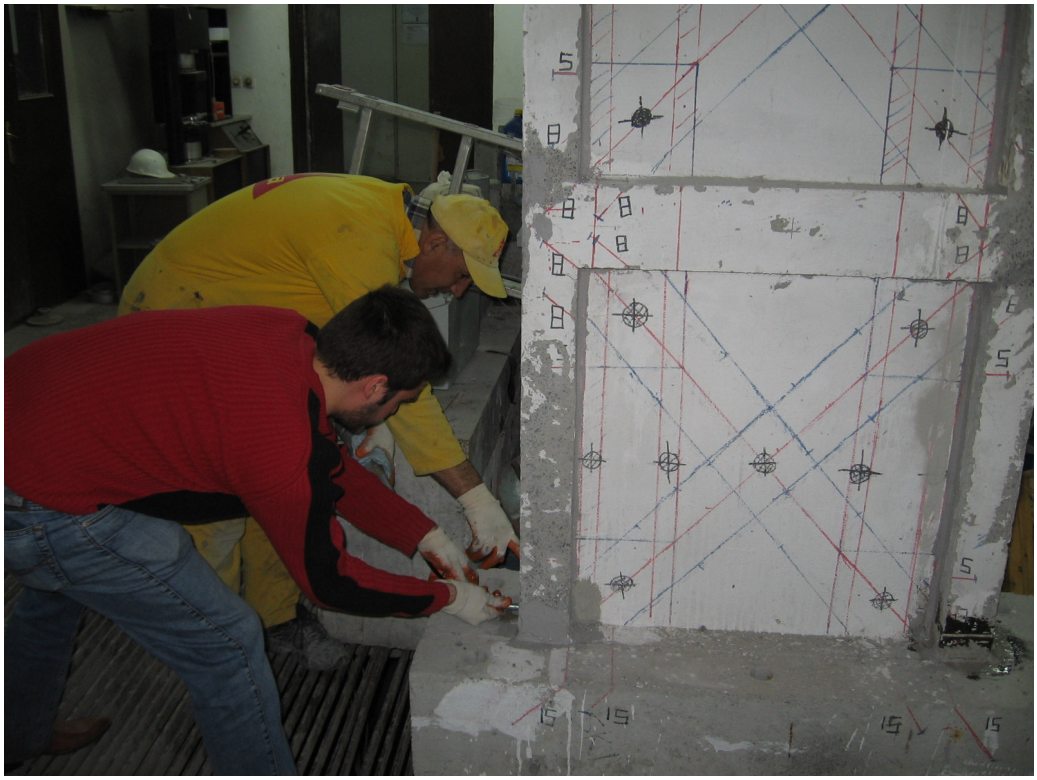

Figure 3.15. Pumping the epoxy resin for specimen O1

Figure 3.16. The flow-out of epoxy resin after injection for specimen O1

3.4.3. CFRP Application

Strengthening was achieved by applying CFRP. Depending on the aspect ratio and previous test results, different strengthening schemes were used. The procedure can be summarized as follows. The places of the anchor holes were determined and drilled into predefined depths. The holes were cleaned by using an air compressor to remove any dust or loose materials. This was done to eliminate any inconvenience for the bond between concrete surface and epoxy impregnated CFRP anchors. As any surface eccentricity could cause early failure of CFRP, any roughness on the surface of the specimens was smoothed by sandpaper. All CFRP were cut in previously determined dimensions prior to application. All strengthened specimens had flag fabrics on the corners and cross diagonal overlays. Some specimens had flags at the mid-span of the beams as well. In some applications, columns were beveled with a radius of about 20 mm. The differences considering CFRP details were illustrated while the strengthening scheme was explained.

Figure 3.17. The preparation of the two-component epoxy impregnation resin

During the strengthening process Sikadur 330, a two component epoxy based impregnating resin, was first applied to the substrate by using a brush and a roller. Before the application of the epoxy resin, dew point, substrate, ambient temperature, and moisture content were checked. The preparation of the two-component epoxy impregnation resin was done by using a mixing spindle attached to a slow speed electric drill as illustrated in Figure 3.17. The mix was stirred at slow speed three or four minutes conforming to the manufacturer's recommendations. Depending on the ambient temperature and application speed, the mix amount was determined because pot life of the mixture started as soon as the components mixed together and it was directly a function of ambient temperature. In the strengthening procedure, corner flag fabrics were stacked preceding the placement of cross diagonals or other overlays (vertical strips, wrapping of columns etc.). Since the fabric was unidirectional, two layers of flags were used horizontally and vertically respectively as shown in Figure 3.18. As soon as CFRP was placed on the wall, a special plastic impregnating roller was used parallel to the fiber direction so that the epoxy resin was evenly distributed over the whole fabric surface and the fabric was not folded. Before the application of second layer of the flag fabric which was parallel to the column axis, the two component epoxy impregnation resin was applied on the previous fabric.

Then cross diagonal overlays were stack on the infill wall at both faces. Excessive amount of the fabric on the corners was cut with a special scissors to fit the corner geometry and to facilitate the anchor application. Application of vertical strips was illustrated in Figure 3.18. Anchor application started following the application of cross diagonals and vertical strips. The holes were filled with the two-component epoxy impregnation resin and the anchors were impregnated with the two-component impregnation resin prior to putting the anchors into the holes. The specimens were left to cure for about 7 days following to the CFRP placement.

Figure 3.18. Vertical and cross FRP application specimen O1

Figure 3.19. Anchorage application for specimen O2

Figure 3.20. Backside of specimen O1

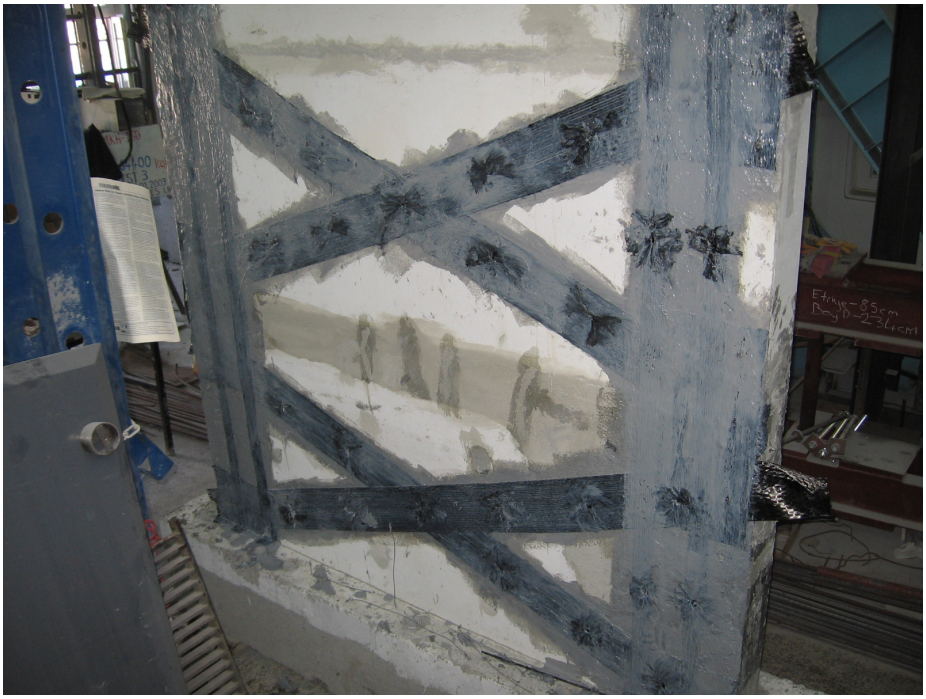

Figure 3.21. Backside of specimen O2

Figure 3.22. Filling the anchorage holes with epoxy resin

Dimensions of the anchors and strips were illustrated in Table 3.9. In order to determine the CFRP anchor widths, it was assumed that 30 to 40% of the anchorage capacity was effectively used. The anchor depth, hole diameter, concrete quality, workmanship, eccentricity on the applied load influenced the performance of the anchors. The detailed information can be observed at Figure 3.23. Since the anchor depths were kept constant, CFRP anchor widths were a function of CFRP strip widths.

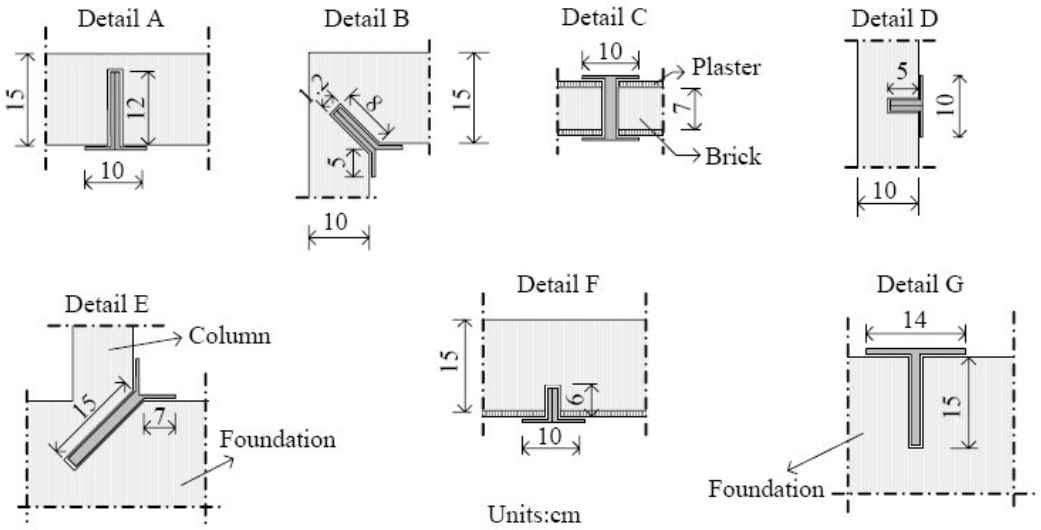

Figure 3.23. Details of CFRP anchor fabrics

Table 3.9. Dimensions of CFRP anchor fabrics

		HOLE	CFRP ANCHOR	
Specimen	Anchor Detail	Depth (mm)	Width (mm)	Length (mm)
O1 and O2	A	120	80	340
	B	80	80	260
	C	90	80	190
	D	50	80	200
	E	150	80	440
	F	60	80	220
	G	150	80	440

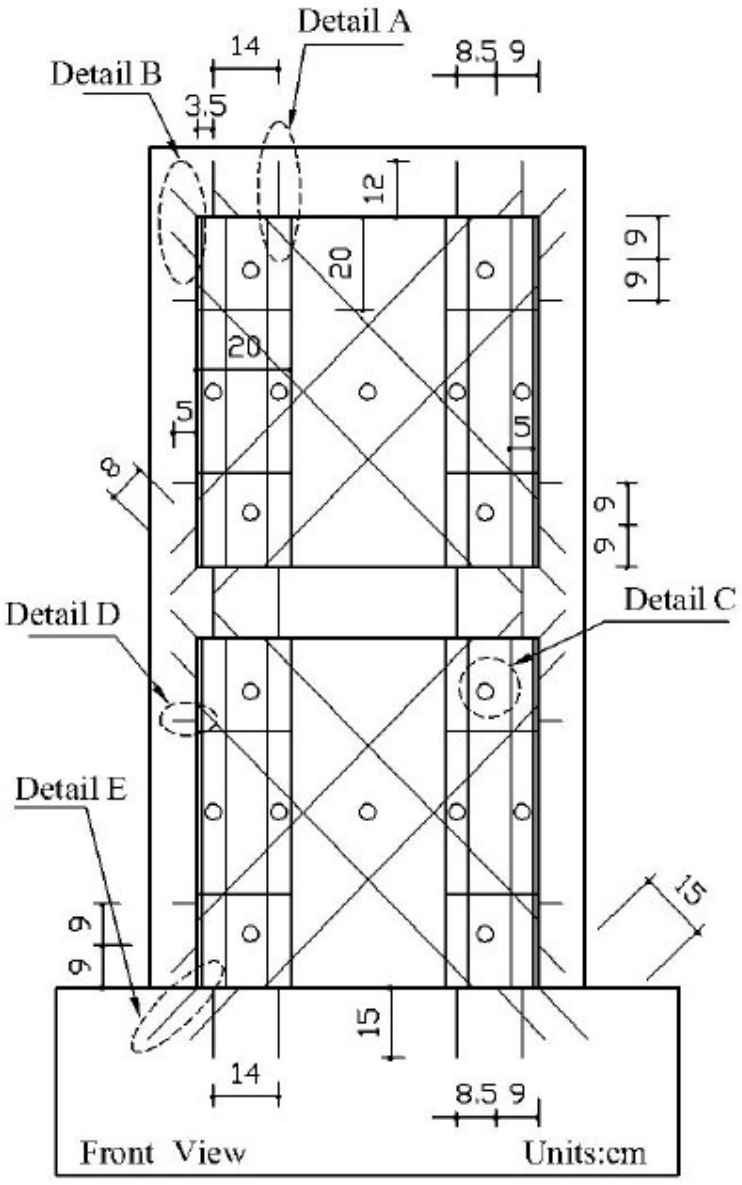

Figure 3.24. Front view of strengthening details of specimen O1

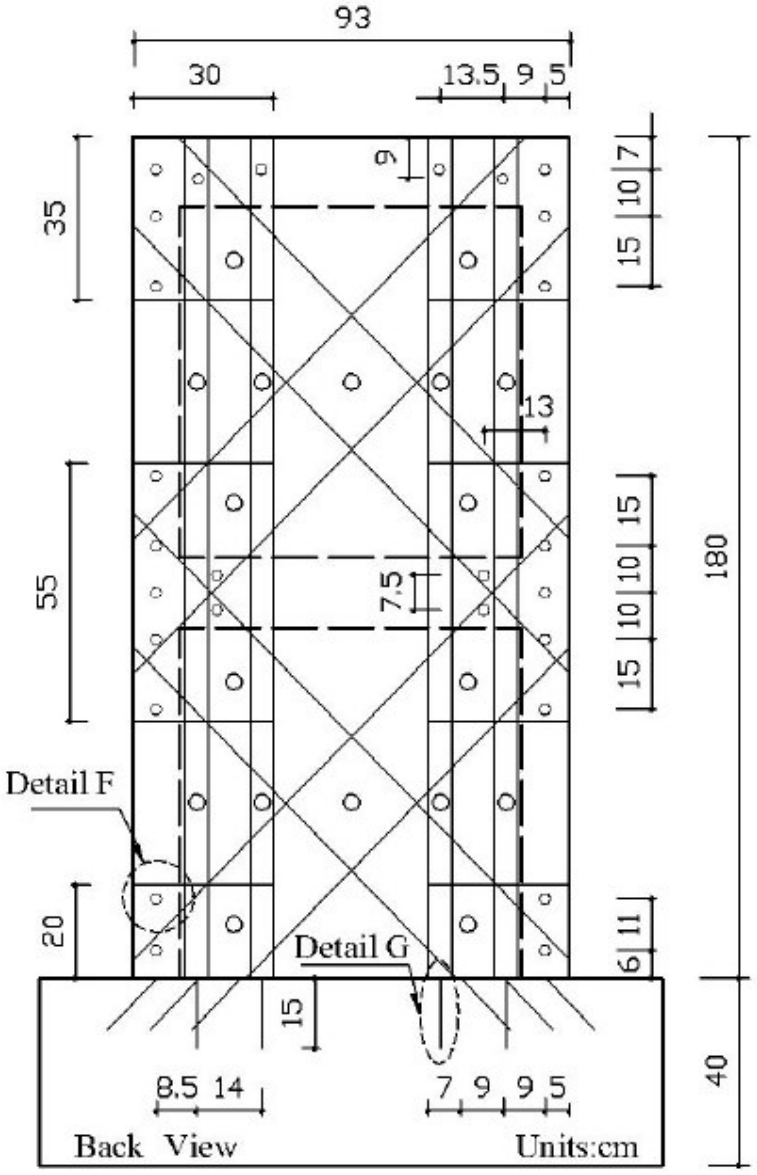

Figure 3.25. Back view of strengthening details of specimen O1

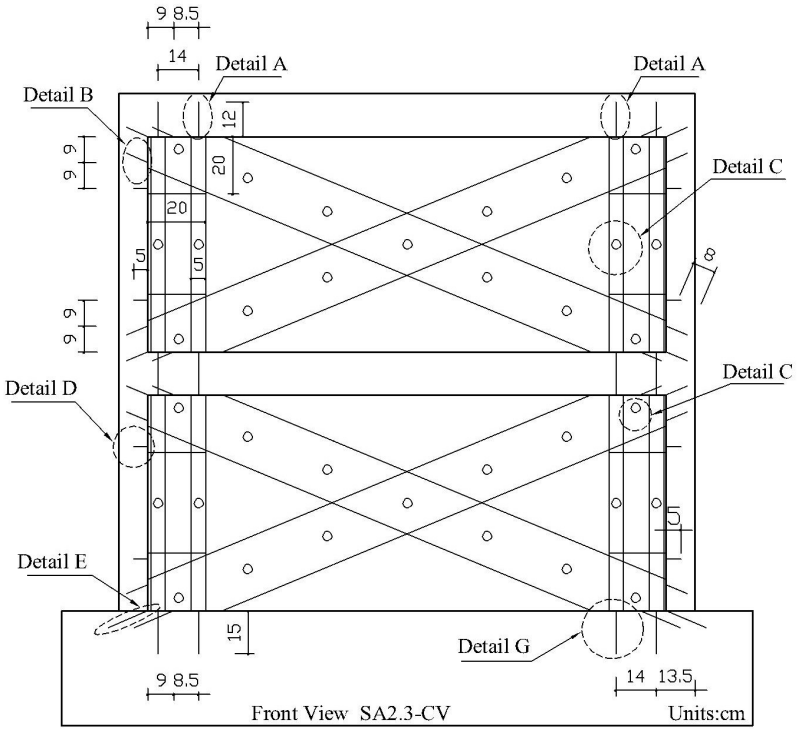

Figure 3.26. Front view of strengthening details of specimen O2

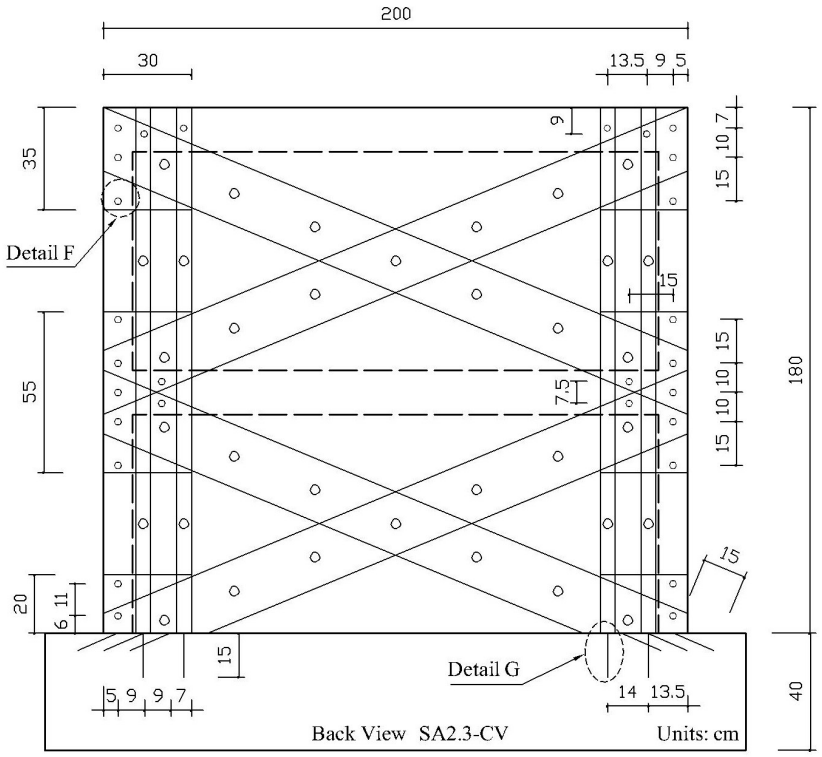

Figure 3.27. Back view of strengthening details of specimen O2

3.5. Test Setup and Instrumentation

The test specimens were attached to the strong floor and loaded until failure. Horizontal and vertical loadings were independently applied throughout the test. Test set up consisted of an auxiliary foundation used to fix the specimen into the strong floor, a steel reaction wall to apply the cyclic horizontal loading, a hydraulic ram and a pumping equipment to apply the vertical load, a 250 kN displacement controlled hydraulic actuator attached to the reaction wall, horizontal and vertical steel spreader beams, restrainers to prevent out of plane deformation of the specimen and a data acquisition system. Each cured specimen was carried into the test rig and prepared for the test. Test set-up is shown in Figure 3.28. The horizontal load was applied by using the 250 kN dynamic actuator which was mounted to the steel reaction wall. One third of the horizontal load was given to the first story and two thirds of the horizontal load was given to the second story by using the horizontal steel spreader beam. Eight steel rods fixed four thick plates on the beam levels to apply the horizontal load. A 40 ton capacity hydraulic ram was placed between two horizontal steel spreader beams over the specimen. One of these spreader beams was placed in the plane of the specimen. The other horizontal spreader beam was located on the top of the hydraulic ram and fixed to the hinge support by using four steel bars. The hinge supports were placed on the auxiliary foundation.

Axial load was applied on the columns by using the manually controlled hydraulic ram and steel bars and kept constant throughout the test. Vertical load was applied prior to test. Application systems of the horizontal and vertical loads were independent. The load obtained by dynamic actuator was not directly used in the calculations. The effect of the axial load on the horizontal force was also calculated and the corrected horizontal load was used in the calculations. To calculate the corrected horizontal load, it was assumed that horizontal load was always horizontal and vertical load had Cartesian components due to horizontal deflection. In other words the horizontal component of the vertical load decreased the effect of the load obtained by the actuator. The corrected horizontal load was calculated in accordance with the Equation 3.1. The variables were shown in Figure 3.25.

$$H_{corrected} = P_{actuator} - N_{vertical} \times \sin(\arctan(\frac{\Delta}{h})) \quad (3.1)$$

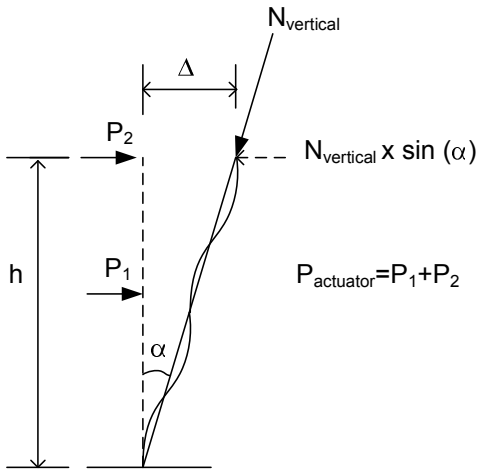

Figure 3.29. Calculation of corrected load

$P_{actuator}$: Total base shear

$N_{vertical}$: Total applied vertical load

H : Height from the hinge support to the top of the specimen

$H_{corrected}$: Corrected base shear

In order to eliminate possible out of plane deformations a steel frame was constructed and steel restrainers were attached to this steel frame. Small steel spherical balls were placed to the ends of these steel restrainers to prevent any frictional forces to develop between the specimen and the steel frame. A total of four restrainers were used at the second story beam level to prevent or limit twisting of the specimen. Installation of loading system preceded the placing of measuring devices (Linear Variable Differential Transducers, dial gages and strain gages). The location of LVDTs and dial gages are schematically given in Figure 3.30.

In order to measure horizontal displacements (drifts) at the first and second story levels 4 LVDTs, two of which were on the second floor level, were mounted on the specimen (1, 2, 3, 4 in Figure 3.30). The measurement frame was mounted on the

foundation of the specimen. Thus all measurements were relative to the foundation of the specimen. Two dial gages were located on the lower part of the left and right columns so that they measured horizontal slip just above the foundation level (6, 8 in Figure 3.30). Two dial gages were located on the bottom outer face of the columns to measure rotation or base rocking of the overall specimens (5, 7 in Figure 3.30). Two dial gages were mounted on the specimen to determine potential out of plane deformations (9, 10 in Figure 3.30). Four dial gages, two of which were in the second story infill panel, were used to measure the shear deformations on the infill panel (11, 12, 13, 14 in Figure 3.30). Specimens with an aspect ratio of 2.3 had two extra dial gages on the infill panel to better understand shear deformations.

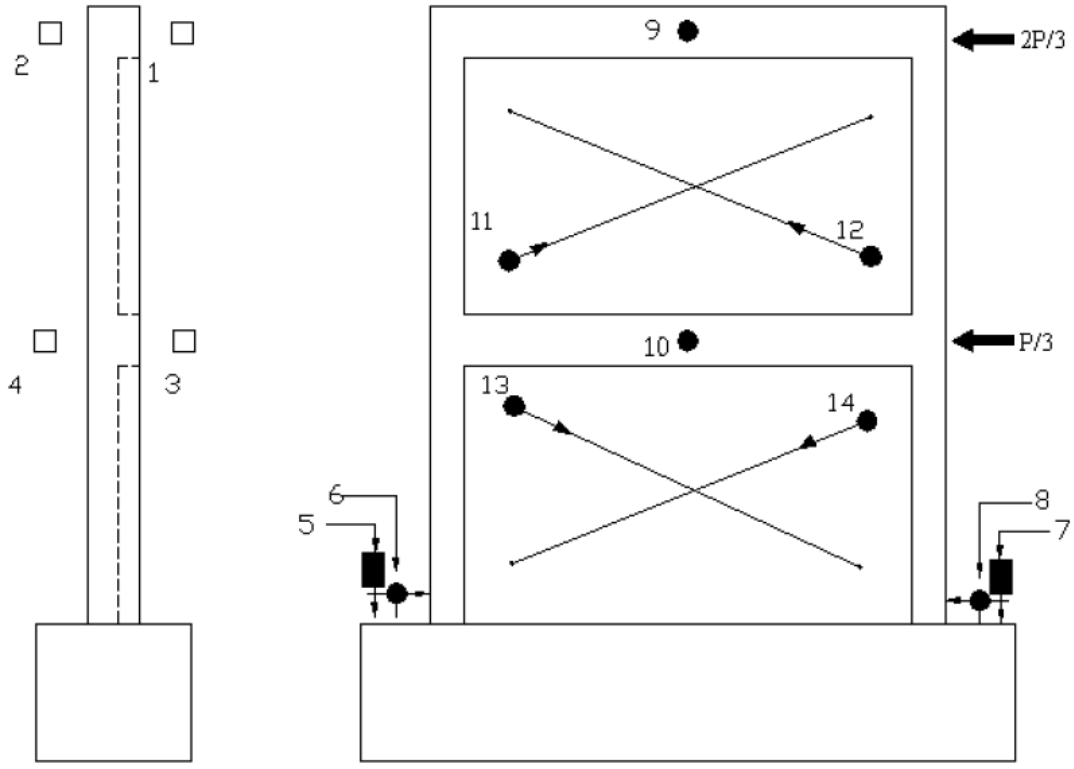

Figure 3.30. Schematical view of LVDTs and dial gages

First the load transfer mechanism was placed, then the instrumentation was mounted on the specimens to the predetermined points, and finally the data acquisition system was connected to the instruments. The data acquisition system included a TML 602 data logger and actuator control panel. All values of the LVDTs, dial gages and strain gages were recorded in this data logger until the test was terminated. During the test, the cracks were marked on the specimen and observations were recorded at each drift level. The specimens were tested in an upright position whereas they were cast in horizontal position.

Loading history was very important for the behavior especially in the nonlinear range. Although it was intended to use the same loading history to do better comparison, it was not possible due to nature of the specimens. In other words failure types of the specimens affected loading history significantly. While flexure dominant systems such as specimens with an aspect ratio of 1.0 can undergo displacement controlled type of loading, shear dominant systems must experience load controlled type of loading in the initial cycles. Load controlled type of loading was followed by displacement controlled type of loading for the specimen with aspect ratio 2.3. Loading histories are given in the following chapter for each specimen. Previous test results done in Bogazici University [Atmaca 2008] were used to find an appropriate loading pattern to be used for displacement controlled phase of the loading. The loading pattern was determined considering the following points:

- The initial drift ratio should be within the linear elastic range,
- The ratio between two consecutive drift amplitudes should be in the range of 1.25 and 1.50
- Three full reversed cycles should be applied at each displacement amplitude.

When load controlled type of loading was used, it was intended to avoid softening caused by loading repetitions. That's why previously determined displacement amplitudes and drift ratios were checked at each drift ratio and the decision was made to shift from load controlled type of loading to the displacement controlled type of loading. Loading increments were approximately 5 kN. The test was halted when the specimens experienced a significant change in ultimate load.

4. TEST RESULTS

4.1. General

In this chapter the reversed cyclic lateral load behavior of the specimens during experiments is presented below by giving the crack patterns, loading history and base shear versus specimen drift graphs for each specimen. The load-deformation behavior of specimens was continuously monitored using the data acquisition system. The specimens were visually inspected at each consecutive loading cycle and cracks were marked and measured on each face of the specimens. While presenting the behavior of the specimens the terms left, right, 1st story, 2nd story lower panel and upper panel are used. For instance, the term right column refers to the member nearest to the actuator, while the term left column or joint on the left side refers to the further side of the frame from the actuator.

Photographs showing the final stage damage level are also given. Load versus drift values in the relevant tables consist of the values attained at the third cycle of each loading step, while the discussions on specimen response are made based on the first cycle values of each loading step. Due to the fact that specimens were damaged and repaired, the initial behavior of them was important in order to compare and evaluate the results. The failure mode and the behavior of undamaged specimens were taken from the test results of the Atmaca 2008.

Before explaining the behavior of these specimens, expected failure modes must be given considering the comparison between damaged and undamaged specimen. The effectiveness of the epoxy injection and CFRP repairing methods were exhibited after the test results. The expected failure modes for the undamaged specimens were reported by Atmaca 2008, such that, if the aspect ratio of the specimen is decreased rocking type of behavior started to govern the behavior as seen in specimen O1. When the aspect ratio increased, specimen behavior changed from a flexure dominant rocking response into a shear dominant one and formation of compression struts became more conspicuous as in the case of specimen O2. Sometimes this rocking action occurred in the strengthened specimens above the foundation level due to the configuration of CFRP cross diagonals. When the specimen started to rock, contact surface started to decrease and this incident

triggered the sliding, and a contact surface sliding type of failure developed. Sliding occurred at the plane where moments of cross diagonals' vertical components were at minimum. This generally coincided with the mid-height of the strengthened specimens. Vertical strips around columns helped to transfer the load from FRP to longitudinal bars at the lap splice region. This occurrence increased the advantages or benefits of the strengthening due to positive effects of continuity. Another failure mode was governed by the anchorage length of FRP anchors into the foundation beam.

If the embedment length of the FRP anchors was not sufficient to develop tensile strength of FRP or debonding initiated before developing tensile strength, pull-out type of failures were observed. The slope of cross diagonals changed as the aspect ratio increased. This affected shear force and normal force interaction of the cross diagonal FRPs and changed the specimens' failure modes. According to these type of expected behaviors, the two damaged specimen were tested under same circumstances comparing the test result and failure modes.

4.2. Specimen O1

The first specimen for the experiment was the specimen O1 which had a low degree damages and an aspect ratio 1.0. This specimen was the control specimen of the Atmaca's experiment and it was tested and damaged until the failure without strengthening. With same conditions, undamaged strengthened one with CFRP was tested, too. In this experiment repaired and rehabilitated specimen O1 tested by applying displacement controlled type of loading for all cycles. The loading drift and cycles were showed at Figure 4.1. The axial load of for each columns were applied as 15 kN (N/N_0=0.11) throughout the test. The base shear versus roof drift graph for the specimen O1 were given in Figure 4.2.

The first visible crack on specimen O1 was observed in cycle 6. This flexural crack with a length of 6 cm was on the both left and right column outer face and located 15 cm away from the foundation level. Maximum applied load for the forward half cycle was about 26.1 kN (0.05% drift). Maximum applied load and corresponding drift for the backward half cycle was about -24.75 kN and -0.049% respectively.

In cycle 7, new cracks formed on the first floor joints both at right and left column. These cracks formed at the same time with a length of 10 cm and on the direction of diagonal CFRP. Maximum applied loads and corresponding drifts for the forward and backward cycles were 27.6 kN (0.10% drift) and -26.3 kN (-0.097% drift) respectively. After the cracks occurred at the first floor joints, the flexural cracks at the foundation did not progress anymore. Moreover, horizontal cracks at different elevations on the left column and right column were formed.

In cycle 9, maximum applied push load for the forward half cycle and corresponding drift were about 43.1 kN (0.19% drift) and 41.2 kN (-0.18% drift) respectively. Some of the previous cracks extended while vertical and diagonal cracks between cross diagonals occurred on the brick infill at first story. New horizontal cracks at the right column and left column were occurred 20 cm away from foundation. Plaster removal started at the backside also at the first story left column and infilled layer

In cycle 12, maximum applied load and corresponding drift for the forward half cycle were 55.2 kN and 0.36% respectively. Horizontal cracks at various elevations between vertical and diagonal strips appeared. Previously formed cracks, 20 cm and 15 cm away from the foundation level on the left column, extended throughout the column front face. Diagonal crack at the first floor joints increased and extended both left and right columns. Observations showed that tensile strength of RC columns was started to be exceeded and horizontal cracks encircled the columns. In addition a new shear crack with a length of 25 cm was observed on the back of the specimen at the 1^{st} story beam level.

In cycle 14, maximum recorded load and corresponding drift for the forward half cycle were 60.1 kN and 0.60% respectively. Separation between plaster and left column back face and brick loss between the X diagonals at the midpoint of first story were observed. Most important behavior was the debonding occurred at one leg of diagonal FRP on both front and back side. Afterwards the cracks occurred on both vertical and diagonal FRP's started to decrease the capacity of FRP and tended to rupture. However, no critical FRP rupture noticed at all 3 consecutive cycles.

In cycle 15, the vertical strips at back side (Figure 4.10) which was on the back of the frame and 13.5 cm away from the outer face of the right column ruptured in the forward half cycle. Afterwards, diagonal strips at the back side of the specimen failed and ruptured consequently due to the failure of both vertical strips. Specimen failed by the rupture of all vertical strips and cross diagonals at the backside .On the other hand; none of the FRP strips on the front side was totally ruptured. Only the one leg of the diagonal strip was buckled and the local cracks occurred on the FRP strips and the lamination epoxy. Vertical strips ruptured just below mid height of the first story. Maximum applied loads and corresponding drifts for forward and backward cycles were 63.1 kN (0.77% drift) and 64.3- kN (-0.72% drift) respectively. After reaching maximum load, the specimen lost its strength suddenly especially in the backward half cycle. Loading type, maximum displacement and corresponding loads for each successive drift level are recapulated in Table 4.1.

The test was terminated at a drift level of 0.018 at the end of the 17th cycle. Figures 4.11 and 4.12 showed the final situation of the specimen. Failure would be attributed to tensile failure of columns, and rupturing of vertical and diagonal FRP at backside under the axial FRP stresses. Due to the tensile failure and FRP failure plastic hinges occurred at the columns on the first story level. Separation between infill and columns around was observed significantly. Masonry infill separated into two main parts due to upper mid-height rocking action of the specimen after rupturing of vertical FRPs as shown in Figure 4.13. On the other hand, formation of horizontal cracks on the infill implied a horizontal movement of the frame. Spalling of unconfined concrete was not observed at the bottom ends of the columns around lap splices. Although the specimen failed with the rupture of vertical FRP strips, the top deformation of the frame was influenced by a sliding shear type of deformation took place at upper midheight of the first story. This resulted in a so- called ductility and anticipated pinching behavior in the hysteretic loops. As a result, compared with the specimen of Atmaca which has not any damage, damaged specimen O1 was approximately same behavior and failure modes with a close lateral load carrying capacity.

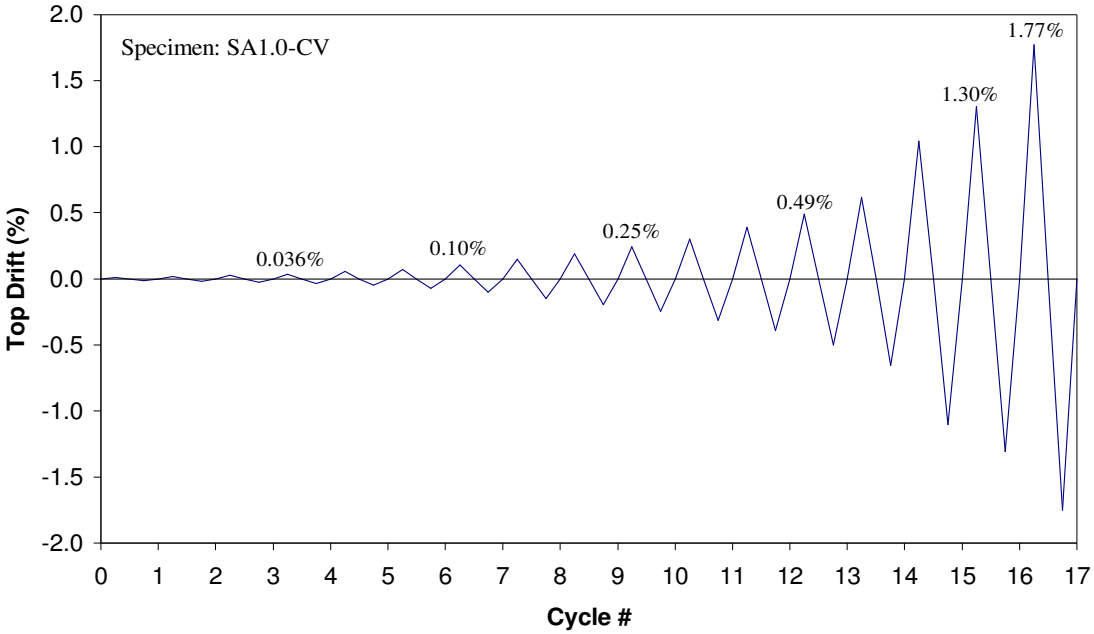

Figure 4.1. Load pattern applied for specimen O1

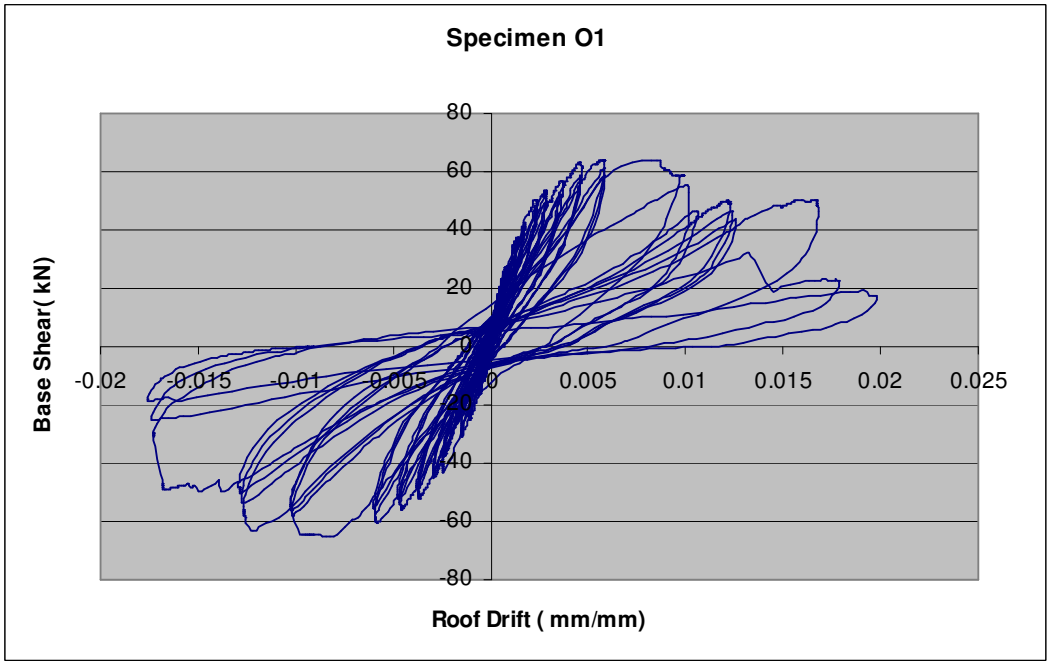

Figure 4.2. Base shear-top drift diagram for specimen O1

Table 4.1. Maximum displacements and corresponding loads for specimen O1

Specimen:O1					
Cycle	Control Type	Maximum Displacement (mm)	Corresponding Load (kN)	Minimum Displacement (mm)	Corresponding Load (kN)
1	DC	0.16	4.34	-0.23	-3.54
2	DC	0.28	9.13	-0.3	-8.79
3	DC	0.43	12.01	-0.42	-13.28
4	DC	0.61	15.39	-0.59	-15.66
5	DC	0.91	17.6	-0.83	-19.88
6	DC	1.2	26.85	-1.21	-25.12
7	DC	1.78	28.6	-1.7	-29.02
8	DC	2.54	36.7	-2.56	-37.65
9	DC	3.26	41.4	-3.33	-42.3
10	DC	4.18	44.7	-4.21	-46.7
11	DC	5.15	50.2	-5.33	-51.23
12	DC	6.64	53.5	-6.64	-55.4
13	DC	8.35	56.85	-8.58	-58.56
14	DC	10.52	60.11	-11.18	-61.65
15	DC	17.75	63.16	-18.78	-64.22
16	DC	22.21	46.56	-22.29	-47.23
17	DC	30.22	20.12	-29.86	-21.54
Note 1: The measurement height was 1705					
Note 2: DC represents displacement controlled type of loading					

Figure 4.3. Rupture of diagonal and vertical FRP for specimen O1

Figure 4.4. Debonding of diagonal FRP for specimen O1

Figure 4.5. Final condition of backside of specimen O1

Figure 4.6. Final condition of frontside of specimen O1

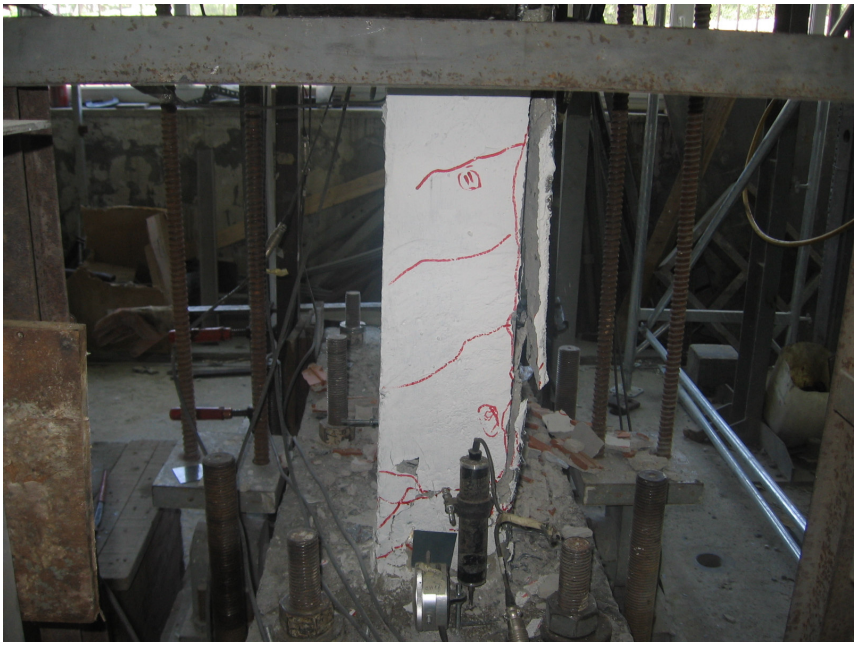

Figure 4.7. Tension cracks on right column of specimen O1

Figure 4.8. Tension cracks on left column of specimen O1

Figure 4.9. Condition of specimen O1 after the test

4.3. Specimen O2

Specimen O2 with an aspect ratio of 2.3 (l/h=2.3) was strengthened with CFRP overlays which were applied in the form of cross diagonals and vertical strips. Load controlled and displacement controlled type of loading were applied to specimen O2 to simulate seismic action. Loading protocol was given in Figure 4.4. Constant axial load of 22 kN (N/N0=0.09) was applied on each column and kept constant throughout the test. Base shear roof drift diagram is shown in Figure 4.3.

Load controlled type of loading was applied in the first cycle. Maximum applied load and corresponding drift for the forward half cycle was 9.20 kN and 0.0000058 respectively. There were no visible cracks in the first nine cycles. At 10^{th} cycle plaster cracks at the backside 1 story beam level .This cycle was the last load controlled cycle.

In cycle 11, displacement controlled cycles began. Maximum applied load and corresponding drift were about 55.8 kN and 0.042% for the forward half cycle. In this cycle the crack between first story panel and the first story beam extended to the length of

97 cm. In cycle 12, some of the previous cracks extended and new cracks formed on the right and left beam-column joint and column outer face. The shear cracks on the joints were about 6 cm in length whereas the flexural cracks were 15 cm and 30cm away from the foundation level. Maximum applied push load and corresponding drift for this cycle was about 66.8 kN and 0.064% respectively.

In cycle 14, maximum applied load and corresponding drift for the forward half cycle were 81.4 kN and 0.19% respectively. The crack located on the right column outer face, 15 cm away from the foundation level, forked out and extended 5 cm toward the front side of columns. Protrusion of plaster was also observed on the back of the specimen on the first story beam level. Previous cracks extended. New cracks on the first story masonry panel appeared. Deboning at the one of the FRP legs from front side and back side occurred after three full cycle completed.

In cycle 16, maximum load and corresponding drift for the forward half cycle and backward cycle were 86.7 kN (0.48%) and 103.2 kN (0.58%) respectively. No new cracks on the surrounding frame were observed. Diagonal cracks which were parallel to cross FRP were observed on the first story masonry panel. A crack on the left column outer face which was about 14 cm away from the foundation level extended throughout the front face of the column. Previous cracks were also extended to different lengths, changing from 2 cm to 10 cm. The cracks at the left beam-column joint started to increase and crushed the concrete cover. 20 cm long diagonal shear crack occurred at the left column started from the joint. Protrusion was observed on the cross diagonals. FRP's were still carrying the maximum load and very close to the failure at that cycle.

In cycle 18, maximum applied load corresponding drift forward was 95.4 kN (0.83%). The diagonal strip on the front side which was deboned, ruptured completely in the forward half cycle as shown in Figure 4.3. As a result of this failure the specimen reached the maximum load capacity and started to lose the capacity. Vertical cracks appeared on the first story masonry panel result in a brick failure at the compression strut. These cracks were almost perpendicular to cross FRP. This event illustrated the restraining effects and effectiveness of the cross FRP.

In cycle 20, maximum applied push load and corresponding drift were 86.9 kN and 0.59% respectively. The specimen started to lose the capacity due to the rupture of diagonal FRP strip at cycle 18. The vertical strip which was 27.5 cm away from the right and left column outer face, ruptured in the forward half cycle with the failure of the diagonal FRP strip at the backside. Shear flexural crack on the left column-beam joint enlarged and crushing of concrete were clearly seen at there. Due to this action, longitudinal reinforcements were buckled and plastic hinge occurred at left column. Beside the FRP failures, shear dominant action were seen and as a result of both actions, specimen had lost the capacity dramatically during the following cycles

In the next two cycles, drift levels corresponding maximum loads for the forward half cycles were about 1.26% and 1.68% respectively. After the FRPs were ruptured, heavy damage occurred as shown in Figure 4.61 and test was terminated at the end of the 22nd cycle. Loading type and maximum values for each successive drift level are summarized in Table 4.2. Failure could be attributed to the rupturing of FRPs and capacity exceedance of the columns. Frame columns failed under a combined action of shear, moment and axial forces. Rupturing of FRPs transferred all the actions from the FRP strengthened frame to the infilled frame and deterioration took place. Buckling of the longitudinal steel on the left column top end, spalling of cover concrete and loss of inadequately confined core concrete which can cause vertical movement implied gravity collapse of the frame after crushing of the infill at the end of the test. Separation of the infill from the surrounding frame was observed clearly after rupturing of the FRPs. Formation of horizontal cracks on the masonry panel was the indicator of sliding but this was not seen as predominant on the failure. At the last cycle, pictures illustrated that the frame and infilled masonry behaviors were not consistent with each other especially after rupturing of FRPs and crushing of masonry around the corner flags. In other words separation was much more notable. Behavior of the specimen showed that axial load failure occurred right after the shear failure of the columns that of which was in good agreement with the literature.

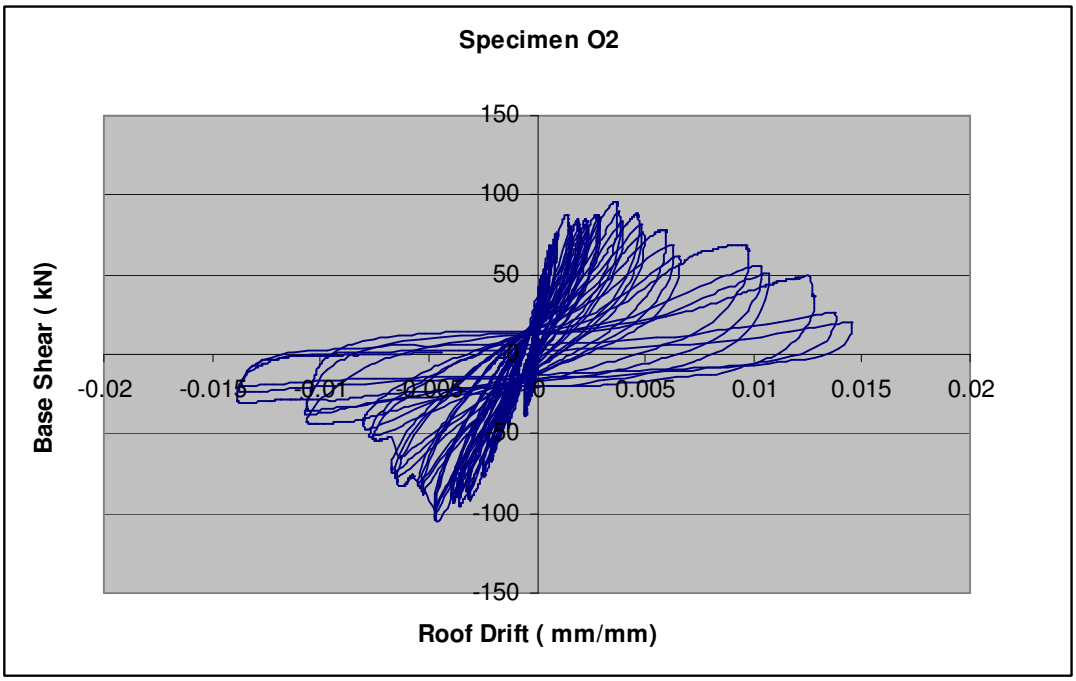

Figure 4.10. Base shear-top drift diagram for specimen O2

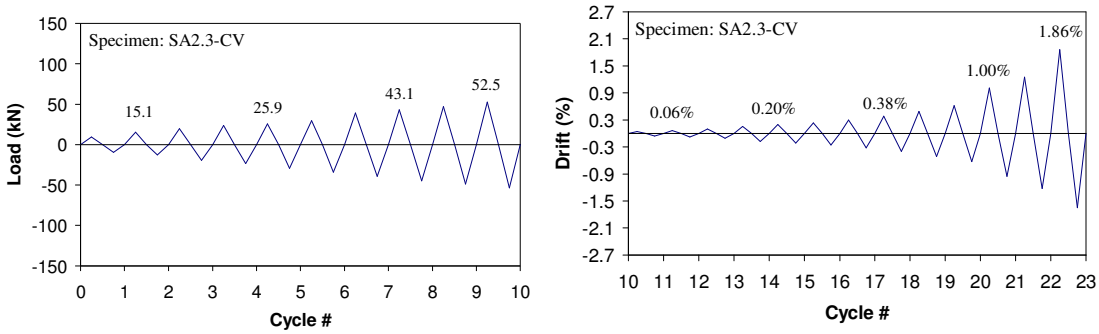

Figure 4.11. Load pattern applied for specimen O2

Table 4.2. Maximum displacements and corresponding loads for specimen O2

Specimen:O2					
Cycle	Control Type	Maximum Load (kN)	Corresponding Displacement (mm)	Minimum Load (kN)	Corresponding Displacement (mm)
1	LC	9.28	0.01	-9.15	-0.13
2	LC	15.13	0.02	-15.2	-0.22
3	LC	19.72	0.07	-19.54	-0.33
4	LC	23.63	0.05	-23.46	-0.38
5	LC	25.92	0.13	-29.37	-0.64
6	LC	29.83	0.27	-34.26	-0.73
7	LC	38.92	0.31	-39.34	-0.81
8	LC	43.08	0.37	-48.61	-0.92
9	LC	47.01	0.5	-52.64	-0.99
10	LC	52.52	0.62	-61.64	-1.00

Specimen:O2					
Cycle	Control Type	Maximum Displacement (mm)	Corresponding Load (kN)	Minimum Displacement (mm)	Corresponding Load (kN)
11	DC	0.74	55.8	-1.01	-66.22
12	DC	1.08	63.8	-1.39	-76.8
13	DC	1.61	74.8	-1.93	-90.6
14	DC	2.61	80.42	-3.08	-94.8
15	DC	3.42	83.7	-3.73	-97.5
16	DC	4.04	84.1	-4.46	-103.3
17	DC	5.05	86.7	-5.57	-100.2
18	DC	6.64	95.43	-6.93	-87.2
19	DC	8.41	86.9	-8.81	-80.4
20	DC	10.66	77	-10.91	-63.4
21	DC	17.38	67.56	-16.49	-50.2
22	DC	22.99	36.9	-23.28	-35.3
23	DC	25.6	15.07	-26.6	-21.2
Note 1: The measurement height was 1730					
Note 2: DC represents displacement controlled type of loading					
Note 3: LC represents load controlled type of loading					

Figure 4.12. Rupturing of diagonal FRP for specimen O2

Figure 4.13. Rupturing of diagonal and vertical FRP for backside of specimen O2

Figure 4.14. Beam-column joint failure for specimen O2

Figure 4.15. Rupturing of diagonal and vertical FRP for front side of specimen O2

Figure 4.16. Spalling of concrete and buckling of reinforcement

Figure 4.17. Condition of specimen O2 after the test

5. EVALUATION OF TEST RESULTS

5.1. General

In this chapter, the seismic behavior of repaired test specimens (Specimen O1 and O2) is explained based on the following observed characteristics and compared with the undamaged strengthened specimens (S.A 1.0-CV and S.A 2.3-CV) tested by Atmaca (2008). These evaluations can be listed as follows:

- Increment in strength and degradation of the stiffness by means of various definitions.
- Energy characteristics of the test specimens considering from viscous damping to cumulative and relative energy dissipation properties.
- Residual displacement and interstory drift characteristics.

5.2. Strength

One of the most important factors that determine the effectiveness of a seismic strengthening technique is the achieved in the lateral load carrying capacity of the structure. In order to evaluate the strength characteristics in detail and make a comparison among the successively repaired and strengthened specimens, the response envelopes are given in the following pages.

For a better understanding, the damaged-repaired specimens and undamaged-strengthened specimens had the same method of FRP application. After the evaluation of the maximum lateral load capacity and response curves, the effectiveness of epoxy injection and FRP repairing technique will be clearly understood. In order to achieve these results, the response envelopes of both repaired test specimens (Specimen O1 and O2) and undamaged strengthened specimens (S.A 1.0CV and S.A 2.3CV) tested by Atmaca (2008) were overlapped and displayed following pages.

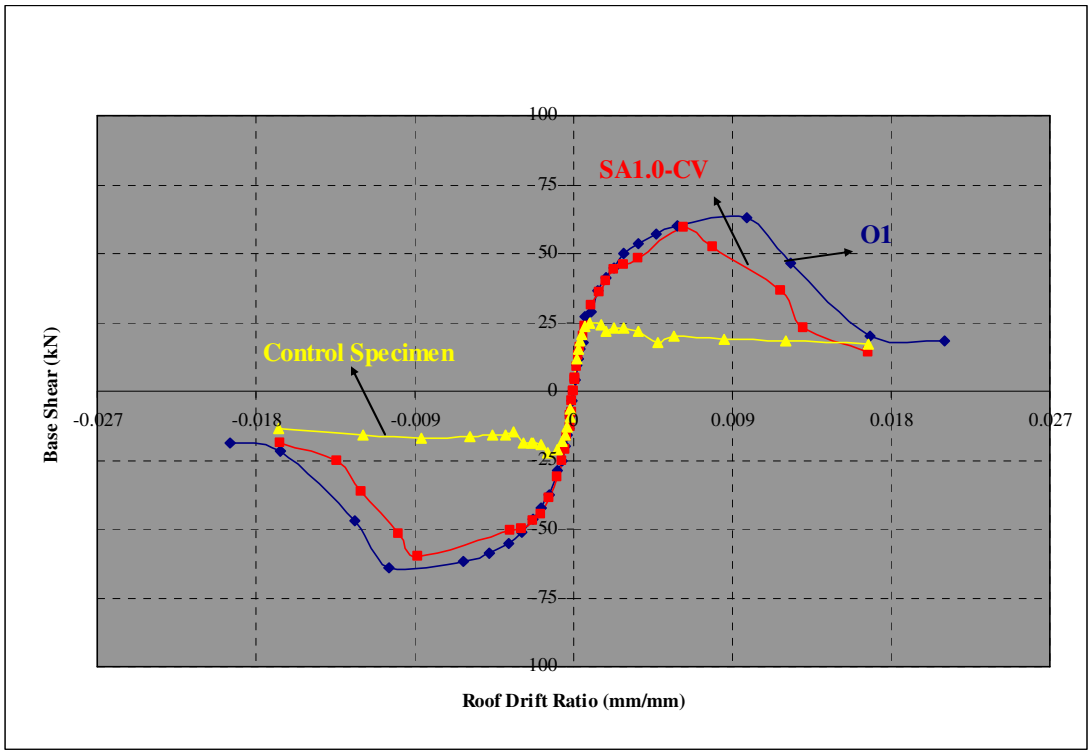

Figure 5.1. Comparison of response envelopes of damaged and undamaged specimens O1 and S.A 1.0 CV

As it is clearly seen at the Figure 5.1, the repairing technique subjected to the damaged frames from the test of Atmaca 2008, was enabled us to reach the approximately the same strength values considering the maximum lateral load capacity. The overall behavior of the repaired specimen (O1) considering the lateral load capacity reached the maximum load capacity of 63 kN at 0.0088 drift ratio, whereas the one conducted by Atmaca 2008 (S.A 1.0CV) was reached 59 kN at the 0.0077 drift ratio. Before repair of the specimen O1, it had lost all the load carrying capacity, however after the epoxy injection and the strengthening with the same method of specimen S.A 1.0 CV, resulted in the recovery of ductility and load carrying capacity. The effect of damage was compensated with this method of repairing.

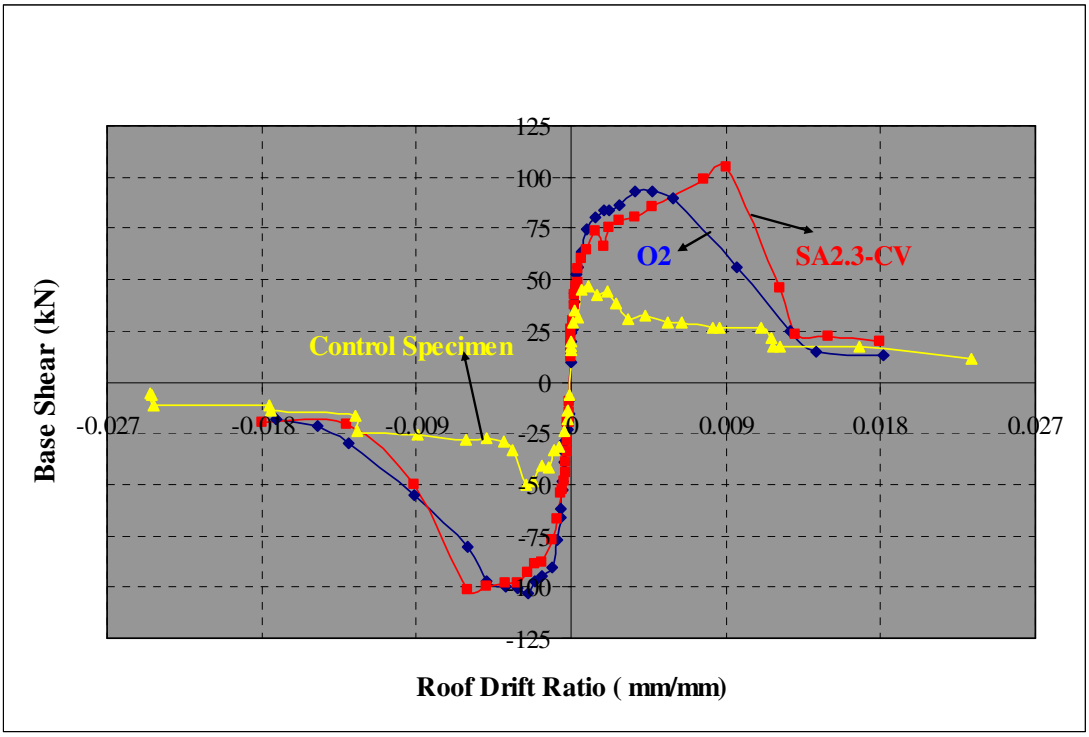

Figure 5.2. Comparison of response envelopes of damaged and undamaged specimens O2 and S.A 2.3 CV

For the case of the specimen with an aspect ratio 2.3, the repairing and strengthening technique was same. However, before the repairing the damage level was much more the one aspect ratio 1.0. There were lots of brick loss due to compression strut existence and largest cracks at beam column joints. After the repairing with the same type of brick infill and epoxy injection wit FRP strengthening, the most of the load carrying capacity was recovered compared with the one Atmaca 2008 (S.A 2.3 CV). The undamaged strengthened specimens (S.A 2.3CV) had the maximum load capacity of 111.3 at 0.0605 drift ratio kN, whereas damaged repaired test specimen O2 was reached 103.5 kN at 0.0041 drift ratio. There is a slight load and deformation capacity drop considering the much more damage level on the case of the Specimen O1. Therefore, one can clearly satisfied with the capacity recovery and repairing method although a capacity loss of 7% considering the damage level.

5.3. Stiffness

Different stiffness descriptions, such as secant stiffness, effective stiffness, and peak to peak stiffness, exist in defining the lateral load response of members and systems. Secant stiffness among these can be defined as the ratio of the load to the corresponding displacement at a given drift level, while the stiffness at cracking can be defined as the effective stiffness. In this study, the peak to peak stiffness is used. The peak to peak stiffness can be defined as the slope of the line which connects the two peak displacements in one load cycle as given in Equation 5.40.

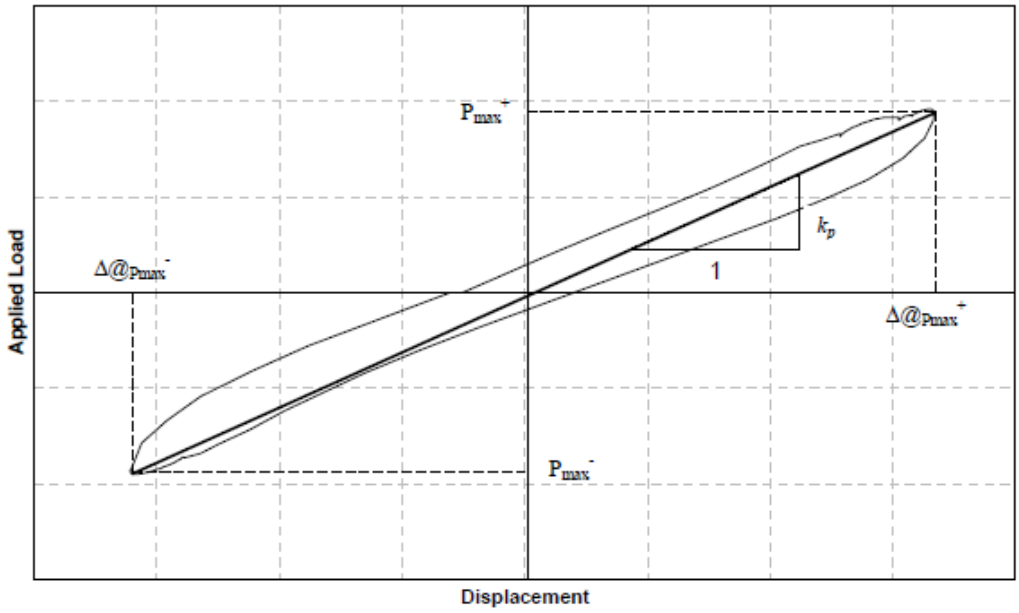

Figure 5.3. Definition of peak-to-peak stiffness

As the terms in the numerator are the loads corresponding to maximum and minimum deformations, the terms in the denominator are maximum and minimum displacement at that specified load cycle. Stiffness calculations were done at each consecutive cycle using the experimental load displacement loops. Peak to peak stiffness values were normalized against that stiffness value at 0.02% drift ratio. At the initial stages of the loading stiffness values were considerably high due to the composite action of the frame, wall, and FRP. At higher displacement amplitudes stiffness degradation took place

due to several reasons such as nonlinear deformations, formation of cracks (flexural and shear), slip of the reinforcement, debonding of FRP from the plaster or brick shell, and rebar bond deterioration.

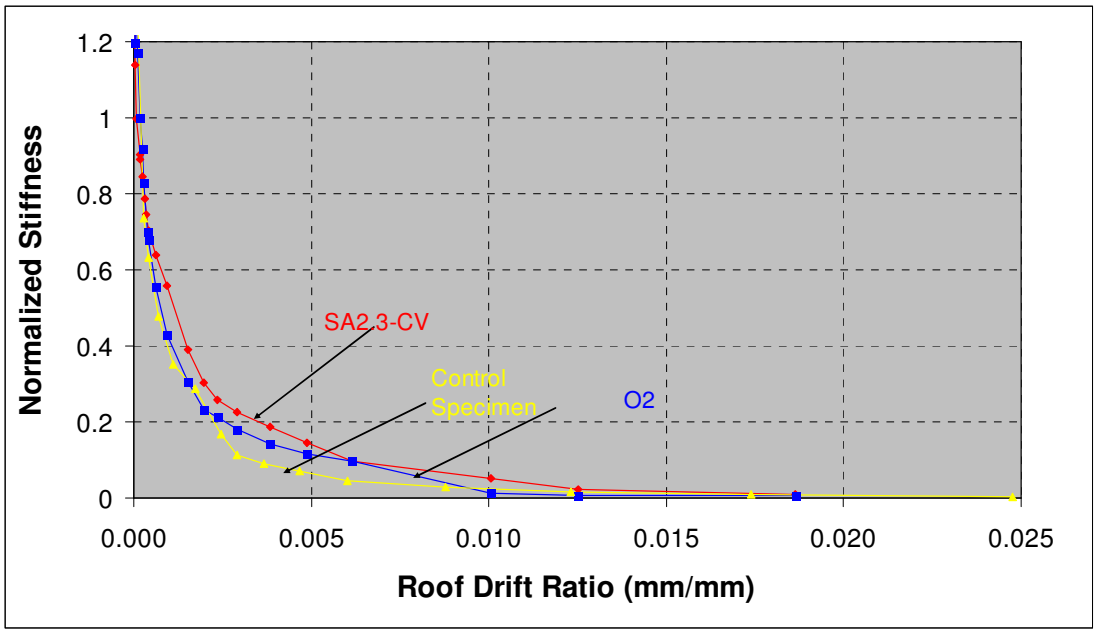

Figure 5.4 Normalized stiffness-roof drift ratio for specimens with an aspect ratio of 2.3

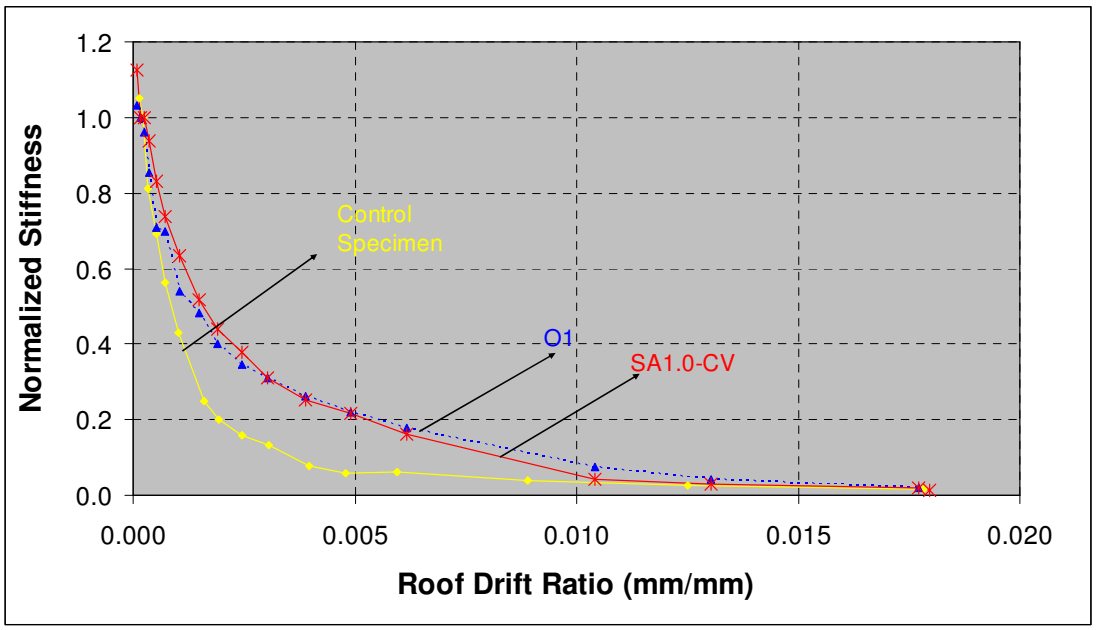

Figure 5.5. Normalized stiffness-roof drift ratio for specimens with an aspect ratio of 1.0

As indicated in Figure 5.4 and Figure 5.5, the infilled control specimen established the lower bound for the stiffness degradation diagram. Encircled points represented the third cycle stiffness values at which the maximum load was attained in the first cycle of that drift level. All the strengthened specimens faced serious stiffness degradation when peak load was reached except control specimen. Figure 5.5 were drawn for the specimens with an aspect ratio of 1.0. Specimen O1 which was damaged and repaired showed a similar stiffness degradation behavior compared with the one undamaged strength specimen SA 1.0 CV. At the beginning, the degradation speed was slightly faster then SA.1.0 CV but, after peak load, it behaved slightly better due to the strengthening quality and epoxy injection. As it is fully considered, the repairing methods were successful enough to behave as undamaged specimen SA 1.0 CV.

The stiffness degradation for specimens with an aspect ratio of 2.3 was similar although they have different response envelope. Normalized stiffness values for the strengthened specimens with aspect ratio of 1.0 and 2.3 at a drift ratio of 0.005 are respectively 0.20 and 0.10 as indicated in Figures 5.4 and 5.5. This shows that the higher aspect ratio increases the stiffness degradation speed. Moreover, consideration of damaged-repaired and undamaged strength specimens' case is another noticeable issue. As

it is mentioned before, specimen O2 had medium level damage with a brick loss and large cracks on the beam column joints. After the repairing methods, the strength degradation ratio of this specimen was approximately coincides with the one Atmaca's (SA.2.3 CV). However, at this aspect ratio the strengthening or repairing methods did not changed the stiffness degradation values dramatically.

5.4. Energy Dissipation

Loading history strongly affects the energy dissipation characteristics, especially in the nonlinear range. However it was not possible to use the same loading protocol for all the specimens. Depending on the aspect ratio of the specimens, their behavior shifted from flexural dominant behavior to a shear dominant one as specimens from O1 to O2. This was the reason to compare the energy dissipation characteristics in 2 different groups, considering the aspect ratios. Cumulative energy and cumulative drift ratios were used for the cross comparison of the aspect ratios and damage level. Energy dissipation was investigated in terms of cumulative values and dissipated energy at each successive story drift ratio.

Dissipated energy is defined as the area enclosed within the load-deformation loops. Input energy was defined as the work of the actuator to deform the specimen up to the predefined displacement amplitude. The work done by axial loads and friction forces were ignored to calculate the input energy. The definitions given for the input and dissipated energy is described in Figure 5.6.

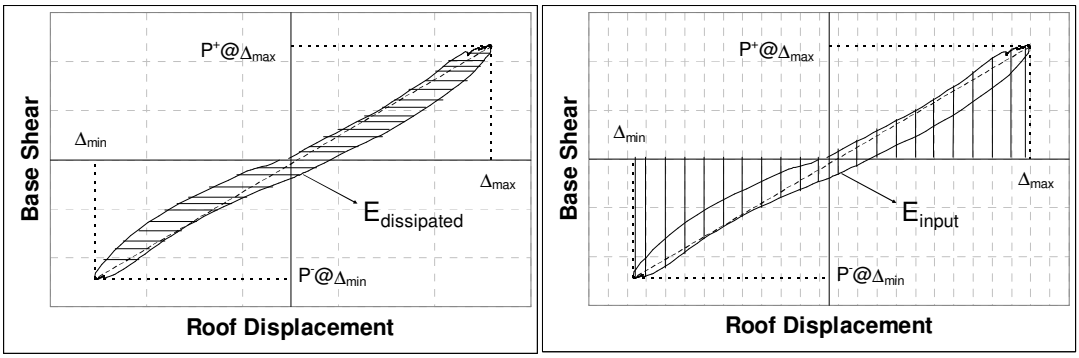

Figure 5.6. Dissipated energy and input energy in one loading cycle

Energy dissipation takes place in several ways. Yielding of reinforcement, cracking of concrete and masonry, crushing of concrete and masonry corners, sliding, and bond failure may be listed as the piers of the energy dissipation. Although FRP influenced the energy dissipation characteristics, it did not have any contribution by itself.

Cumulative dissipated energy and cumulative roof drift ratio graphs are given in Figure 5.7 and 5.8 for different aspect ratios and damage levels. As indicated in Figure 5.7, cumulative dissipated energy values of the specimens having A.R. of 1.0 were almost the same until the cumulative drift ratio of 0.027. The same trend is valid for the specimens with an aspect ratio of 2.3 at the same cumulative drift ratio as shown in Figure 5.8. After the cumulative drift level of 0.027 was attained, the dissipated energy started to deviate for the strengthened and non strengthened infilled frames. However, it still coincides with the undamaged repaired specimen O1 as the cumulative drift increases. At the cumulative drift level of 0.1, undamaged strengthened specimen and damaged repaired specimen with A.R. of 1.0 dissipated almost as much as 2 times energy as infilled control specimen. Strengthened specimens having A.R. of 2.3 dissipated less than 2 times energy that the companion control specimen dissipated in this group. Comparing with the damaged specimen O2, it has more dissipation capacity approximately 10%. Although behavior of O1 and SA 1.0 CV was so close, higher damage level and aspect ratio of specimen O2 result in a lower energy dissipation capacity. When the ultimate drift ratios were attained, cumulative drift ratios differed slightly. In other words, it can be said that energy loss due to change in drift ratio was almost equal to the energy gain due to increase in ultimate load.

Although the specimen O1 and O2 were damaged and had lost the energy capacity before rehabilitation, the repairing with same CFRP method and epoxy injection compensated the lack of energy capacity compared with the undamaged strengthened specimens SA 1.0 CV and SA 2.3 CV. One can observe that very good agreement was traced considering cumulative dissipated energy as indicated in Figure 5.6 and 5.7. This also showed that lap splice deficiency, the main deficiency in this group which affected behavior significantly, was successfully quenched.

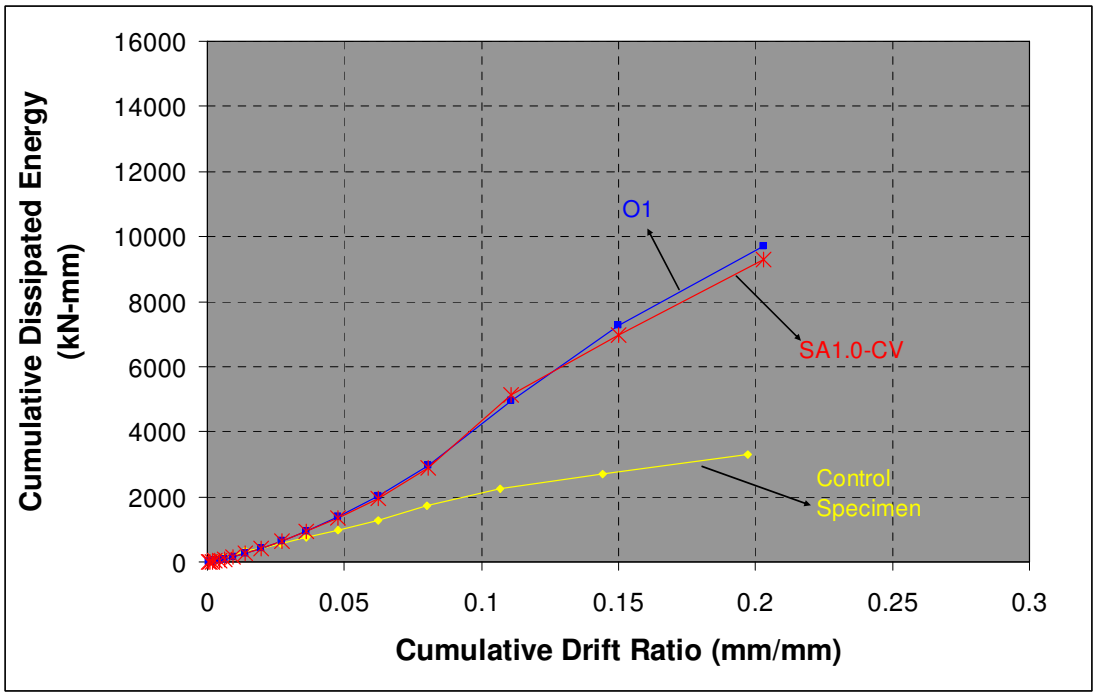

Figure 5.7. Cum. dis. energy vs. cum. drift ratio for the specimens with A.R. of 1.0

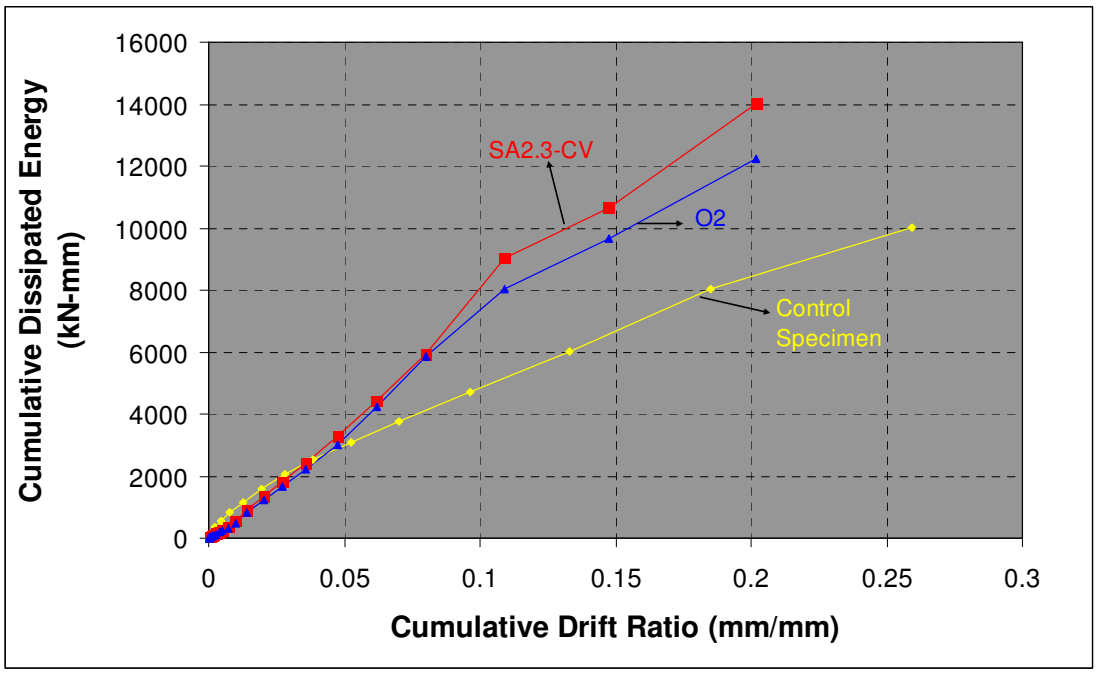

Figure 5.8. Cum. dis. energy vs. cum. drift ratio for the specimens with A.R. of 2.3

The ratio of dissipated energy to input energy per drift level was calculated and drawn with respect to roof drift ratio for each specimen. The area enclosed by each loop at a specific drift level was described as the dissipated energy. As shown in Figure 5.9, the ratio tended to decrease in the first several cycles. During the test, no damage was observed in these cycles. The system was in the elastic range. Once the cracks occurred, energy dissipation mechanisms activated and input energy dissipated by the system started to increase. This trend was much clearer for the strengthened specimens. When the strengthened specimens with an aspect ratio of 1.0 reached their peak loads, SA1.0-CV dissipated almost 80% of the input energy at that drift level as indicated in Figure 5.9 (0.01mm/mm). It is observed that the damaged-repaired specimen O1 showed a good trace compared with the specimen SA 1.0 CV, and at the ultimate drift levels same strengthening methods with epoxy injection increased this ratio 5% much which can be evaluated as the same behavior.

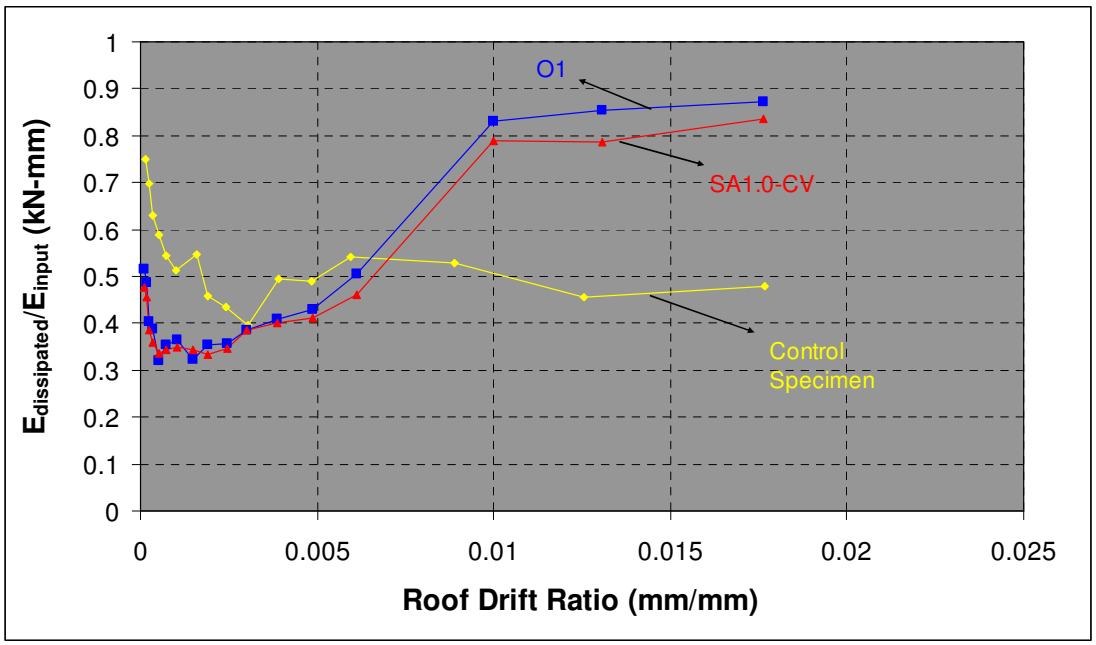

Figure 5.9. The ratio between dissipated and input energy at each drift level for specimens with A.R.of 1.0

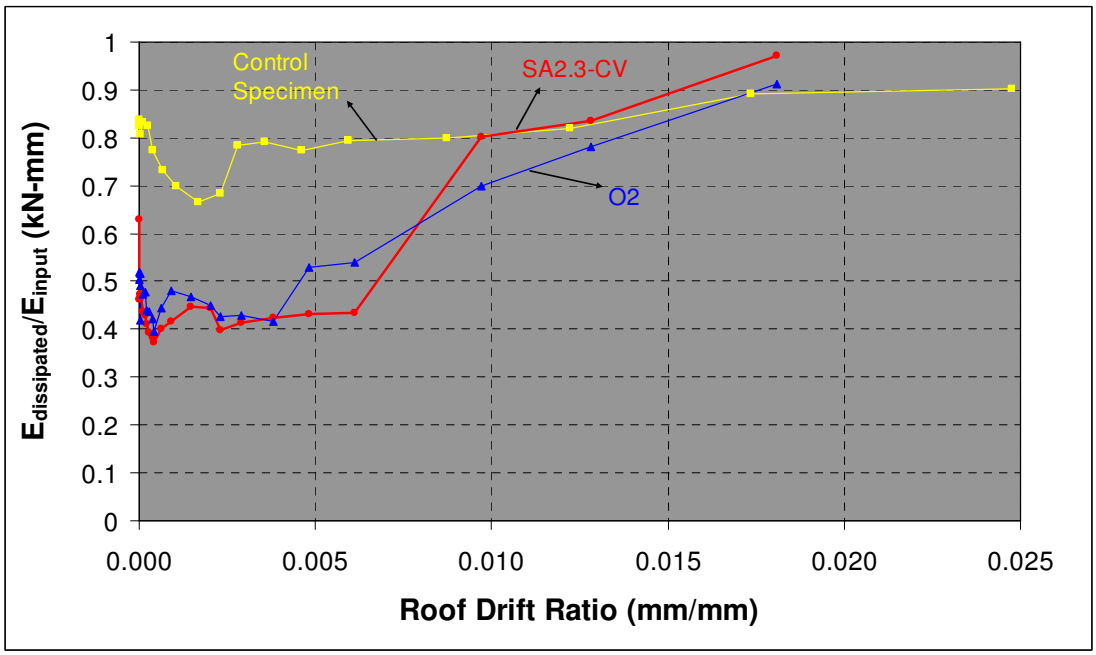

Figure 5.10. The ratio between dissipated and input energy at each drift level for specimen with A.R.of 2.3

As indicated in Figure 5.10, the dissipated energy ratio tended to decrease during the load controlled type of loading for the specimens' aspect ratio 2.3. One explanation is that the specimen behaved mostly elastic during these load controlled cycles, as the increase in displacement for each load increment was very little compared to the previous cycle. Due to the fact that, specimen O2 had a higher level of damage the ratio between dissipated and input energy was tended to be lower comparing with the undamaged strengthened specimen SA 2.3 CV. The increase started earlier for the specimen O2 but at the ultimate drift ratio, dissipation over input ratio decreased approximately 10 %.

Figures 5.11 and 5.12 illustrate the general trend for all the specimens tested in this study. As indicated, SA2.3 CV was the closest specimen to the y=x line. This line showed that all of the input energy dissipated by the given system. Comparing with the damaged repaired case, specimen O2, it had a positive energy dissipation behavior. SA1.0 CV and O1 was also very close to this line. All the strengthened specimen and repaired strengthened specimens tended to deviate from the y=x line. For the aspect ratio 1.0, the graph fits well and observed that the damage effect compensated.

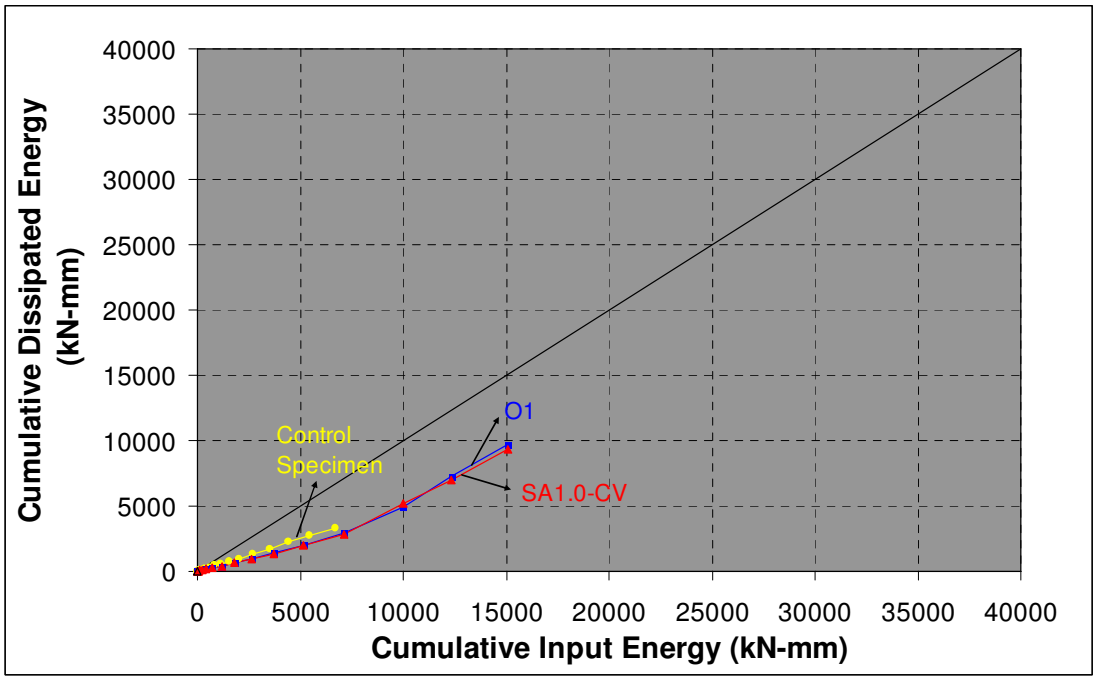

Figure 5.11. Cumulative dissipated energy vs. cumulative input energy for specimens with an aspect ratio of 1.0

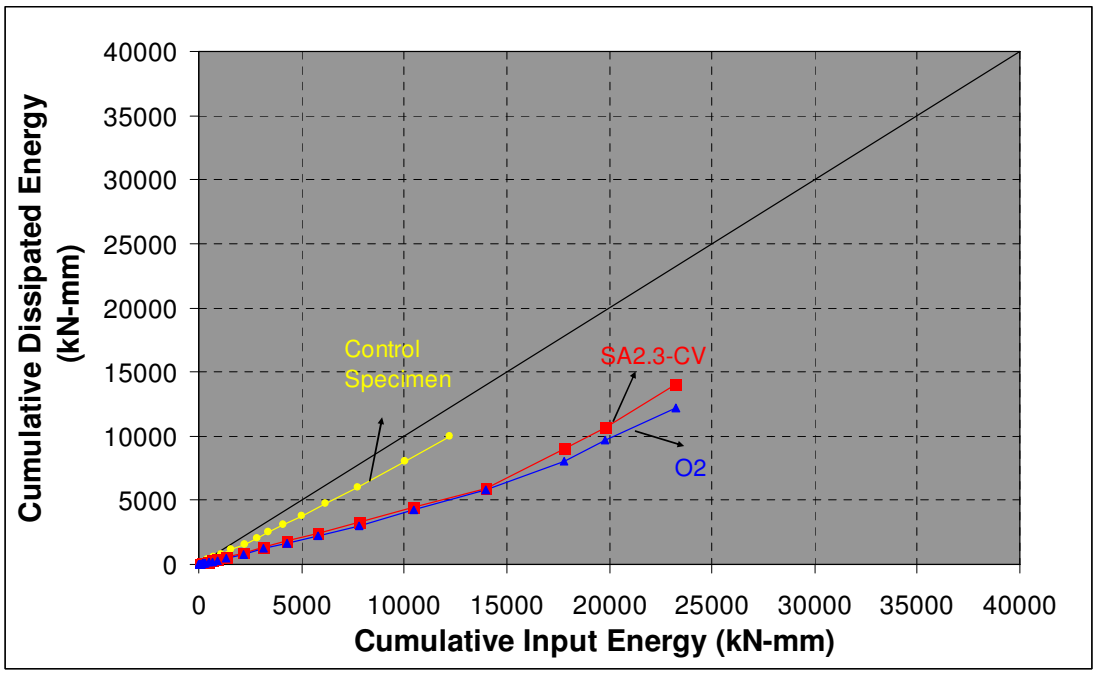

Figure 5.12. Cumulative dissipated energy vs. cumulative input energy for specimens with an aspect ratio of 2.3

5.5. Equivalent Damping Ratio

One of the most important parameters in earthquake engineering is the energy dissipation, and the equivalent damping ratio is directly related to the energy dissipation of the system. There are several definitions of the equivalent viscous damping. In this formula E_D represents the energy dissipated in one loading cycle in the actual structure as E_S is the strain energy defined as the triangular areas between stiffness line and x axis. (Figure 5.13)

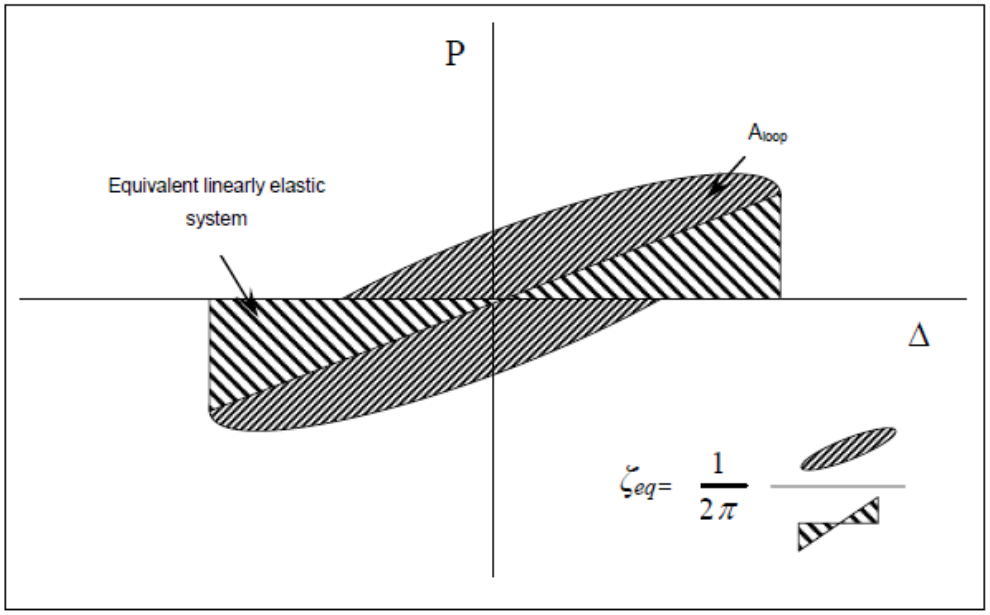

Figure 5.13. Definition of energy loss and equivalent viscous damping in a cycle

$$\zeta_{eq} = \frac{1}{2\pi}\frac{E_D}{E_S} \tag{5.1}$$

Equivalent damping ratio is discussed in the following paragraphs considering the three different diagrams drawn for each aspect ratio. Equivalent damping ratio values stand for that of the third cycle of each successive drift ratio. Cumulative drift ratios are the sum of the all drift ratios obtained from the sets of three cycles. The stiffness values in the diagrams correspond to the third cycle value, same as in the case of equivalent damping ratio.

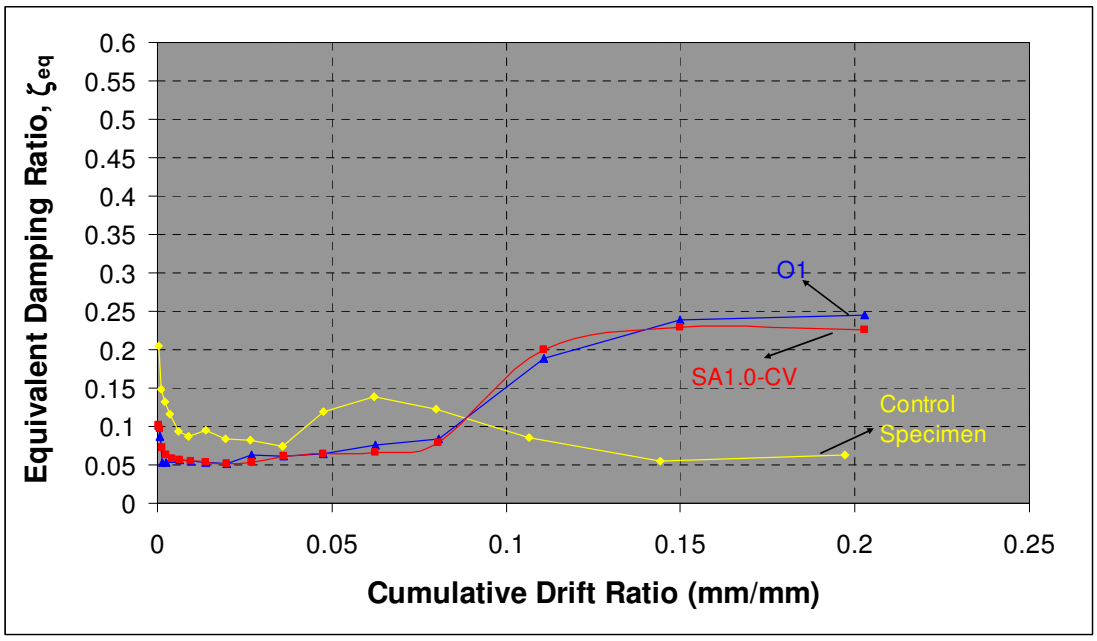

Figure 5.14. Equivalent damping ratio vs. cumulative drift ratio for A.R. 1.0

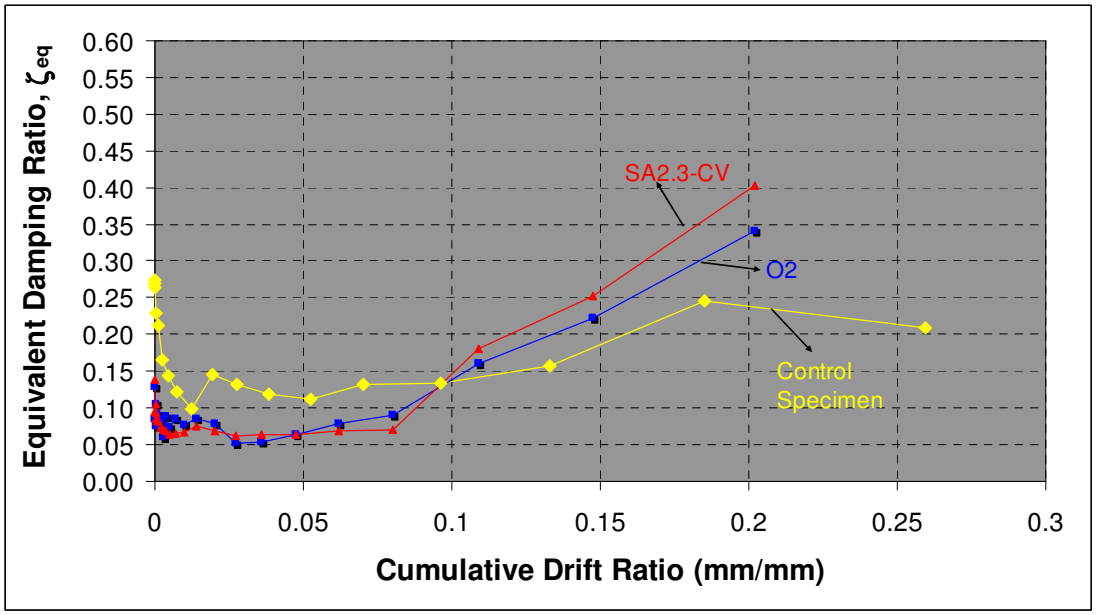

Figure 5.15. Equivalent damping ratio vs. cumulative drift ratio for A.R. 2.3

Figure 5.14 and 5.15 illustrate the changes in equivalent damping ratios of the third cycles of each set with respect to cumulative drift ratios. For the strengthened specimens with an aspect ratio of 1.0, the equivalent damping ratio experienced a sudden drop then stabilized at approximately 0.05 until the cumulative drift level of 0.027. After this point it deviated from the value of 0.05. When the undamaged strengthened and damage strengthened specimens reached peak loads, both O1 and SA1.0-CV had close equivalent damping ratios however, it was observed that repaired specimen O1 had a slight higher value as 0.24. The effect of repair and strengthening result in a good trace of damping ratio compared with the undamaged strengthened case. Specimens with an aspect ratio of 2.3 experienced sudden drops in equivalent damping ratio as indicated in Figure 5.15. However this drop was in the small drift ratio range. Equivalent damping ratio of the strengthened specimens in this group stabilized about 0.065 between cumulative drift ratios of 0.017 and 0.068. In this case, the repaired specimen O2 showed a similar behavior with the SA 2.3 CV at the elastic range but after the early failure load, observed damping ratio was lower than the undamaged specimen. However, this behavior can be evaluated as a good manner considering the damage level of specimen O2.

Figure 5.16 and 5.17 illustrate the changes in the equivalent damping ratio with respect to the stiffness values of the third cycles of each drift ratio level. As indicated in Figure 5.16 specimens having aspect ratio of 1.0 showed a very good convergence while stiffness was degraded. Equivalent damping ratio for this group converged to 0.05 in the large range of stiffness degradation. However, the equivalent damping ratio was inclined to rise after 75%-80% stiffness degradation, especially for the strengthened specimens with an aspect ratio of 1.0. As shown in Figure 5.17, the strengthened specimens experienced better convergence than the infilled specimens. However, the scatter in the specimens with aspect ratio of 2.3 was greater than the other two groups. This can be attributed to the effect of the infill's aspect ratio on the behavior. As explained before, changes in aspect ratio influenced the behavior appreciably from the flexural dominance into the shear dominance. The effect of damage and aspect ratio can be summarized that, for the specimens with lower aspect ratio and damage level, the behavior was closer to the undamaged case. It also shows us that specimen O1 behaved more stabile and result in good trace compared with the specimen O2 with higher damage level before repairing.

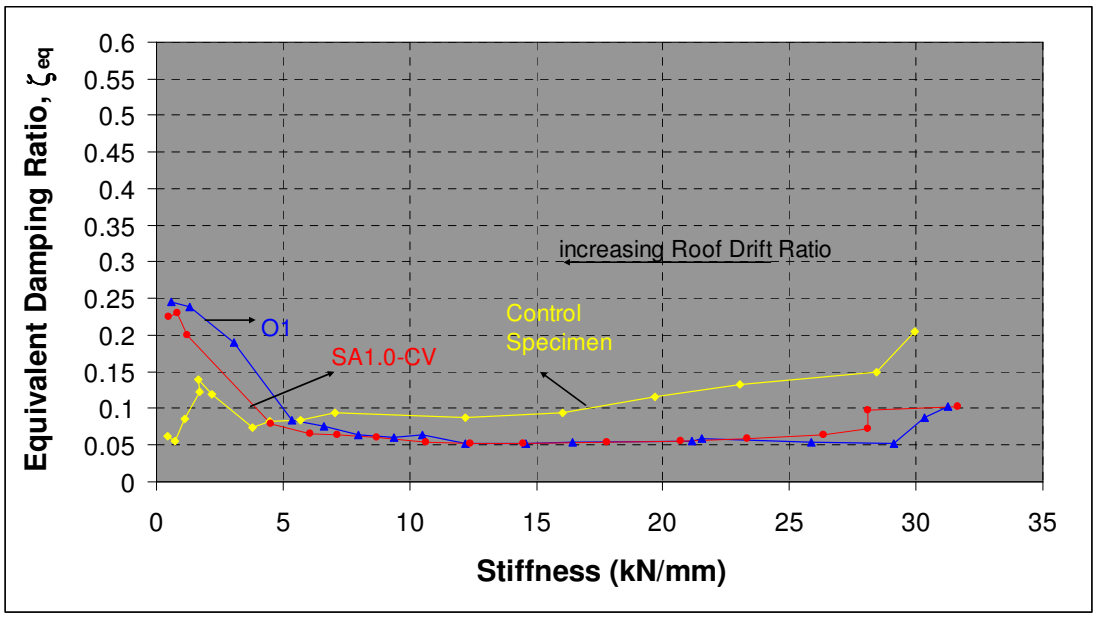

Figure 5.16. Equivalent damping ratio vs. stiffness for A.R. 1.0

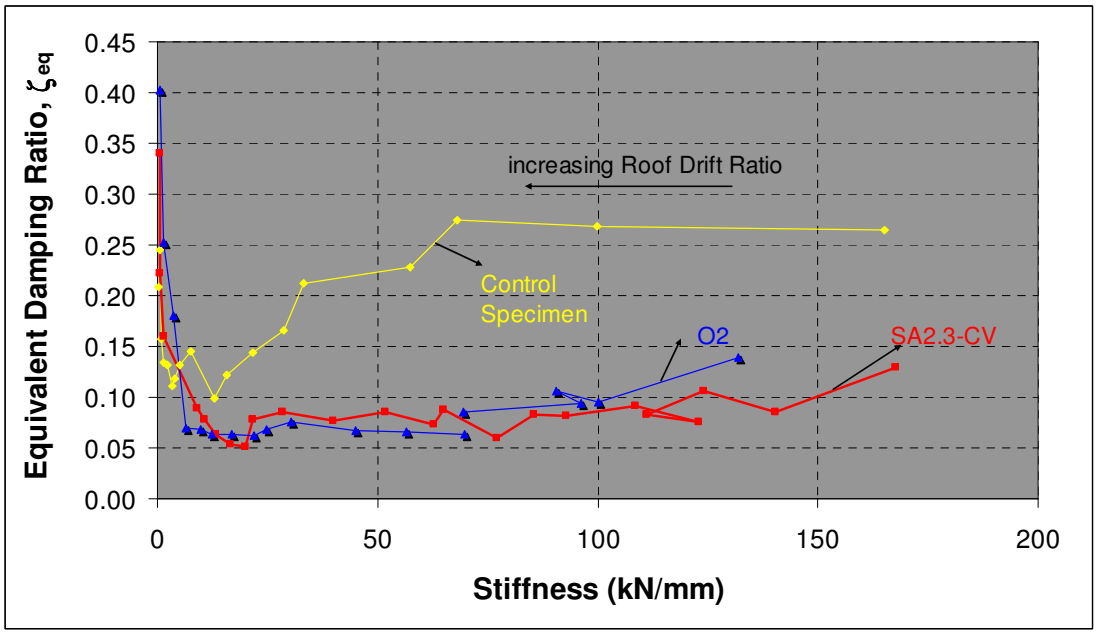

Figure 5.17. Equivalent damping ratio vs. stiffness for A.R. 2.3

5.6. Residual Displacement Ratio

Residual displacement is a measure of the plastic deformation that the specimen undergoes. Residual displacement ratio is one of the indicators showing the damage accumulation behavior of the specimen. Stiffness and strength degradation along with the residual displacements are affected from the same reasons. Some of the reasons for the residual displacement are the formation of cracks (on the masonry or surrounding frame), yielding of steel, bond deterioration (either in concrete and steel or concrete and FRP), FRP failures (debonding, peeling off, rupturing), nonlinear deformations, and failures in the masonry and the surrounding frame (crushing of the masonry corners, sliding, interaction of the masonry panel and surrounding frame). Residual displacement ratio can be defined as the ratio between the residual displacement and the positive maximum displacement in each cycle as figure 5.18. Residual displacement ratios at the third cycles are drawn with respect to the corresponding roof drift ratios.

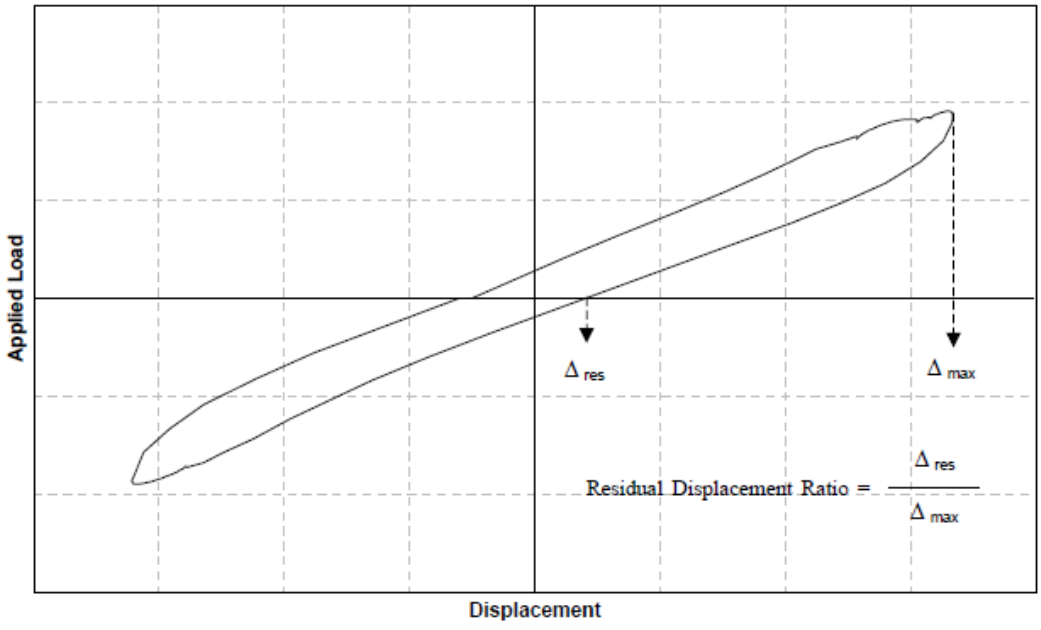

Figure 5.18. Definition of residual displacement

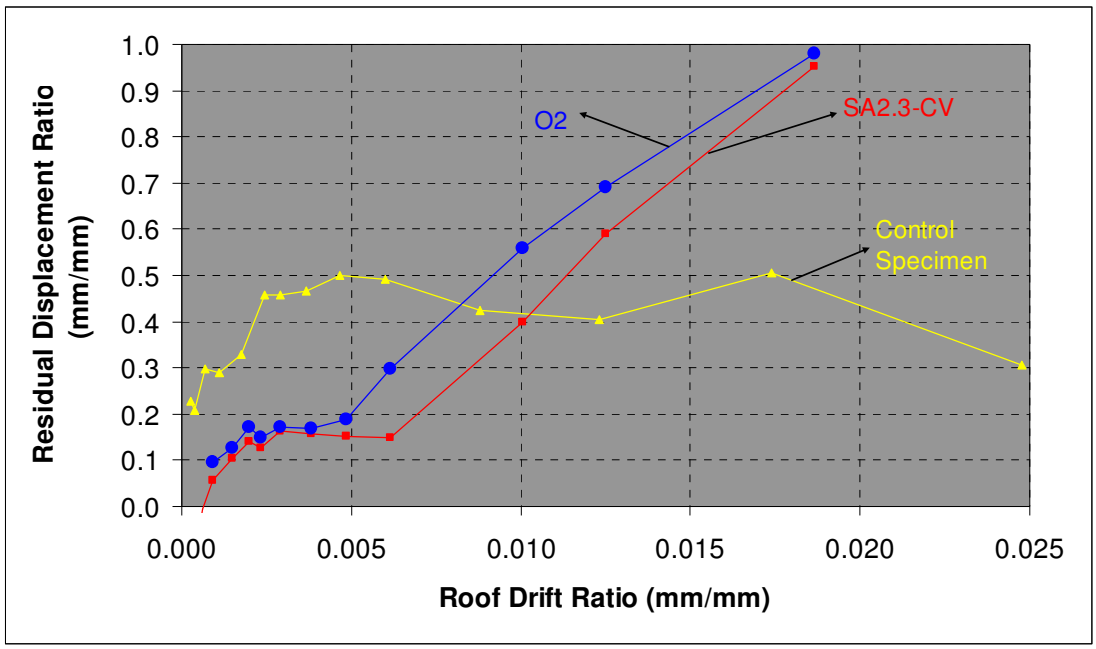

Figure 5.19. Residual displacement ratio vs. roof drift ratio for A.R. 2.3

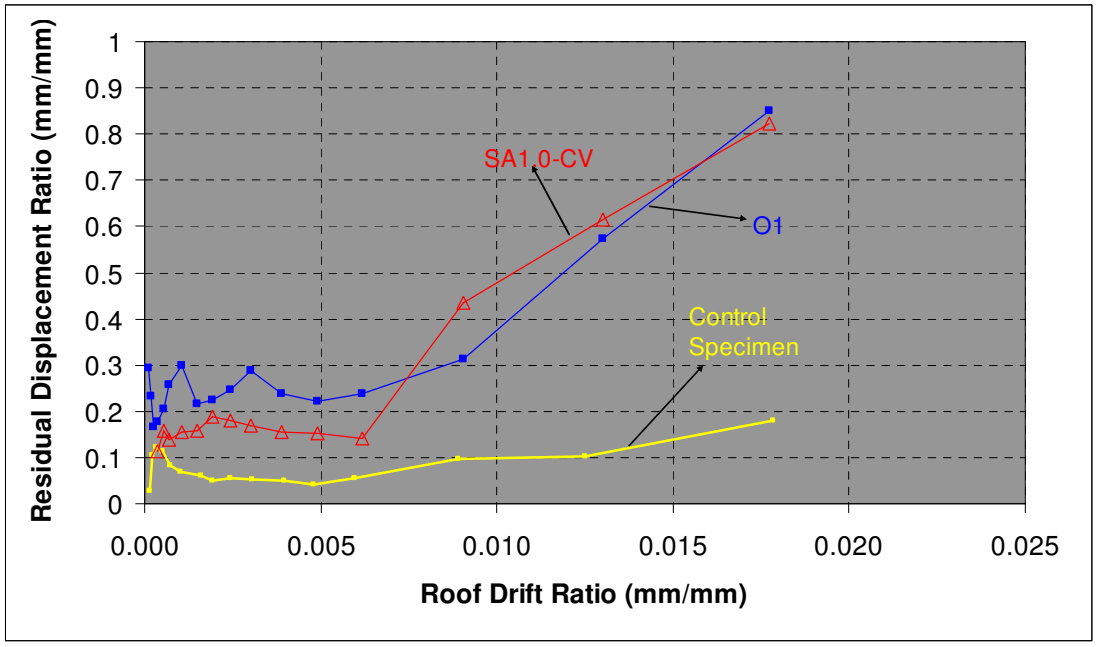

Figure 5.20. Residual displacement ratio vs. roof drift ratio for A.R. 1.0

Figures 5.19 and 5.20 depicted changes in residual displacement ratio considering the aspect ratios and damage levels. Specimen O1 has the higher residual displacement before the drift ratio 0.005.As the drift ratio increases, the undamaged specimen SA 1.0 CV and damaged specimen O1 have close residual displacement values for each drift ratio. As indicated in Figure 5.20 residual displacement ratio was not affected with the damaged case considering the behavior of O1 and SA. 1.0 CV.

Figure 5.19 illustrates the residual displacement ratio trend for the specimens with an aspect ratio of 2.3. Fluctuation in small drift levels was quite high. This can be due to some imperfections of the measuring devices. The highest residual displacement ratio was attained in this group. The damage effect can be clearly observed at this graph. Residual displacement ratio of specimen O2 was higher at all drift ratio compared with specimen SA 2.3 CV. Comparing with the specimens having aspect ratio 1.0 all of the specimen have the higher damage level and residual displacement ratio.

6. ANALYTICAL STUDY BASED ON CAPACITY CALCULATION

6.1. Failure Modes

Strengthening of the specimens with FRP increased the ultimate loads depending mainly on FRP configurations and on the frame aspect ratio. Also, application of FRP changed the failure modes of the infilled specimens depending on the aspect ratio (frame bay length/story height). Stress-strain relation of CFRP is assumed linearly elastic under uniaxial loading. However, FRP showed relatively poor behavior under the combined action of shear and axial tensile forces. That's why high strains that can be obtained from FRP coupon tests could not possibly be obtained during the test of the frame specimens. Analytically and experimentally obtained ultimate loads of the strengthened specimens are compared and listed in Table 6.1. The ratios between calculated and measured capacities are given in the last column of Table 6.1. The formulations developed in this chapter are inspired from the Paulay's approach and Atmaca S. 2008. [27]

As indicated in Table 6.1, capacities can be calculated more accurate for flexural dominant system (smaller aspect ratio) whereas there was scatter for shear dominant systems. However, the calculated values can satisfactorily predict failure loads. For the tested specimens, some combination of the following failure modes can be described:

- Tension failure of the tension column,
- Flexural or shear failure of the columns,
- Sliding shear failure,
- Compression failure of the diagonal strut,
- Overturning mode of failure,
- Anchorage failure of the FRP anchorages, and rupturing of FRP overlays,

Low aspect ratio (l/h_1), and high moment/shear ratio results in tension failure of the tension column which can be identified as an overall flexural type of failure. Tension failure of the tension column can also be considered as a part of the overturning mode of failure. The lateral load capacity of the columns, either flexure or shear is included in the overall shear sliding type of failure of the specimens. Diagonal tensile cracking of the panel generally takes place before the compression failure of the diagonal strut or the flexural or shear failure of the columns. Therefore, such a failure is not stated as one of the failure modes. Local debonding of FRP strips from the substrate surface generally took place right before the complete loss of strength. Hence, this type was also not listed as one of the failure modes as it happened at low load levels compared to the failure load. Rupturing of FRP was not considered as a failure mode since it was already included in the shear sliding and overturning type of failures. Mainly three failure modes out of above listed ones were described as following; the sliding shear failure mode, the compression failure of the diagonal strut mode, and the overturning mode of failure.

At low load levels, the frame and the panel acted together. As deformations increased, infill and frame behaved differently and all of shear was assumed to be carried by infill panel at this stage due to high infill to frame stiffness ratio. Different behavior tendency, which were shear and flexural modes, resulted in separation between infill and the surrounding frame. An infilled frame could be idealized as diagonally braced pin-jointed frame. As the lateral deformations increased, the response mechanism shifted from a diagonally braced pin jointed frame to a knee-braced frame. Effective height of the column decreased due to the formation of hinges which were about at mid-height and top or bottom of the column. Hinge formation at about mid-height and top or bottom of the columns and imminent shear failure of the columns resulted from the masonry panel which was in contact with the lower left portion of the left column and upper right portion of the right column. Pin jointed frame and knee braced frame with shear sliding at mid-height are shown in Figures 6.1 and 6.2.

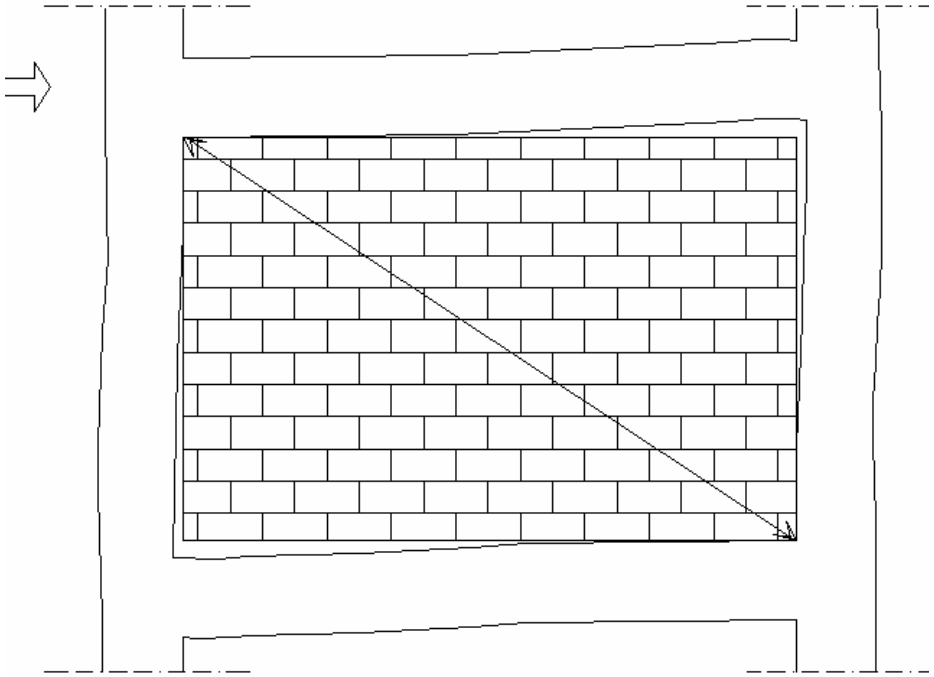

Figure 6.1. Pin jointed frame behavior

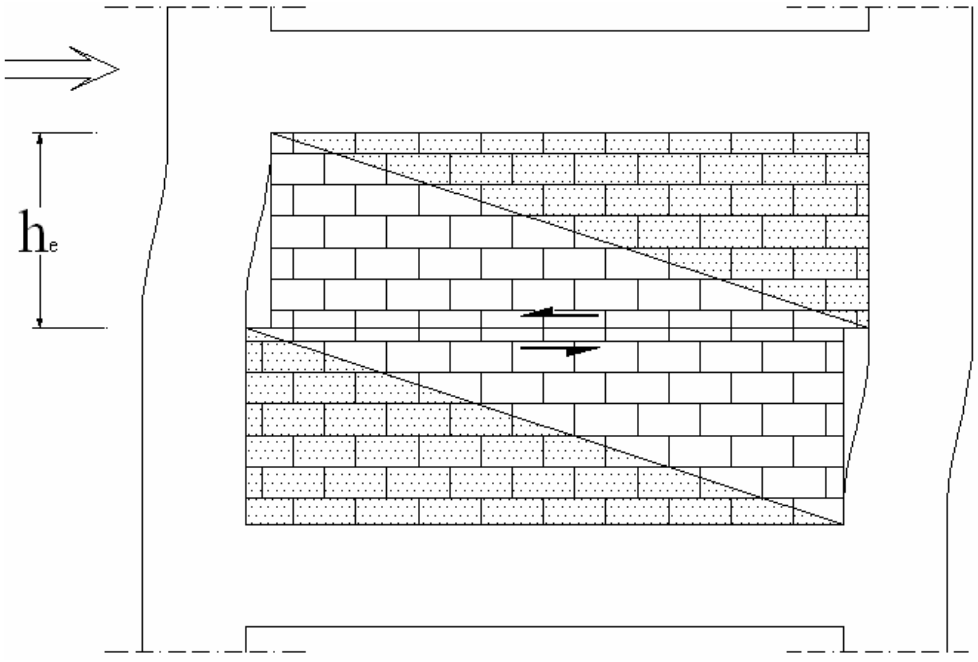

Figure 6.2. Knee braced frame behavior

6.2. Procedure for Capacity Prediction

In the light of the failure modes described above, a procedure is developed to predict the failure modes and capacities of the specimens tested. For the ease of defining the procedure, the specimens are grouped according to their CFRP configuration and discussed in the following sections. The capacity prediction has conducted by Atmaca 2008 for undamaged strengthened case, however the same type of calculation method is also applicable for the damage strengthened case specimen O1 and O2. Due to the close behavior types and capacity values observed after the experiment, following analytical capacity prediction can be assumed both damaged (Atmaca 2008) and undamaged case

Shear sliding mode of failure, as described above, is one of the three main failure modes. The following equations are used to predict the shear sliding capacity of the specimens and they are in SI units unless otherwise indicated. The modulus of elasticity of the masonry infill (E_{bm}), inclination of the diagonal strut (θ), the modulus of elasticity of concrete in the frame (E_c), the maximum stress that can be developed in the rebars of the tension column (f_s) due to the insufficient lap splice length (l_b), and the characteristic tensile strength of concrete (f_{ctk}) are calculated according to Equations 6.1~6.7.

6.2.1 Specimens: SA1.0-CV, O1, SA2.3-CV, O2

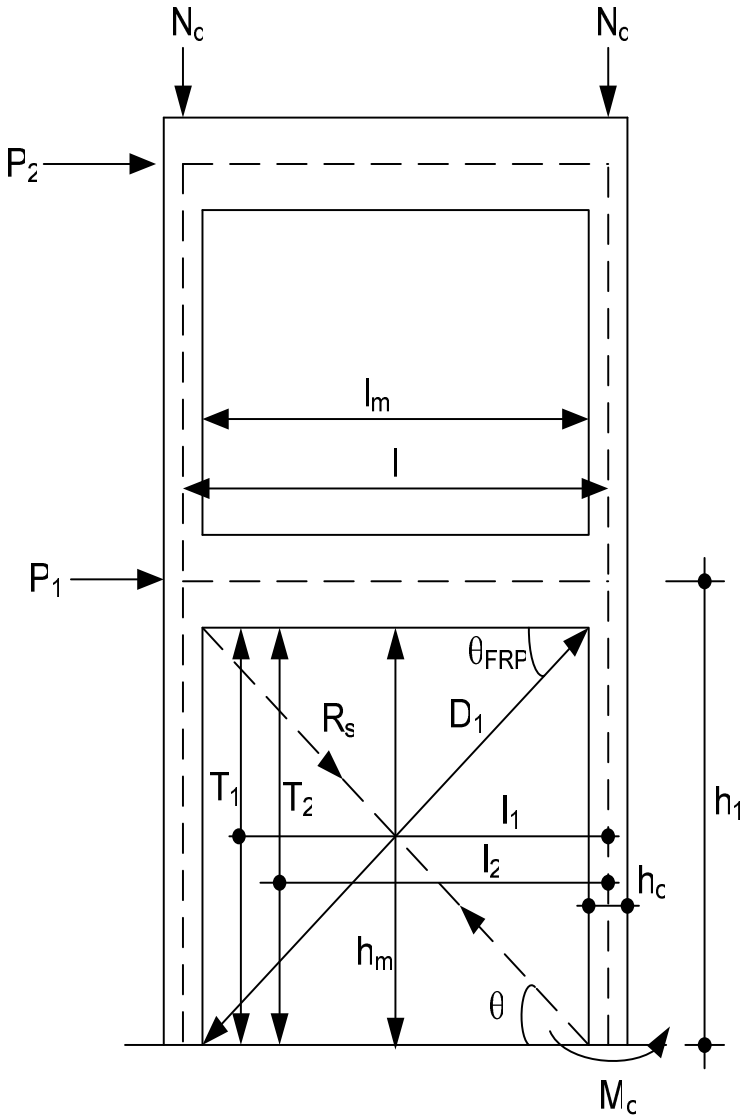

Figure 6.3. Forces and dimensions for the specimens with vertical and diagonal strips on the panel

$$E_{bm} = 750 \times f_{bm} \le 20600 \qquad \text{(in accordance with UBC 1997)} \qquad (6.1)$$

$$E_p = 5500\sqrt{f_p} \qquad (6.2)$$

$$E_{bmp} = E_{bm} \times \frac{t_{bm}}{t_{bm} + 2 \times t_p} + E_p \times \frac{2 \times t_p}{t_{bm} + 2 \times t_p} \qquad (6.3)$$

$$\theta = \tan^{-1}\left(\frac{h_{bmp}}{l_{bmp}}\right) \text{ (} \theta \text{ is in radian)} \qquad (6.4)$$

$$E_c = 3250\sqrt{f_{ck}} + 14000 \text{ (in accordance with TS500 [94])} \qquad (6.5)$$

$$f_s = \frac{l_b}{l_{b0}} \times f_{yk} \qquad \text{where } l_{b0} = 0.67 \times 0.24 \times \phi \times \frac{f_{yk}}{f_{ctk}} \qquad (6.6)$$

It should be noted that the constant 0.24 should be 0.12 in case of deformed reinforcing bars.

$$f_{ctk} = 0.35\sqrt{f_{ck}} \qquad (6.7)$$

The maximum shear force resisted by the panel (V_f) is calculated assuming that the vertical load on the infill panel is zero. The following formulations are used to calculate the V_f. At first, the entire shear is assumed to be taken by infill. The lateral load capacity of the columns, either flexure or shear, is developed at further drift levels.

$$\begin{aligned} V_f = {} & \tau_{bm} \times l_{bmp} \times t_{bm} + \tau_p \times l_{bmp} \times 2 \times t_p + \mu \times R_s \times \sin\theta \\ & + 2 \times \mu \times t_{frp-cross} \times b_{frp-cross} \times \sigma_{frp-cross} \times \sin\theta_{FRP} \\ & + 4 \times \mu \times t_{frp-vertical} \times b_{frp-vertical} \times \sigma_{frp-vertical} \end{aligned} \qquad (6.8)$$

The diagonal compression strut force (R_s) shown in Figure 6.3 is a function of the shear friction stresses, inclination of the strut (θ) and the aspect ratio of the frame. The summation of the horizontal component of R_s and the cross diagonal CFRP can also be assumed equal to the panel shear capacity as given in Equation 6.9.

$$V_f = R_s \times \cos\theta + 2 \times t_{frp-cross} \times b_{frp-cross} \times \sigma_{frp-cross} \times \cos\theta_{FRP} \tag{6.9}$$

By equating the Equations 6.8 and 6.9, R_s can be written as follows;

$$R_s = \frac{1}{\cos\theta - \mu \times \sin\theta} \begin{Bmatrix} \tau_{bm} \times l_{bmp} \times t_{bm} + \tau_p \times l_{bmp} \times 2 \times t_p \\ +2 \times \mu \times t_{frp-cross} \times b_{frp-cross} \times \sigma_{frp-cross} \times \sin\theta_{FRP} \\ +4 \times \mu \times t_{frp-vertical} \times b_{frp-vertical} \times \sigma_{frp-vertical} \\ -2 \times t_{frp-cross} \times b_{frp-cross} \times \sigma_{frp-cross} \times \cos\theta_{FRP} \end{Bmatrix} \tag{6.10}$$

The diagonal tension cracking capacity of concrete columns both in compression ($V_{cr\text{-}compression}$) and in tension ($V_{cr\text{-}tension}$) are given in Equations 6.11 and 6.12 respectively, while the contribution of transverse steel to the shear capacity is given in Equation 6.13.

$$V_{cr-compression} = 0.65 \times f_{ctk} \times b_{column} \times d_{column} \times \left[1 + 0.07 \times \frac{N_d}{b_{column} \times h_{column}} \right] \tag{6.11}$$

$$V_{cr-tension} = 0.65 \times f_{ctk} \times b_{column} \times d_{column} \times \left[1 - 0.3 \times \frac{N_d}{b_{column} \times h_{column}} \right] \tag{6.12}$$

$$V_w = A_{sw} \times f_{ywk} \times \frac{d_{column}}{s} \tag{6.13}$$

The shear capacity of the frame columns are calculated in accordance with Equation 6.14.

$$V_{column} = V_w + 0.8 \times V_{cr} \tag{6.14}$$

When a knee braced frame mechanism takes place imminent to the failure, hinges occur at approximately mid-height and top or bottom of the columns or column shear failure takes place. In this condition, moment induced shears are calculated as follows. These moment-induced shears included axial load effects due to gravity loads.

$$V_{up} = \frac{M_{p-upper} + M_{p-middle}}{h_{eff}} \qquad \text{where} \qquad h_{eff} = \frac{h_m}{2} \tag{6.15}$$

$$V_{down} = \frac{M_{p-lower} + M_{p-middle}}{h_{eff}} \tag{6.16}$$

Total shear force carried by concrete columns, $V_{f\text{-column}}$, under the action of moment, shear and axial load can be calculated in accordance with Equation 6.17.

$$V_{f-column} = \min(V_{up},\ V_{colum-tension}) + \min(V_{down},\ V_{column-compression}) \tag{6.17}$$

The sliding shear failure capacity of the infilled frame strengthened with the CFRP overlays can be calculated by adding the shear forces carried by panel and the column as shown in Equation 6.18.

$$V_i = V_f + V_{f-column} \tag{6.18}$$

The second type of failure defined previously is the compression failure of the compression strut, where the compressive strength of the masonry constitutes a failure criterion. Diagonal compression failure force, R_c, is directly proportional to the compressive strength of the strengthened masonry (f_{bmpF}) and contact length (z_{clm}) between panel and the column.

$$z_{clm} = \frac{\pi}{2}\left(\frac{4 \times E_c \times I_g \times h_{bmp}}{E_{bmp} \times t_{bmp} \times \sin 2\theta}\right)^{\frac{1}{4}} \tag{6.19}$$

$$R_c = \frac{2}{3} \times z_{clm} \times t_{bmp} \times f_{bmpF} \times \sec\theta \tag{6.20}$$

$$f_{bmpF} = \left[f_{bm} \times \frac{t_{bm}}{t_{bm} + 2 \times t_p} + f_p \times \frac{2 \times t_p}{t_{bm} + 2 \times t_p} \right] \times k \tag{6.21}$$

The overturning mode of failure capacity as the last mode of failure defined previously is calculated in accordance with the Equation 6.22.

$$P = P_1 + P_2 = \frac{1}{\frac{h_1 + 2h_2}{3}} \begin{Bmatrix} N_d \times l + A_s \times f_s \times l + 2 \times b_{FRP-vertical} \times t_{FRP-vertical} \times \sigma_{FRP-vertical} \times l_1 \\ +2 \times b_{FRP-vertical} \times t_{FRP-vertical} \times \sigma_{FRP-vertical} \times l_2 \\ +2 \times b_{FRP-cross} \times t_{FRP-cross} \times \sigma_{FRP-cross} \times \cos\theta_{FRP} \times h_1 + M_c \end{Bmatrix} \tag{6.22}$$

In the above formulations masonry compressive strength was determined by linear regression using the formulation $f_{bm}=0.1063f_m+3.8875$ which was developed from laboratory tests specifically for the mortar and brick quality used. In order to determine the shear strength of the brick masonry, quadlet tests were performed and shear strength is determined by linear regression analysis. In the lights of these experiments shear stress values for mortar and brick were determined for each specimen using Formula 6.23 and 6.24.

$$\tau_{bm} = (0.0133 \times f_m + 1.3783) \times 0.3 \tag{6.23}$$

$$\tau_m = 0.15 \times (f_m \times 0.30) \tag{6.24}$$

$$\tau_p = 0.15 \times (f_p \times 0.30) \tag{6.25}$$

It is assumed that the mortar shear strength is 15% of the mortar compressive strength, and approximately 30% of the panel length is assumed in contact at mid-height when the crack which caused sliding or rocking appears at this level. The above assumptions were found quite prudent considering the test results. The cross diagonals and flags used on the corners of the masonry panels improved the compressive strength of the masonry panel and increased diagonal compression failure load. The following formulation (Equation 5.26) is used to modify the masonry compressive strength improved by FRP. (l/h) defined the aspect ratio and the constant 0.67 was found from the experiments.

$$k = \left[\frac{0.67}{(l/h)} \times \left(\frac{L_{flag} + L_{flag} + \sum W_{cross-diagonals}}{L_{diagonal}} \right) + 1 \right] \tag{6.26}$$

6.3 Predicted Capacities

The procedure defined in the previous pages is used to determine the lateral load capacity and the failure mode of the specimens. The results of the model predictions are given in Table 5.1. Predictions on specimens with small aspect ratio show good correlation with the experimental results on the basis of both failure loads and failure modes. On the other hand, failure mode predictions for SA2.3 series specimens scatter. As indicated in Figure 5.6, the ratios were very close to the ordinate of 1.0. This was the indicator of the success of the capacity predictions. However, the same trend was not observed in the case of the aspect ratio of 2.3. The scatter in Figure 5.7 indicated that calculated and predicted values differed more than the specimens with an aspect ratio of 1.0. Since the specimens with an aspect ratio of 2.3 were not flexure dominant systems, the accuracy in the results were not as close as that of specimens with the aspect ratio of 1.0

Table 6.1. Experimental and analytical capacity for damaged and undamaged specimens

	EXPERIMENTAL		ANALYTICAL				RATIO
Specimen	P_{max} (kN)	Failure Mode	$P_{overturning}$ (kN)	$P_{shear\ sliding}$ (kN)	R_c (kN)	$P_{diagonal\ compression}$ (R_c*cosθ) (kN)	$P_{exp.}/P_{an.}$
O1	64.3	Tensile failure of columns and rupturing of FRP's	59.3	68.2	188.3	131.3	1.08
SA1.0-CV	58	Tensile failure of columns and rupturing of vertical FRP	59.3	68.2	188.3	131.3	0.98
O2	103.2	Capacity exceedance of columns and Rupturing of FRPs with shear failure	118.0	108.5	130.2	120.2	0.95
SA2.3-CV	111.6	Capacity exceedance of columns and Rupturing of FRPs	118.0	108.5	130.2	120.2	1.03

7. SUMMARY, CONCLUSIONS AND RECOMMENDATIONS

7.1 Summary

Strengthening of existing vulnerable buildings to an impending earthquake is of great importance in Turkey. There are various methods to increase the supply of the buildings, which could be divided mainly into two categories: member strengthening (jacketing of columns and beams…etc.), and system strengthening (adding of shear walls, steel bracing, or seismic isolators…etc.). If the number of members to be strengthened is limited, the former method can be used to improve the overall performance. However, the latter is more appropriate if the number of members to be strengthened is excessive or the structure suffers from inadequate lateral stiffness resulting excessive deformations. Although the above techniques are effective, they mostly require the evacuation of the dwellers. Presence of large building stock in Turkey, which is vulnerable to an imminent earthquake, entails fast, relatively easier and feasible alternative methods. Application of CFRP materials onto the infilled frames is considered as an alternative strengthening method for the low to mid-rise buildings. In this method, CFRP is adhered to the infill surface by using an appropriate adhesive and anchored to the surrounding frame with CFRP anchors.

7.2. Conclusions

The efficiency of strengthening and repairing methods are investigated in this thesis, comparing the undamaged strengthened specimens with damaged, repaired and strengthened specimens. The main variable was the damage level. All other variables were constant throughout the test. With the help of this comparison, it enabled us to evaluate the effectiveness of the strengthening for damaged buildings after the earthquake. All in all, results showed that low damage levels can be fully recovered with CFRP application and epoxy injection. For the other case, the medium damage levels can be also recovered, however the performance of this repaired specimen dropped approximately 10% compared with the undamaged specimen. If the ease of application for the repairing method is taken into account, this level of recovery is acceptable for the damaged case.

The following conclusions can be drawn based on the test results and comparisons between the test results and analytical study.

- The rehabilitation of damaged infilled frames with CFRP application with epoxy injection was generally successful considering the lateral load capacity, energy absorption and residual displacement.

- The stiffness values were not increased dramatically with same strengthening methods considering the unstrengthened frames with aspect ratio 1.0. It is more remarkable for the specimens with aspect ratio 2.3.

- Level of damage is the critical variable for the general behavior of the repaired specimen, such that medium damage level with brick loss was not fully compensated with same strengthening by CFRP and epoxy injection. For the low damage level (Specimen O1), application of repairing and strengthening enabled fully recovered lateral load capacity and energy absorption capacity.

- The failure modes, crack patterns and general behavior of the damaged-repaired specimens were very close to the undamaged strengthened specimen which was conducted by Atmaca in 2008.

- Damages occurred after the earthquake, can be recovered up to the acceptable level with same strengthening methods of undamaged case and epoxy injection. Applying the same methods to the damaged frames helps us to increase the capacity of them even after the earthquake without any additional high cost and hard applicable strengthening method.

- Analytical predicted capacity calculation for the undamaged strengthening case successfully fits the damaged, repaired and strengthened specimens O1 and O2. It is showed that experimental capacity values for damaged specimens, was very close to the values calculated as undamaged case. This analytical method can be applicable for the strengthening before and after earthquakes.

- CFRP diagonal overlays controlled the crack widths on the infill wall and caused an increase in the number of the cracks. Due to the restraining effects of CFRP overlays, the effect of the infill wall on the strength of the specimens was significant. However, the failure of FRP's results in sudden losses in the load carrying capacity and the frame itself can not pick up such a capacity loss since it is not designed for such load levels.

7.3. Recommendations for Future Studies

- Full scale tests should be performed to highlight the size effects on the behavior and ensure the reliability of the scaled tests.

- In addition to cyclic quasi-static tests, pseudo-dynamic and shake table tests should also be performed for the strengthened infilled frames.

- Long term behavior of FRP composites should also be investigated carefully. The research on the non-flammable, ductile adhesives should be developed.

- Different cost saving repairing techniques with fewer amounts of CFRP and without epoxy injection has to be developed in order to recover the damage effect and to strengthen the frames.

- Same tests have to be conducted with two actuators in order to see more appropriate damages both at 1st and 2nd story.

APPENDIX A: EXAMPLE OF THE CAPACITY CALCULATIONS

A.1. Capacity Calculation of Specimen SA1.0-CV and O1

Table A.1. Mechanical and geometric properties of specimen O1

Geometric Properties (SA1.0-CV)		**Mechanical Properties (SA1.0-CV)**			
Infill		**Masonry, Steel, Concrete**		**Cross FRP**	
		E_{bmp} (Mpa)	5130		
l_m (mm)	730	f_{bmp} (Mpa)	4.6		
h_m (mm)	750	f_m (Mpa)	5.2	ε_{FRP}	0.0045
d_m (mm)	1046.6	μ	0.3	E_{FRP} (Mpa)	230000
θ_strut (rad)	0.799	τ_{bm} (Mpa)	0.43	t_{FRP} (mm)	0.13
Frame		τ_p (Mpa)	0.23	b_{wFRP} (mm)	200
		E_c (Mpa)	23696	θ_{FRP}(rad)	0.799
l (mm)	830	I_g (mm^4)	12500000		
h_1 (mm)	825	E_s (Mpa)	195000	**Vertical FRP on the Wall**	
b_c (mm)	150	f_{ywk} (Mpa)	241		
h_c (mm)	100	f_{yk} (Mpa)	347	ε_{FRP}	0.0045
A_s (mm^2)	201	f_{ck} (Mpa)	8.9	E_{FRP} (Mpa)	230000
s_c (mm)	95	f_{ctk} (Mpa	1.04	t_{FRP} (mm)	0.13
d_c (mm)	80	N_d (kN)	14.7	b_{wFRP} (mm)	50

$$\theta = \tan^{-1}(\frac{750}{730}) = 0.799 \ radian$$

$$f_{bm} = 0.1063 \times 5.2 + 3.8875 = 4.4 \text{ MPa}$$ Linear Regression

$$f_p = f_m = 5.2 \text{ MPa}$$ Experimental Test

$$f_{bmp} = 4.4 \times \frac{70}{70 + 2 \times 8.5} + 5.2 \times \frac{2 \times 8.5}{70 + 2 \times 8.5} = 4.6 \text{ MPa}$$

k=1.49 (6.26)

$$f_{bmpF} = 4.6 \times 1.49 = 6.82 \text{ MPa} \tag{6.21}$$

$$E_{bm} = 750 \times 4.4 = 3330.2 \text{ MPa} \tag{6.1}$$

$$E_p = 5500\sqrt{5.2} = 12541.9 \text{ MPa} \tag{6.2}$$

$$E_{bmp} = 3330.2 \times \frac{70}{70 + 2 \times 8.5} + 12541.9 \times \frac{2 \times 8.5}{70 + 2 \times 8.5} = 5130 \text{ MPa} \tag{6.3}$$

$$\tau_{bm} = (0.0133 \times 5.2 + 1.3783) \times 0.3 = 0.43 \text{ MPa} \tag{6.23}$$

$$\tau_p = 0.15 \times (5.2 \times 0.30) = 0.23 \; MPa \tag{6.25}$$

R_s=14917.65 N (6.10)

$$Cos(0.799) = 0.697$$
$$Sin(0.799) = 0.717$$

$$R_s = \frac{1}{0.697 - 0.3 \times 0.717} \begin{Bmatrix} 0.43 \times 730 \times 70 + 0.23 \times 730 \times 17 \\ +2 \times 0.3 \times 0.13 \times 200 \times (0.0045 \times 230000) \times 0.717 \\ +4 \times 0.3 \times 0.13 \times 50 \times (0.0045 \times 230000) \\ -2 \times 0.13 \times 200 \times (0.0045 \times 230000) \times 0.697 \end{Bmatrix} = 14917.65 \; N$$

$$V_f = \frac{(14917.65 \times 0.697 + 2 \times 0.13 \times 200 \times (0.0045 \times 230000) \times 0.697)}{1000} = 47.94 \; kN \tag{6.9}$$

Stresses in reinforcing steel and corresponding plastic moments at different elevations can be calculated as follows:

$$f_{s\_bottom} = \frac{20 \times 8}{0.67 \times 0.24 \times 8 \times \frac{347}{1.04}} \times 347 = 130.5 \; MPa \qquad M_{p\_bottom}=1.46 \text{ kN-m} \tag{6.6}$$

$$f_{s\_middle} = \frac{46.9 \times 8}{0.67 \times 0.24 \times 8 \times \frac{347}{1.04}} \times 347 = 305.9 \; MPa \qquad M_{p\_middle}=2.51 \text{ kN-m} \tag{6.6}$$

$$f_{s\_top} = \frac{39\times 8}{0.67\times 0.24\times 8\times \frac{347}{1.04}}\times 347 = 254.5\ MPa \qquad M_{p\_top}=2.2\ \text{kN-m} \tag{6.6}$$

Increasing deformations caused separation between columns and masonry panel and columns carried shear and moments. When sliding developed at the mid-height of the panel, shear due to plastic hinge moments at the top of the left column and at the bottom of the right column can be calculated as follows:

$$V_{up} = \frac{2.2+2.51}{(0.75/2)} = 12.56\ kN \tag{6.15}$$

$$V_{down} = \frac{1.46+2.51}{(0.75/2)} = 10.59\ kN \tag{6.16}$$

Shear capacity of column under compression (Equation 6.14);

$$V_{column\_comp.} = \frac{25.13}{95}\times 241\times 80 + 0.8\times (0.65\times 1.04\times 150\times 80\times \left[1+0.07\times \frac{14700}{150\times 100}\right]) = 12.06\ kN$$

Shear capacity of column under tension (Equation 6.14);

$$V_{column\_tension} = \frac{25.13}{95}\times 241\times 80 + 0.8\times (0.65\times 1.04\times 150\times 80\times \left[1-0.3\times \frac{14700}{150\times 100}\right]) = 9.70\ kN$$

Total shear force that can be carried by column under the combined action of moment, shear and axial loads;

$$V_{f-column} = 9.70+10.59 = 20.3\ kN \tag{6.17}$$

Sliding shear failure load;

$$V_i = 47.94+20.3 = 68.2\ kN \tag{6.18}$$

Contact length between column and panel;

$$z_{clm} = \frac{\pi}{2}\left(\frac{4\times 23696\times 1.25e+7\times 750}{5130.2\times(70+17)\times\sin(2\times 0.799)}\right)^{\frac{1}{4}} = 331.8\ mm \tag{6.19}$$

The coefficient used to modify compressive strength of the masonry can be found as follows;

$$f_{bmpF} = f_{bmp}\times\left[\frac{0.67}{(830/825)}\times\left(\frac{280+280+200}{1046}\right)+1\right] = 4.6\times 1.49 = 6.82\ MPa \tag{6.21}$$

Compression failure load of the diagonal strut;

$$R_c = \frac{2}{3}\times 331.8\times(70+17)\times 6.82\times\sec(0.799) = 188.3\ kN \tag{6.20}$$

Overturning failure load;

$$P = \frac{1}{\frac{825+2\times 1725}{3}}\begin{Bmatrix} 14700\times 830+(100.5\times 2)\times 130.5\times 830 \\ +2\times 50\times 0.13\times 1035\times 745 \\ +2\times 50\times 0.13\times 1035\times 605 \\ +2\times 200\times 0.13\times 1035\times 0.697\times 825+1460000 \end{Bmatrix} = 59.3\ kN \tag{6.22}$$

Minimum of V_i (68.2 kN), P (59.3 kN), and R_c*cos(0.799) (131.3 kN) is called the analytical failure load

APPENDIX B: LOCATION OF THE SENSORS

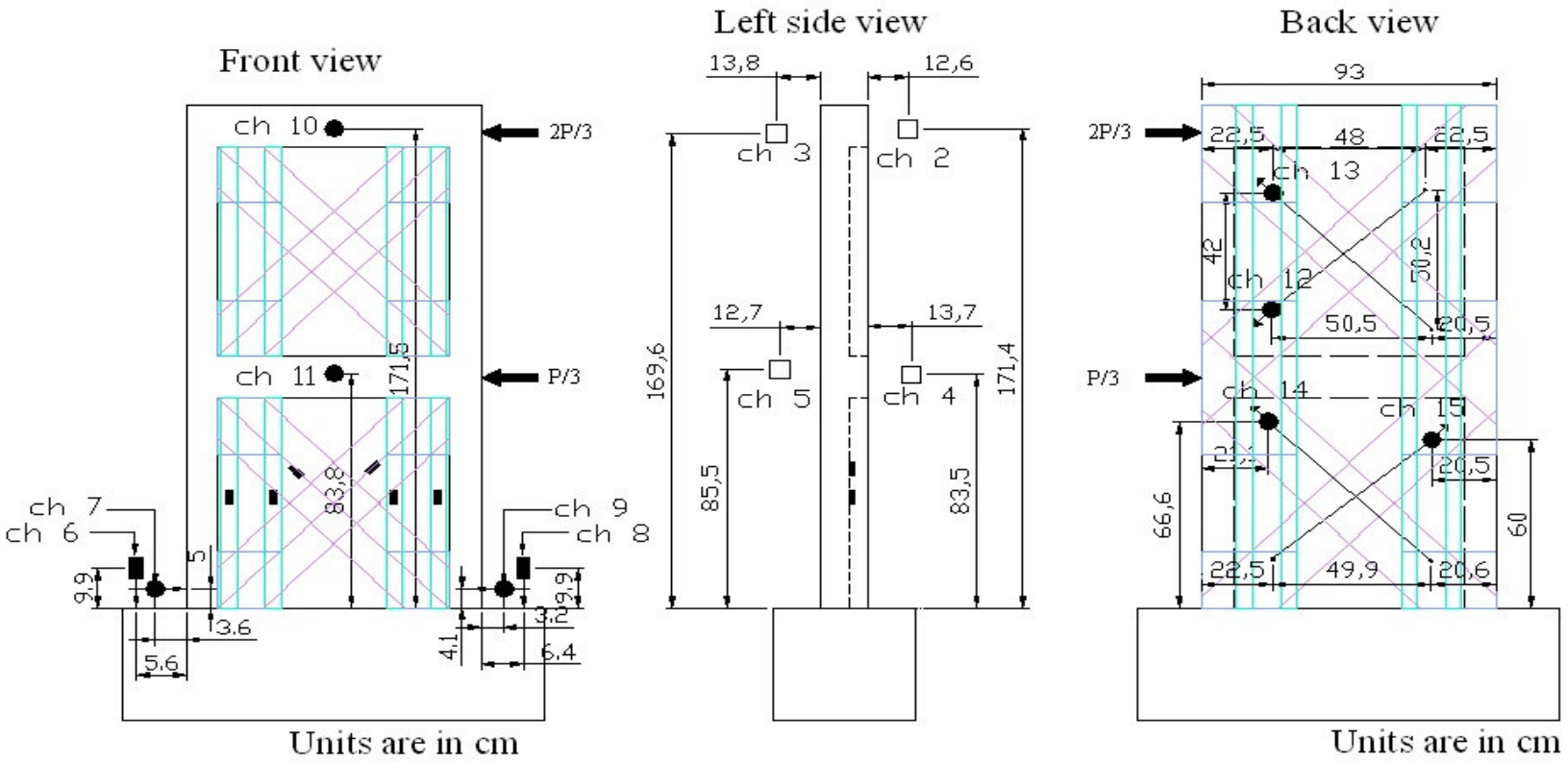

Figure B.1. Position of measuring sensors of specimen O

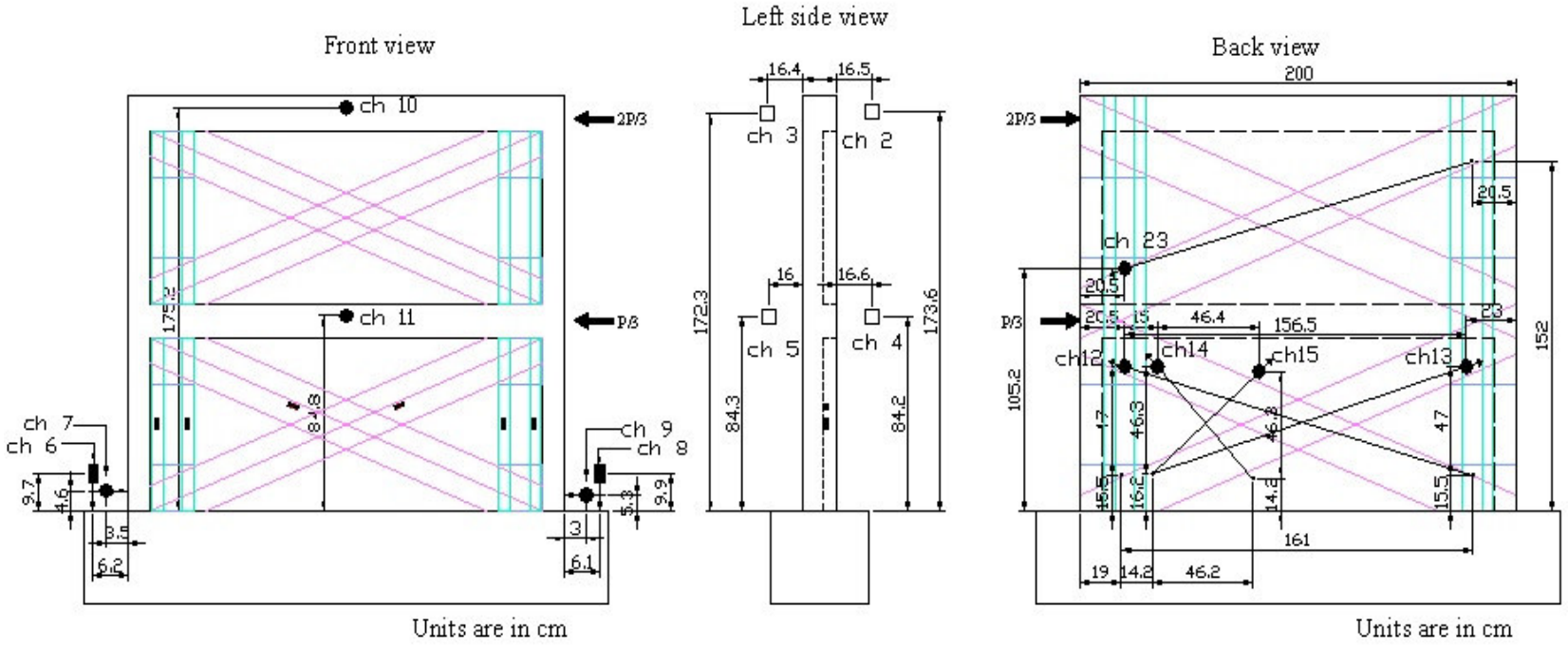

Figure B.2. Position of measuring sensors of specimen O2

REFERENCES

1. Ersoy, U and S. Uzsoy, *The Behavior and Strength of Infilled Frames*, Report No. MAG 205 Tubitak, Ankara, Turkey, 1971.

2. Mainstone, R.J., "On the Stiffness and Strength of Infilled Frames" *Proceedings of the Institute of Civil Engineers*, Vol. 49, Supplementary Paper 7360S, pp. 57-90, 1971.

3. Altın, S., *Strengthening of Reinforced Concrete Frames with Reinforced Concrete Infills,* Ph.D. Thesis, Department of Civil Engineering, Middle East Technical University, and February 1990.

4. Weeks, J., F. Sieble, G. Hegemier, and M. J. N. Priestley, The US-TCMMAR *Full-Scale Five Story Masonry Research Building Test: Part V-Repair and Retest,* Rep. SSRP-94/05, Struct. Sys. Proj., University of California, San Diego, 1994

5. Marjani, F., *Behavior of Brick Infilled Reinforced Concrete Frames Under Reversed Cyclic Loading*, Ph.D. Thesis, Department of Civil Engineering, Middle East Technical University, September 1997.

6. Ehsani, M. R., H. Saadatmensh and A. Al-Saidy, "Shear Behavior of URM Retrofitted with FRP Overlays", *ASCE Journal of Composites for Construction,* Vol. 1, No. 1, pp. 17-25, February 1997.

7. Triantafillou, T. C., "Strengthening of Masonry Structures Using: Epoxy Bonded FRP Laminates", *ASCE Journal of Composites for Construction,* Vol. 2, No. 2, pp. 96-104, May 1998.

8. Kolsch, H., "Carbon Fiber Cement Matrix (CFCM) Overlay System for Masonry Strengthening", *ASCE Journal of Composites for Construction*, Vol. 2, No. 2, pp. 105-109, May 1998.

9. Marshall, Jr., O. S., S. C. Sweeney and J. C. Trovilion, "Seismic Rehabilitation of Unreinforced Masonry Walls", *Fourth International Symposium on Fiber Reinforced Polymer Reinforcement for Reinforced Concrete Structures,* ACI International, SP 188 26, pp. 287-295, 2000.

10. Albert, M.L., A.E. Elwi and J.J.R. Cheng, "Strengthening of Unreinforced Masonry Walls Using FRPs", *ASCE Journal of Composites for Construction*, Vol. 5, No. 2, pp. 76-84, May 2001.

11. Hamilton, H.R. III and C.W. Dolan, "Flexural Capacity of Glass FRP Strengthened Concrete Masonry Walls", *ASCE Journal of Composites for Construction*, Vol. 5, No. 3, pp. 170-178, August 2001.

12. J.G. Tumialan and A. Nanni, "Strengthening of Masonry Walls with FRP Bars," *Composites Fabricator Magazine,* March 2002, Arlington, VA

13. Li, T., P. F. Silva, A. Belarbi, A. Nanni and J. J. Myers,*" Retrofit of Unreinforced Infill Masonry Walls with FRP*", Proceedings of the First International Conference Composites in Construction, Porto, Portugal, October 2001.

14. Ghassan Al-Chaar, "Rehabilitation Of Infilled Nonductile Concrete Frames Using Carbon Fiber Reinforced Polymer" *Composites Fabricator Magazine,* March 2002

15. Borri, A., M. Corradi and A. Vignoli, *"Strengthening Technique Tested on Masonry Structures Struck by Umbria-Marche Earthquake of 1997-1998",* Construction and Building Materials, 2002

16. Hanoglu, K.B., *Fiber Reinforced Plastic Overlay Retrofit of Hollow Clay Tile Masonry Infilled Reinforced Concrete Frames*, Ph.D. Dissertation, Department of Civil Engineering, Bogazici University, 2002.

17. Valuzzi, M. R., D. Tinazzi and C. Modena, *"Shear Behavior of Masonry Panels Strengthened by FRP Laminates",* Construction and Building Materials, Vol. 16, pp. 409-416, 2002.

18. Mertol, H. C., *Carbon Fiber Reinforced Masonry Infilled Reinforced Concrete Frame Behaviour,* M.S. Thesis, Department of Civil Engineering, Middle East Technical University, July 2002.

19. Akguzel, U., *Seismic Retrofit of Brick Infilled RC Frames with Lap Splice Problem In Columns*, M.S. Thesis, Department of Civil Engineering, Bogazici University, 2003.

20. Stratford, T., G. Pascale, O. Manfroni and B. Bonfiglioli, "Shear Strengthening Masonry Panels with Sheet Glass-Fiber Reinforced Polymer", *ASCE Journal of Composites for Construction*, Vol. 8, No. 5, pp. 434-443,October 2004.

21. Erdem, I., U.Akyuz, U. Ersoy and G. Ozcebe, "An Experimental Study on Two Different Strengthening Techniques for RC Frames", *Engineering Structures*, Vol. 28, pp. 1843-1851, 2006.

22. Yuksel, E., A. Ilki, G. Erol, C. Demir and H. F. Karadogan, "Seismic Retrofit of Infilled Reinforced Concrete Frames With CFRP Composites", *Advances in Earthquake Engineering for Urban Risk Reduction,* S.T. Wasti and G. Ozcebe (editors), pp. 285-300, Springer, Amsterdam, Netherlands, 2006.

23. ElGawady, M.A., P. Lestuzzi and M. Badoux, "Static Cyclic Response of Masonry Walls Retrofitted with Fiber-Reinforced Polymers", *ASCE Journal of Composites for Construction*, Vol. 11, No. 1, pp. 50-61, February 2007.

24. Tarek H. Almusallam, "Behavior of FRP Strengthened Infill Walls under In-Plane Seismic Loading", *ASCE Journal of Composites for Construction* Page 308-318 May/June 2007.

25. Gaetano Della Corte, Luigi Fiorino and Federico Massimo Mazzolani "Lateral-Loading Tests on a Real RC Building Including Masonry Infill Panels with and without FRP Strengthening", *ASCE Journal of Composites for Construction* pp. 419-431 June 2008.

26. Han Tae Choi; Jeffrey S. West; and Khaled A. Soudki "Analysis of the Flexural Behavior of Partially Bonded FRP Strengthened Concrete Beams", *ASCE Journal of Composites for Construction* pp. 375-386 July/August 2008.

27. Atmaca S, "*Strengthening Of Brick Infilled RC Frames With Different Aspect Ratios By Means Of CFRP Overlays*" Phd. Thesis, Department of Civil Engineering, Bogazici University, 2003.